Investigation on shear behaviour and design for Aluminium alloy with circular edge stiffened holes with shear span ratio 1.

Esther Mariya Manoj

A thesis submitted fulfilling the requirements for the Master of Engineering degree.

Supervised by

Dr Zhiyuan (Arthur) Fang and Prof James Lim

THE UNIVERSITY OF WAIKATO
Te Whare Wānanga o Waikato

Department of Civil and Environmental Engineering

The University of Waikato

New Zealand

2025

Abstract

Cold-formed aluminium (CFA) structural members are increasingly being adopted in engineering applications due to their favourable strength-to-weight ratio, corrosion resistance, recyclability, and long-term durability in harsh environments. A promising application lies in lightweight framing systems, where circular service holes in the web accommodate mechanical, electrical, and plumbing (MEP) installations. However, such openings significantly reduce shear capacity, leading to premature buckling and distortion.

This study investigates the shear behaviour of CFA channel sections with unstiffened and edge-stiffened circular web holes through nonlinear finite element (FE) analysis, validated against experimental results from the literature. The FE models demonstrated strong predictive capability, with mean FEA-to-test ratios of 1.02 for aluminium and 1.07 for cold-formed steel, and low coefficients of variation (<0.06). A comprehensive parametric study is done by simulations evaluated the effects of hole size, stiffener length, section depth, thickness (2.0–3.5 mm), and alloy grade (H36 and H38). The results showed that unstiffened holes reduced shear capacity by up to 60% (at dw/d1=0.6), while edge stiffeners effectively regained 15–40% of the lost strength. Increasing thickness from 2.0 to 3.5 mm more than doubled shear capacity, and the H38 alloy consistently outperformed H36 due to its higher yield strength.

Comparisons with international design standards ([AISI 2016], [AS/NZS 2018], and [ADM 2015]) revealed that current provisions are conservative for plain webs but underestimate the strengthening contribution of edge stiffeners. To address these shortcomings, new design equations based on a modified Direct Strength Method (DSM) were proposed, incorporating shear reduction factors and elastic buckling coefficients tailored for aluminium members with web perforations. The findings contribute to safer and more efficient design of cold-formed aluminium systems, supporting the integration of perforated channels in modern construction practice.

Keywords

Cold-formed aluminium, cold-formed stainless-steel edge-stiffened circular holes, finite-element models, shear ratio, parametric study, proposed design equations.

Preface

This thesis is submitted to the University of Waikato, New Zealand in fulfilment of the requirement for the master's degree in civil engineering, The work contained in this thesis has not been previously submitted for a degree or diploma in any other higher educational institution. To the best of my knowledge and belief, the thesis contains no material previously published or written by another person except where due reference is made.

Acknowledgements

Firstly, my sincere thanks go to my supervisor, Dr. Zhiyuan (Arthur) Fang, and my co-supervisor, Professor James B.P. Lim, for their unwavering support throughout my research. Their constant guidance and contributions were integral to the successful submission of my journal paper and the completion of this thesis.

I extend my heartfelt gratitude to Dinesh Lakshmanan for his continuous support and encouragement. I am also sincerely thankful to my well-wishers and friends in New Zealand, whose invaluable support and motivation have been a source of strength throughout this journey.

I am deeply grateful to my family—my father Manoj, my mother Lissy Manoj, my brother Ebenezer, and my sister Elhanna—for their unwavering love, encouragement, and belief in me, which have played a vital role in the completion of this project.

Finally, I would like to thank the University of Waikato, School of Engineering, for providing access to computing resources and research assistance, which were essential for the successful execution of this work.

Table of Content

List of Figures

List of Tables

List of Equations

List of Abbreviations

- **AI** – Artificial Intelligence
- **AISI** – American Iron and Steel Institute
- **AS** – Australian Standard
- **BS** – British Standard
- **BSI** – British Standards Institution
- **CAD** – Computer-Aided Design
- **CAE** – Computer-Aided Engineering
- **CEH** – Circular Edge-Stiffened Hole
- **CEN** – European Committee for Standardization
- **CFA** – Cold-Formed Aluminium
- **CFS** – Cold-Formed Steel
- **CNN** – Convolutional Neural Network
- **CUH** – Circular Unstiffened Hole
- **CoV** – Coefficient of Variance
- **DBN** – Deep Belief Network
- **DSM** – Direct Strength Method
- **EH** – Edge-Stiffened Hole
- **EN** – European Norm
- **EXP** – Experimental
- **FE** – Finite Element
- **FEA** – Finite Element Analysis
- **FRP** – Fibre Reinforced Polymer
- **FU** – Flange Unstiffened
- **ISO** – International Organization for Standardization
- **MEP** – Mechanical, Electrical, and Plumbing
- **NH** – No Hole (plain web)
- **NZ** – New Zealand
- **NZS** – New Zealand Standard
- **RC** – Reinforced Concrete
- **RMSE**- Root Mean Square Error
- **MSE**- Mean Square Error
- **MAE**- Mean Absolute Error

- **MBE**- Mean Bias Error
- **NRMSE**- Normalized Root Mean Square Error
- **PCC**- Pearson Correlation Coefficient
- **R^2**- Coefficient of Determination
- **SS_{res}**– Residual sum of squares
- **SS_{tot}** – Total sum of squares
- **UH** – Unstiffened Hole
- **USA** – United States of America
- **VEXP** – Experimental Shear Capacity
- **VFE** – Finite Element Shear Capacity
- **VFEA** – Finite Element Analysis Shear Capacity
- **VP** – Variation of Proposed Equation

Chapter 1. Introduction

1.1 General Background

In modern structural engineering and architectural work, the structural efficiency of elements in use in terms of strength/weight relation, cost and material consumption is of great concern. The elements of structures e.g., beams, plates, and columns are often exposed to complicated loading conditions of the combined axial force, bending and shear. Web openings are typically cut into the members to allow installation of mechanical, electrical and plumbing (MEP) systems within the confined space in the modern building. Such openings, especially when located in web panels or shear walls, allow the structure to be serviced, but reduce load-carrying capacity dramatically by fragmenting stress paths and possibly creating stress concentrations. The utilization of edge-stiffened holes is one solution to this dilemma. Edge stiffeners are thin material reinforcements placed along the periphery of the web openings to counteract the reduction in local stiffness and mitigate the risks of buckling and other localized failures. This design intervention has shown positive results in restoring the lost strength and stiffness in steel members (see Fig: 3), especially cold-formed steel (CFS) members [4], [5]. But still the performance of aluminium alloys in comparable constructions is not well appreciated although it is gaining more and more popularity in structures.

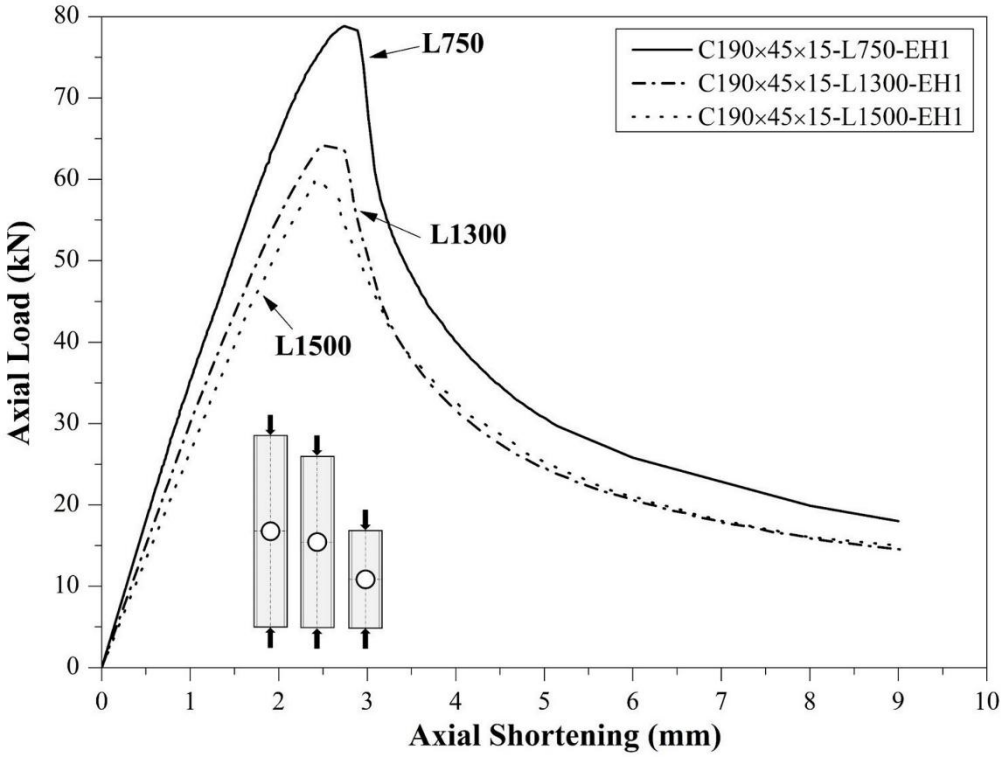

Fig: 1 Load versus axial shortening curves for specimens with various lengths [6]**.**

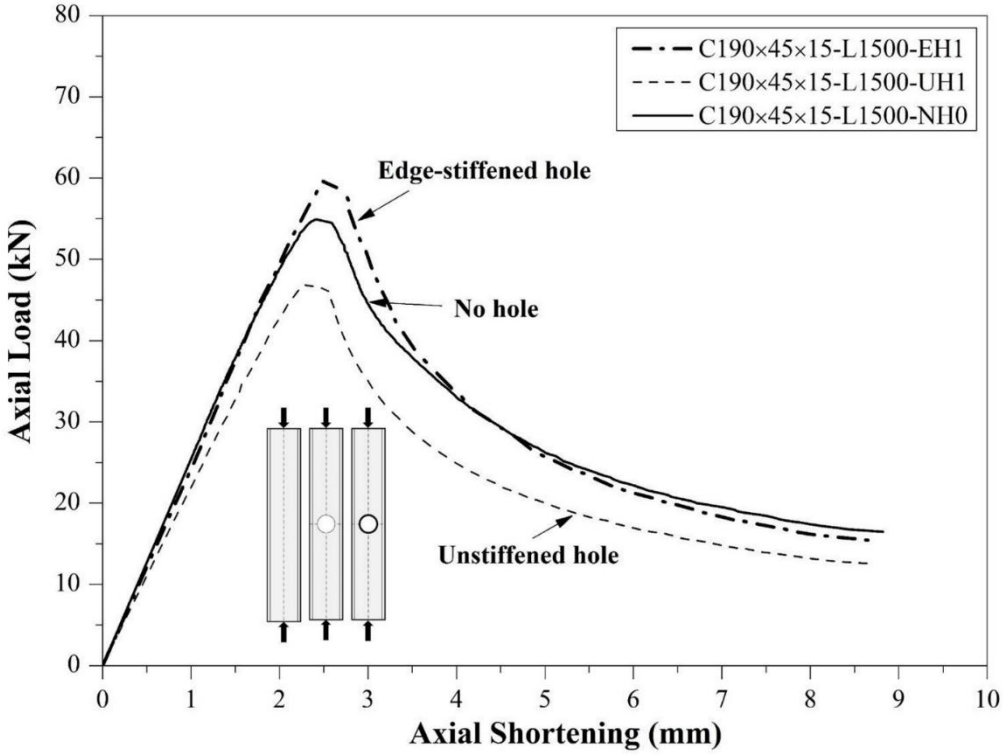

Fig: 2 Comparison of load-displacement response for specimens with and without web openings [6]**.**

The strengthening effect of edge-stiffened web openings has been clearly demonstrated in experimental research on cold-formed steel (CFS) channel sections. Chen et al. [6] investigated the axial compression behaviour of CFS members with unstiffened and edge-stiffened holes, and the results highlighted the efficiency of stiffeners in restoring and even improving load-carrying capacity. As shown in Fig: 1, column length influenced the ultimate resistance, with shorter members achieving higher axial strength. More importantly, Fig: 2 demonstrates that while unstiffened web openings reduced resistance by nearly 20% compared to plain webs, the addition of edge stiffeners increased the strength by up to 21% above the plain section. These results confirm that edge stiffening not only mitigates the loss of capacity associated with service openings but also enhances overall stability. However, while such behaviour has been extensively validated in cold-formed steel, similar investigations in aluminium alloy sections remain limited, creating a critical research gap that motivates the present study.

Due to favourable properties, including light weight, corrosion resistance homogeneous building materials, high strength-to-weight ratio, and recyclability, aluminium alloys are rapidly gaining traction in many industries by replacing the conventional structural materials.

They have applications in different fields such as aerospace, automotive, transportation and most recently modular and prefabricated building systems. Such advantages have necessitated the need to derive material-specific design and performance analysis techniques, particularly where structural forms are varied outside of conventional norms including the use of web openings and edge stiffeners.

Geometric parameters like shear span ratio, i.e., a/d can also have substantial effects on the modes of failure, and the capacity of any given load. At a small ratio between the shear span and overall span (approaching 1), members are likely to fail not by being bent but by being broken by shear mechanisms, and would require a different modelling and design approach. This is a notoriously-documented behaviour in the case of cold-formed steel, but little is known about the response of aluminium alloy members under these conditions.

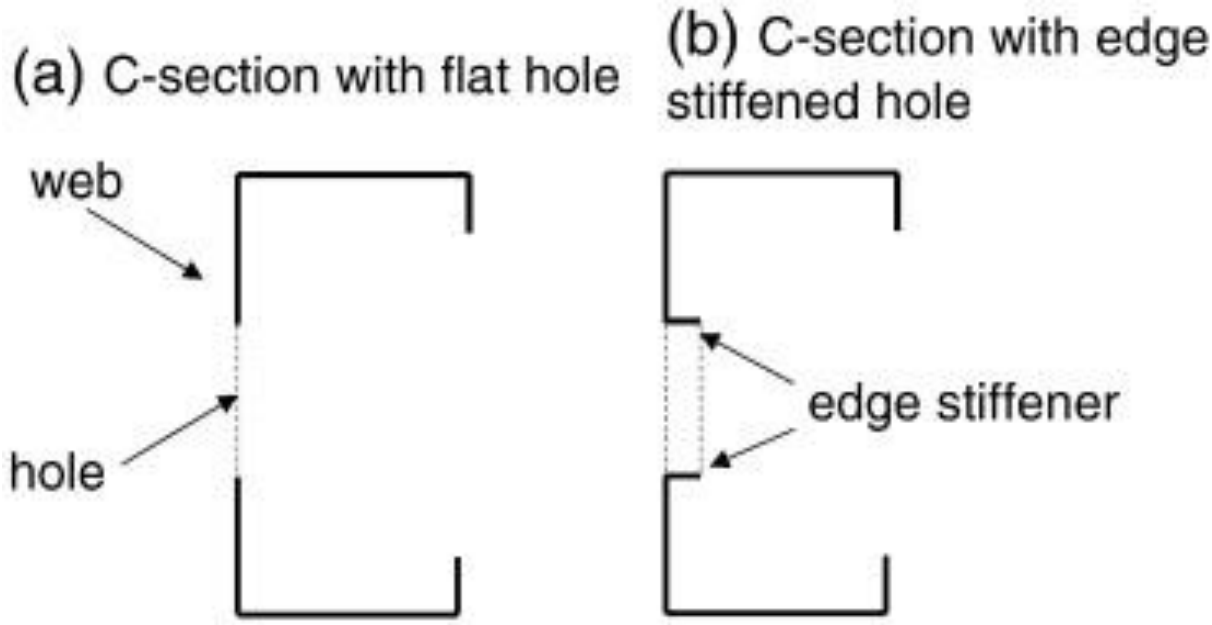

Fig: 3 Cold-formed steel flexural member with edge stiffened holes [7]

Given these complexities, the current investigation aims to explore and quantify the effects of edge-stiffened circular holes on the shear behaviour of aluminium alloy plates (see Fig: 4), particularly under low shear span ratios of 1.0 and 1.5. This study utilizes finite element modelling to simulate structural behaviour and validates results against existing design standards such as AISI (2016) [1] and AS/NZS (2018) [2].

Fig: 4 Aluminium structure frame [8].

In recent decades, research on cold-formed aluminium (CFA) and related lightweight structural systems has grown rapidly, reflecting the global interest in sustainable and efficient construction materials. A bibliometric search revealed more than 2,116 publications indexed in Scopus and 1,810 in Web of Science (Clarivate) on the subject area, highlighting a sharp upward trend in scholarly contributions, particularly after 2005. This surge in publications (Fig: 5) indicates the increasing recognition of aluminium and thin-walled structures as a critical research frontier, reinforcing the timeliness and relevance of the present study.

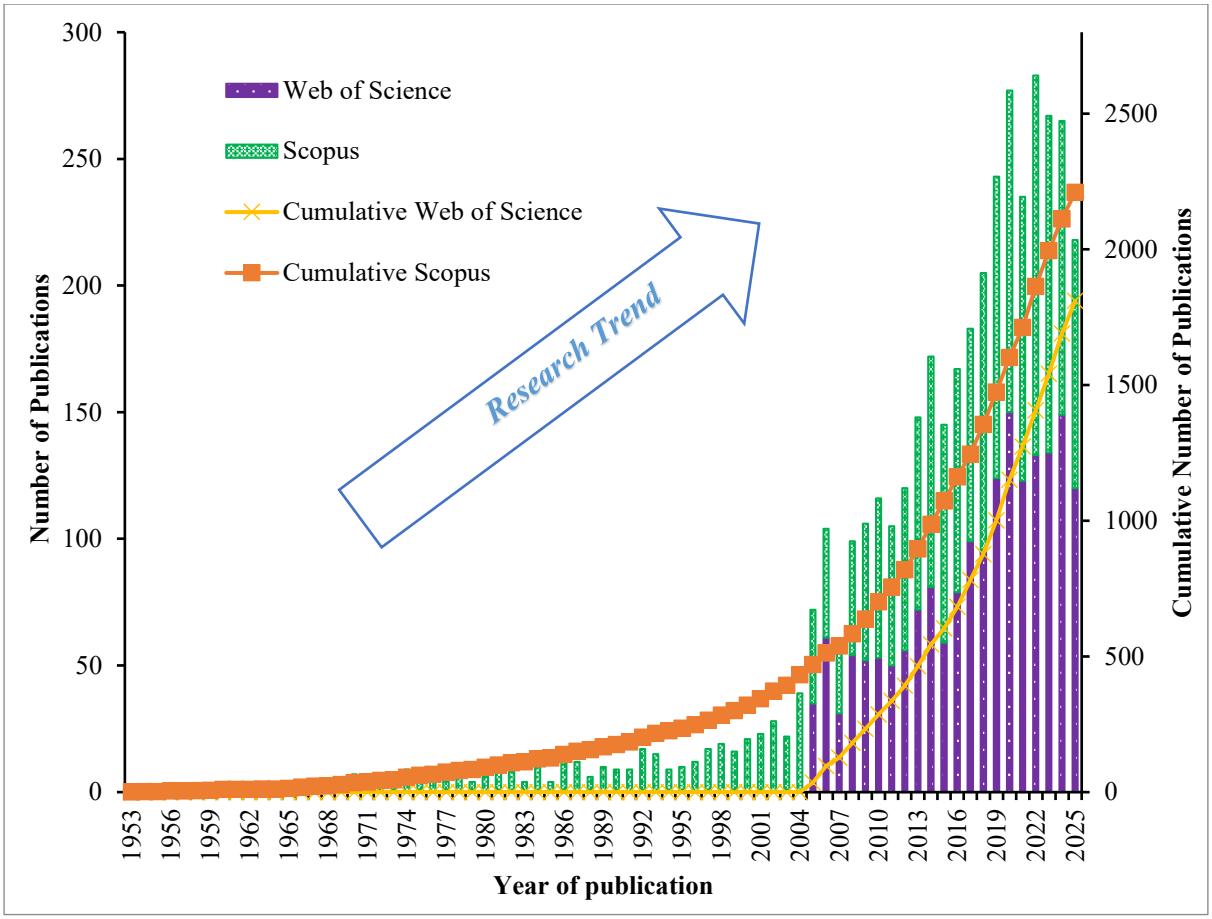

Fig: 5 Research trend in cold-formed aluminium and related structural systems based on Scopus and Web of Science databases.

1.2 Problem Identified

This critical review of the literatures indicates a critical research gap in a current knowledge and structural design approach of aluminium alloy sections with web openings. Although steel-based structures are an established model that has various analyses, aluminium elements are largely evaluated utilizing the underlying principles of methods applied in cold-formed steel structures (AISI, 2016; AS/NZS, 2018) [1] [2]. This is the case since aluminium has fundamentally different mechanical characteristics to that of steel, namely lower modulus of elasticity, non-linear stress-strain behaviour, and higher tendency to local buckling.

The lack of special design provisions to edge-stiffened holes in aluminium alloy sections cause engineers to use conservative design assumptions or employ cumbersome and time-consuming numerical computation. Also, the effect of the stiffener geometry, hole size and shear span ratio

is not adequately covered in most standards and design manuals that involve further complicating the process of design and analysis.

In addition, the available numerical and experimental studies investigate members loaded by standard loading conditions and ignore more realistic cases such as low shear span ratios. These are normally experienced in practice in short span beams, base plates, and support structures. Under these loading conditions, the risk of structural failure may become a hazard due to lack of proper knowledge and predictive ability which creates a risk to safety and serviceability issues.

As such, there is a strong case to fill the missing information by performing specific study on shear capacity of aluminium alloy plates with circular edge-stiffened holes subjected to different shear span ratios. This would not only improve the body of knowledge but there would be development of more accurate and efficient designs models.

1.3 Aim of the Study

The primary aim of this study is to investigate the shear behaviour and design of aluminium alloy plates containing circular edge-stiffened holes, with an emphasis on evaluating their performance under different shear span ratios (1.0). Specific objectives include:

- To model and analyse the shear capacity of aluminium alloy plates with circular edge-stiffened holes using finite element analysis (FEA).
- To assess the influence of shear span ratio on failure modes, stiffness, and ultimate load capacity.
- To compare the FEA results with predictions from existing design standards such as AISI (2016)[1] and AS/NZS (2018) [2].
- To propose improved design recommendations or modification factors for better alignment with observed behaviour.

1.4 Need for the Study

This research renders a gap in structural engineering research and practice. Although aluminium alloys are emerging as promising materials due to their favourable characteristics, structural behaviour of those alloys, especially under shear, is not well understood when they are subjected to complex geometries such as edge-stiffened hole. This is particularly the case in the ones with the low shear span ratios, which have been ignored in the past studies to a great extent.

It is evident that due to the wide gaps existing in current design codes that fail to differentiate between materials such as steel and aluminium design criteria based on their respective behaviour of deformation and failure modes, the need exists to have material-specific design provisions. The result is conservative designs that can neutralize the weight and cost saving advantages of using aluminium or, on the other hand, unsafe designs in those cases where the inherent differences in behaviour are underestimated.

Additionally, the need to adopt modular and prefabricated building methods requires accuracy and effective designing methods. Such systems can use aluminium because of its ease of transportation and assembly and so it is important that sufficient structural integrity is achieved without excessive design. Accurate prediction of shear behaviour of the members with web opening can play a great role in the economic and safe deployment of such system.

Besides practical relevance, the research also makes a contribution to the academic literature because the parameter set which is being studied, namely, edge-stiffened circular holes in aluminium plates with different shear span ratios has not been well researched before. The findings of this work will be used to modify code, experiments and the educational materials.

1.5 Structure of the Thesis

This thesis is organized into seven main chapters, each addressing a distinct aspect of the research on the shear behaviour of cold-formed aluminium (CFA) channel sections with edge-stiffened web openings.

Chapter 1 introduces the research topic by providing the general background, identifying the research problem, and outlining the aims, objectives, and need for the study. It also includes an overview of research trends and bibliometric analysis of published literature, followed by a description of the overall thesis structure.

Chapter 2 presents an extensive literature review covering previous studies on the shear behaviour of cold-formed steel (CFS) and aluminium sections with web openings. It discusses the effects of edge stiffeners, advances in numerical and artificial intelligence-based modelling approaches, and the influence of shear span ratio on failure behaviour. Current design standards are reviewed, and major research gaps are identified. The chapter concludes by outlining the contribution of the present study and summarizing key experimental investigations by Rouholamin et al. and Chen et al.

Chapter 3 details the numerical investigation carried out using finite element analysis (FEA) in ABAQUS. It describes the material properties, meshing schemes, boundary and loading conditions, and geometric imperfections considered in the models. Validation of the FEA

models against published experimental results is performed, and comparative graphs between experimental and numerical outcomes are presented.

Chapter 4 describes the comprehensive parametric study conducted on the verified FE models. It examines the influence of key parameters such as web thickness, alloy grade, web depth, hole geometry, and stiffener configuration on the shear capacity of CFA sections. The section presents tabulated and graphical results for varying thicknesses (2.0, 2.5, 3.0, and 3.5 mm) and compares unstiffened and edge-stiffened configurations.

Chapter 5 provides an in-depth discussion of the results obtained from the FE analyses. It interprets the effects of hole geometry, stiffener length, material grade, and section thickness on shear performance. Comparisons are made with existing international design standards (AISI 2016 and AS/NZS 2018), and typical failure modes are identified. The key findings of the study are summarized at the end of this chapter.

Chapter 6 focuses on the formulation of design rules. It compares the design strengths obtained from current design guidelines with those derived from the FE results. Modified shear reduction factor-based equations are proposed for aluminium members with stiffened web openings, followed by a reliability analysis to validate their applicability.

Chapter 7 concludes the thesis by summarizing the major findings and contributions of the research. It highlights the practical significance of the proposed design recommendations, outlines limitations of the current work, and suggests directions for future research and code development.

Chapter 2. Literature review

2.1 Introduction

Modern construction frameworks with lightweight performance requirements exploit beams and channels to shear forces extensively because they need high-performance materials. These applications demonstrate rising popularity of cold-formed steel (CFS) and aluminium alloys since they provide enhanced strength-to-weight ratio as well as corrosion resistance alongside easy fabricability (Fig: 6). Web openings incorporated into structural members reduce their load-bearing potential when treating shear and axial compression loads because they affect their structural strength.

Modern research into edge-stiffening techniques yields promising results that strengthen weakened areas created by structural opening installations. The review within this chapter presents detailed study regarding the shear performance and design methods and modelling approaches of edge-stiffened web openings within cold-formed and aluminium alloy sections while examining shear span ratios at the forefront. The review bases its investigation on numerical simulation results along with deep learning applications and international design standard insights to establish the foundation for both numerical theory and experimental research within this study.

(a) Unstiffened web holes

(b) Edge-stiffened web holes

Fig: 6 CFS channels studied in this paper: (a) CFS channels without holes; (b) CFS channels with unstiffened web holes; and (c) CFS channels with edge-stiffened web holes. [9].

2.2 Structural Behaviour of Cold-Formed Steel Sections with Web Openings

The field of shear behaviour research related to cold-formed channel sections containing web openings has progressed through multiple studies after LaBoube and Yu's initial work in 1978 that evaluated web strength under combined loading. Their research provided fundamental principles for upcoming shear-buckling investigations because they revealed how web openings affect stress distribution and accelerate shear failure in web parts.

[10] provided further research by studying web elements with different movements under shear forces to show both stress patterns and reinforcement options. Unstiffened web holes according to traditional design prove detrimental to shear capacity which requires modern design approaches according to this research. Experimental studies on lipped channel beams with web openings were carried out by Keerthan and Mahendran (2013a, 2013b) who noted that the shear failure occurred at corners of openings because of local buckling. They also have come up with new design propositions in shear strength prediction [5], [11], [12], which suggests that edge stiffening can be used as a mitigation measure. In a later publication (2015) the two researchers confirmed these working rules in more detailed experimental and finite element (FE) work, stressing the importance of hole geometry and stiffening schedule.

Analogously, Pham and Hancock (2009, 2010a) investigated channel sections and high-strength C-sections, respectively, and examined respectively buckling and strength under

combined bending and shear [13], [14]. Conventional analysis of structure reflects the fact that, as the strength of material increases, its predictions are conservative because unconsidered post-buckling effects are present. While these studies established fundamental shear behaviour for cold-formed steel members with web openings, their conclusions cannot be directly applied to aluminium alloys because of differences in modulus, ductility, and post-buckling response. This thesis builds on those steel-based insights but extends the investigation to aluminium sections with edge-stiffened circular holes under low shear span ratios, an area largely absent from previous research.

2.3 Edge Stiffened Web Holes and Other Holes Enhancing Structural Performance

Web opening stiffening techniques are facing extreme popularity as a successful means of structural reinforcement. The approach provides reinforcement of the hole circumference that helps to overcome the stress concentration that usually leads to buckling and crippling failure. Research led by Chen et al. (2019) analysed the influence that edge-stiffened web openings possess on cold-formed channel sections while they undergo compressive stress [15]. The research results demonstrated that properly designed edge-stiffeners achieve restoration and sometimes improved lateral capacities in comparison to uniform web structures. The edge-stiffened specimens demonstrated enhanced performance in terms of both local and global buckling resistance according to the conducted test results.

New research by Chen et al. (2020) studied how edge-stiffened beam designs outperform unstiffened and plain web configurations under combined stressful conditions through both examination samples and FE models. Both FE modelling and experimental tests confirmed the findings of this research [4], [16].

Chen et al. (2021) conducted a research study which investigated web crippling strengths when beams were subjected to two-flange loading conditions. Edge-stiffened web holes produced superior performance than un-stiffened holes and plain webs because they exhibited lower failure strains and elevated load-carrying capacities [16]. The research findings proved that hole geometry together with stiffener design elements affect the structural ultimate strength. Prior research, especially by Chen et al., has shown that edge stiffeners can restore or even enhance the strength of cold-formed steel members. However, these findings remain untested in aluminium alloys, which display distinct constitutive behaviour. The present study therefore adapts similar stiffening concepts to aluminium channel sections, quantifying their shear capacity through validated FE modelling and parametric analysis.

2.3 Advances in Numerical Modelling and Machine Learning Approaches

Structural engineers use computational tools and artificial intelligence (AI) to create advanced predictions and designs for complex behaviour in thin-walled and cold-formed structures. Standard design methods prove effective yet limited in their application to members that have edge-stiffened web openings. Various studies have studied numerical methods and machine learning methods for enhancing design accuracy and efficiency.

FEA represents the leading computational technology for structure simulation because it provides both flexibility and realism in duplicate actual conditions. [4], [15], [16] effectively simulated cold-formed steel (CFS) channel sections using FEA for edge-stiffened and unstiffened web holes in their respective research. FE model simulations validated experimental findings which proves that these models efficiently reproduce complicated buckling processes in different sections. Edge stiffeners deploy stresses differently throughout the material to both improve shear strength and overall axial resistance of the section. The research findings establish the base for this thesis that utilizes comparable FE-based analysis methods to examine aluminium alloy sections.

Modern design optimization along with predictive modelling has benefited from the implementation of deep learning-based methods. The deep learning framework developed by [17] optimized the compression resistance of CFS channels that incorporate web openings. According to their model a Convolutional Neural Network (CNN) achieved superior accuracy in axial load capacity assessments than the traditional empirical and semi-empirical formulas especially when dealing with non-standard code designs. Engineers benefit from this artificial intelligence-based method to conduct speedy correct assessments across various section dimensions and loading parameters.

[18] developed a Deep Belief Network (DBN) to assess CFS channel section axial capacity where their method demonstrated strong prediction accuracy with scarce dataset information. The research proved that machine learning computational models successfully recognize non-linear structural response patterns which traditional regression design approaches usually cannot identify. The increasing popularity of data-based engineering solutions becomes evident through these research works because they address the unmet need for complete empirical rules within the space of aluminium members with stiffened holes. Here, the FE simulations follow the processes of Chen et al. but are applied in the context of aluminium alloys - a material that has distinct constitutive behaviour. The combination of these two previous studies will allow the models in use to be not only methodologically sound but also based on validated research practice, especially with regard to the parameters such as a shear span ratio and the shape of

stiffeners. Although finite element and machine learning approaches have been successfully applied to cold-formed steel, their application to aluminium alloys with perforations remains underdeveloped. This research contributes by developing and validating nonlinear FE models for aluminium with CUH/CEH, and by aligning the results with design equations that can complement emerging AI-based prediction methods.

2.4 Influence of Shear Span Ratio in Structural Design

The shear span length-to-depth ratio (a/d) i.e. the ratio of the length between the point where the structural member is experiencing the load and the support to the depth of the section is major determinant of the failure mode of structural members. The ratio determines which type of failure occurs in a section, shear failure, flexure failure or the combination. In cold-formed and thin-walled sections, sections that are often susceptible to local instability and post-buckling phenomena, the influence of shear span ratio is critical to safe and efficient design.

[11], [12], [19] carried out parametric studies on CFS channel beams and found that the ratio of shear span verifies the contribution of web and flange to the overall strength. They discovered that shorter shear lengths (a/d $\approx$ 1) encourage shear-dominated collapsing behaviours, in which web-buckling is the most likely to occur at openings. Instead, greater ratios (a/d $\approx$ 2–3) earned 81.76 up to 50 in the temperature range 200 to 400 C. Their work also showed that web openings, especially unstiffened ones accentuate stress concentration and thus cause premature local buckling. This underscores the need for shear span-specific design checks.

[13] researched the shear buckling properties of thin-walled C-sections while validating that shear span parameters affect critical buckling loads especially under different hole shape conditions. The 2010 study by the researchers added complexity by investigating combined effects of high-strength materials which mandated that design calculations incorporate separate considerations for material strength and geometric properties.

Two distinct shear span ratios (see Fig: 7) corresponding to 1.0 were chosen in this research to demonstrate shear-dominated and transition shear conditions. Research by Li and Young (2019) validated that bearing and bending strength levels from high-strength steel tubular sections depend extensively on distance between load points and span length [20]. Wrong selection of shear span can result in two unfavourable outcomes including excessive design capacity or unsafe material failure prediction.

The literature review shows extensive investigation of shear span effects on Channels with Flange Splices but fails to provide sufficient knowledge about aluminium alloy members

incorporating web stiffeners. The research adds essential knowledge since aluminium displays different stress responses through its ductility and strain hardening properties thus serving lightweight construction needs. Existing studies confirm that shear span ratio strongly influences failure modes in thin-walled steel sections. Yet, there is a notable lack of evidence for aluminium members with service openings at a/d ≈ 1.0, a regime critical for shear-dominated behaviour. The present thesis addresses this gap by systematically assessing aluminium edge-stiffened webs under low shear span ratios.

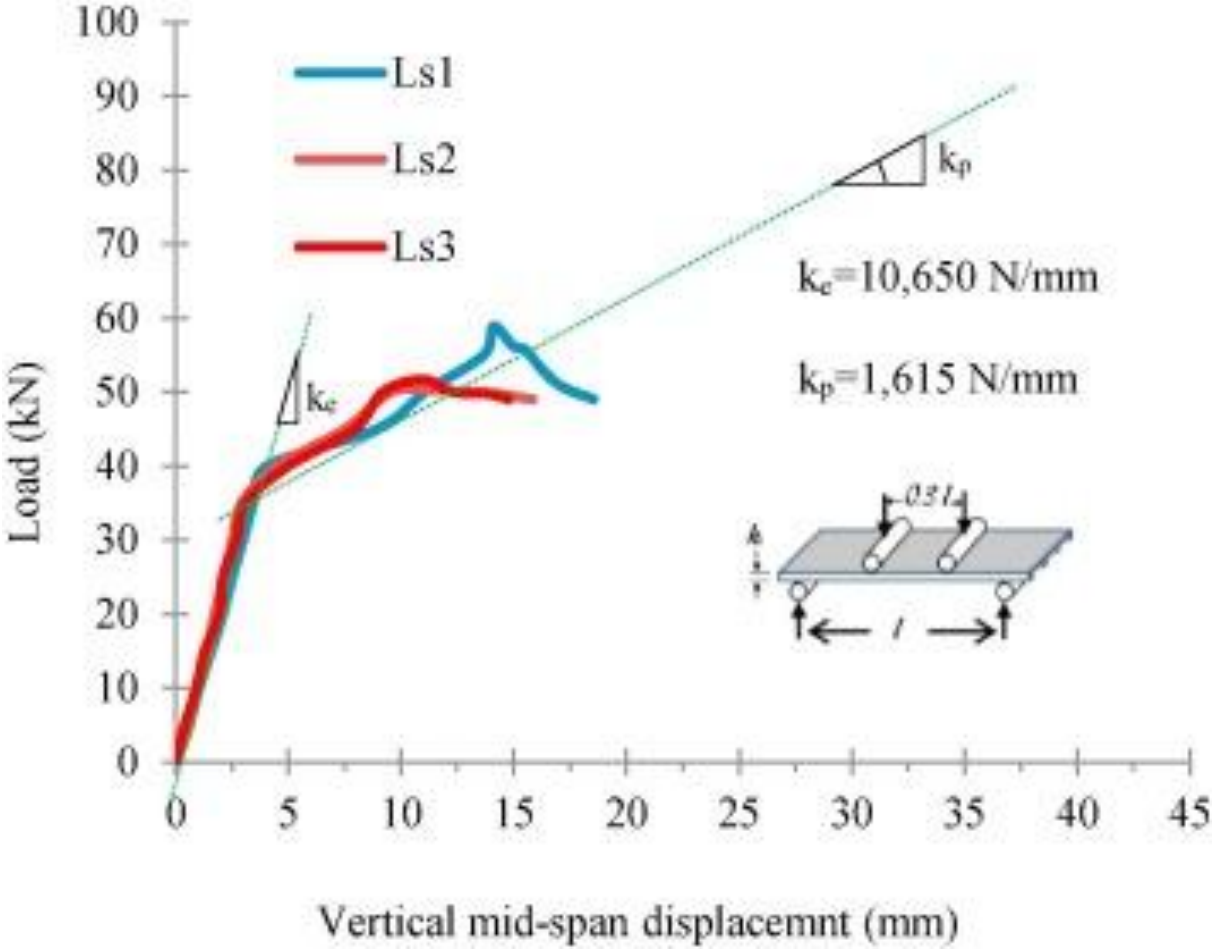

Fig: 7 Shear span ratio overview [20]**.**

2.5 Behaviour of Aluminium Sections with Edge-Stiffened Web Openings

Modern construction applications choose aluminium material because it offers lightweight construction and strong corrosion protection properties and easy recyclability benefits. The application of aluminium alloy members with web openings specially designed as edge-stiffened holes has limited study in available academic research. Research studies primarily concentrated on cold-formed steel elements while Aluminium sections remain under documented regarding valid design models together with experimental data.

The thesis fills this academic void by assessing aluminium plates with circular edge-stiffened holes through various shearing span ratio tests. [4], [15], [16] demonstrated through their work that steel members with web holes receive significant reinforcement from edge-stiffening creating higher buckling resistance and ultimate strength values. The general concept of edge-stiffening benefits aluminium structures but produces different response and magnitude effects due to its elastic and ductile properties.

Application of aluminium beams in construction projects necessitates service openings which requires edge-stiffening to act as performance enhancing design structure as well as a functional requirement. Numerical results in this thesis validate edge-stiffeners as an efficient design tool because they evenly distribute shear stresses while minimizing stress concentrations and postponing plate local buckling in aluminium structural components.

The research of Eiler et al. (1997) and LaBoube and Yu (1978) provided supplementary evidence for these findings by demonstrating major behaviour differences in web elements with and without reinforcing under shear and combined load conditions [10], [21]. The research tested cold-formed steel in the beginning yet the findings about load path optimization and local reinforcement apply to aluminium design.

Furthermore, the use of numerical modelling approaches validated against ISO 6892-1 (2009) standards ensures that the material-specific response of aluminium is accurately captured in simulations [22]. The application of non-linear material models and geometric imperfections allows for realistic prediction of failure patterns in aluminium alloy members.

Thus, this section of the literature reveals a major contribution of the current research: it is among the first to systematically evaluate the shear performance of aluminium alloy plates with edge-stiffened holes, under specific design scenarios relevant to lightweight and high-performance structures. Only limited attempts have been made to extend stiffener benefits from steel to aluminium, and available work does not comprehensively capture shear behaviour under practical loading. This thesis is among the first to provide a systematic study of aluminium channels with CUH and CEH, validated against test data and expanded into parametric design recommendations.

2.6 Current Design Standards and the Need for Revision

Structural design standards such as the American Iron and Steel Institute (AISI 2016)[1] and the Australian/New Zealand code (AS/NZS 2018) [2] provide detailed formulas and provisions for the design of cold-formed steel sections. However, their applicability to non-standard

geometries such as web openings with edge-stiffeners, and especially to aluminium members is questionable.

The research has established that AISI (2016) [1] and AS/NZS (2018) [2] provide a 4.5% conservative prediction for cold-formed stainless steel members having edge-stiffened web holes. Security issues emerged when the codes underestimated the strength of some configurations while selecting incorrect load directions. The results support previous research by Keerthan and Mahendran (2013c; 2014) which demonstrated the need for updated rules to determine shear strength of lipped channel sections with non-standard openings [11], [12].

Chen et al. (2020) together with Chen et al. (2021) stressed the existing design standards have several constraints [4], [16]. The researchers showed that neglecting edge-stiffening effects causes limited prediction accuracy of ultimate capacity so new design equations are required to include hole geometry characteristics and stiffening configurations specifically.

A piece of numerical simulation-derived equation serves as a basis for this thesis to calculate the moment and shear capacities found in aluminium plates with edge-stiffened holes. The proposed mathematical expressions received reliability analysis to conform with the theory of limit state design.

The proposed research of [17], [18] introduces machine learning technology which demonstrates potential applications in future structural code revisions. These analytical models show ability to predict various section shapes under different loading conditions which make them suitable for modern engineering applications involving aluminium alloys.

Current design standards require immediate revision because they need to integrate new materials with emerging structural geometries and edge-stiffened features. This revision of design standards receives vital support from the current research through its validated experimental data and newly developed equations and structural information for aluminium alloy sections. Current international standards (AISI, AS/NZS) offer provisions mainly for cold-formed steel and unstiffened webs, often proving conservative or unsafe for aluminium with stiffened openings. The present study responds to this gap by proposing modified DSM-based equations and reliability-checked reduction factors, specifically calibrated for aluminium members with perforated webs.

2.7 Summary and Research Gap

Research examines the structural characteristics of cold-formed steel (CFS) sections with web openings both individually and in compression applications as well as bending and shear conditions. The research shows that edge-stiffened holes represent an effective strategy to

combat strength reduction from openings in structures. Despite notable advancements various research gaps continue to exist for aluminium alloy sections since these materials gain prominence because of their desirable engineering characteristics such as low weight and resistance to corrosion and high flexibility.

Research by [4], [15], [16] proved that attaching edge stiffeners to web openings creates an effective strengthening mechanism which boosts the axial and shear performance in CFS channel sections. Research findings based on experimental testing and validated finite element (FE) models from these scientist's form foundations to develop improved design specifications. The research by Chen et al. focuses on cold-formed steel sections but does not explore aluminium alloys because these materials exhibit different mechanical behaviour when loaded due to their low elastic modulus, heightened strain hardening effects and stress–strain non-linear characteristics.

Research carried out by Keerthan and Mahendran (2013a–2015) and Pham and Hancock (2009, 2010a) on thin-walled section shear behaviour has confirmed the impact of dimensional alterations and loading conditions on shear strength [5], [11], [12], [13], [14], [23], [24]. Research findings demonstrate how shear performance depends on three primary elements including web design aspects alongside material attributes and testing setup characteristics. The fundamental examination of aluminium edge-stiffened web openings has not been performed for low shear span ratios (a/d = 1) even though such conditions heighten shear-dominant failure modes.

Fang et al. (2021a, 2021b) presented deep learning-based approaches for structural optimization but these methods remain in their early stages since their work primarily concentrates on actions along the axial direction [17], [25]. Widely published evidence to support their shear performance prediction methods is lacking especially when applied to edge-stiffened holes and aluminium alloys. The development of new research should focus on linking AI prediction algorithms and physical testing results and simulation outcomes applied to aluminium structural components.

The current design standards including AISI (2016) [1] and AS/NZS (2018) [2] offer reliable advice for cold-formed steel characteristics but fail to address properly edge-stiffened web holes adequately and these standards are incompatible with aluminium alloy element applications. The thesis evaluation demonstrates that standard predictions for edge-stiffened designs lead to 4.5% over conservative results and particular cases show they produce unacceptably low strength predictions resulting in unsafe structural designs. The development of better rules for efficient assessment of CFS beams with web openings was presented by

Keerthan and Mahendran (2013c, 2014) yet similar research is insufficient for aluminium alloy structures. Experimental data reveals a gap from current standardized design procedures thus demonstrating why updated design equations are essential for specific materials[11], [12].

Research is absent regarding combined effects between shear span ratios and edge stiffening mechanisms on aluminium plates and channels when exposed to shear-dominant loading conditions. Research has failed to investigate the combined impact of CFS geometry along with loading pathways on material performance despite the extensive knowledge about CFS section behaviour. Structural systems require a reliable design that includes aluminium elements because this material displays enhanced susceptibility to local buckling yet lacks sufficient analysis research.

While prior studies established the benefits of edge-stiffening primarily for cold-formed steel, their conclusions cannot be directly transposed to aluminium because of aluminium's lower modulus, stronger nonlinearity, and higher local-buckling susceptibility as per shown in Table 1. Moreover, most works either excluded shear-dominant regimes ($a/d \approx 1.0$) or addressed only unstiffened openings. In contrast, this thesis focuses on aluminium 5052-H36/H38 channels with circular CUH/CEH under $a/d=1.0$, builds a large FE–validated dataset, and proposes modified DSM reduction/enhancement factors and reliability-checked equations specifically calibrated for aluminium.

Table 1 Comparative map: prior studies vs. the current studies.

Study (short)	Material	Geometry & loading focus	Method & scope	Key findings	Limits/gaps in prior work	How this thesis extends / addresses
LaBoube & Yu [19], [25] [21]	CFS	Webs under bending, shear, and combined	Experiments + early design guidance	Web openings alter stress paths; early shear-buckling insights	No edge-stiffening; not aluminium; limited perforation types	Applies concepts to aluminium with circular edge-stiffened holes under shear-dominant a/d≈1.0.
Eiler et al. [10]	CFS	Web elements with openings under varying shear	Experimental	Showed stress concentration and need for reinforcement	No quantitative rules for stiffeners; no aluminium	Quantifies stiffener benefits for aluminium via FE + parametric; proposes design factors.
Young & Chen [20], [26]	CFS	Shear of beams with perforated webs	Tests + design recommendations	Baseline reduction factors for unstiffened openings	No edge-stiffened cases; steel only	Builds reduction/enhancement factors for aluminium CUH/CEH; calibrates vs FEA.
Pham & Hancock [13], [14]	CFS (incl. high-strength)	Shear buckling; bending–shear interaction	Tests + analysis	Importance of shear span and slenderness	Limited hole stiffening; no aluminium	Treats a/d=1.0 regime; maps hole depth ratio & stiffener length effects in aluminium.
Keerthan & Mahendran [5], [11], [12], [23], [27]	CFS	Lipped channels with web openings (shear)	Tests + FE + design rules	Edge stiffening improves capacity; rules for steel	Rules do not cover aluminium properties or CEH geometry specifics	Transfers methodology to 5052-H36/H38 aluminium; updates factors for E, σ–ε behaviour.

Study (short)	Material	Geometry & loading focus	Method & scope	Key findings	Limits/gaps in prior work	How this thesis extends / addresses
Fang et al. [17], [18]	CFS	Shear of beams with circular/large openings	FE + experiments	Quantified capacity loss vs. hole size	No aluminium; no CEH for aluminium	Uses similar FE rigor to generate aluminium CEH/CUH datasets and trends.
Chen et al. [4], [16], [28], [29], [30]	CFS	Edge-stiffened openings (compression, bending, crippling)	26 tests + FE + parametrics	CEH can even outperform plain webs in compression; validated FE	Focused on steel; not shear-dominant with aluminium	Motivates your Intro figures and sets the stiffening rationale; your work fills aluminium + shear gap.
Li & Young [20]	High-strength steel	Bearing/bending; span effects	Experiments	Strength depends strongly on load positions/span	Material and geometry differ; no perforated aluminium	Justifies a/d selection and load path sensitivity for current aluminium study.
Standards: AISI (2016), AS/NZS (2018) [1], [2]	CFS	Code provisions (plain/unstiffened)	Specifications	Provide qs reductions for steel	No specific CEH rules for aluminium; conservative/unsafe in cases	You propose modified DSM with new reduction/enhancement factors for aluminium CEH/CUH.

2.8 Key Research Gaps Identified

1. Lack of studies on aluminium alloy sections with edge-stiffened web holes subjected to shear loading—most prior work focuses on cold-formed steel.
2. Minimal experimental or numerical investigation into the influence of shear span ratio on the failure mechanisms of aluminium members with web holes.
3. Current design codes (AISI 2016 [1]; AS/NZS 2018 [2]) do not adequately cover configurations involving edge-stiffened openings or provide specific provisions for aluminium materials.
4. The use of deep learning has not yet been expanded to predict shear capacity in complex configurations, nor validated for aluminium alloy members.
5. No unified framework exists to compare edge-stiffened and unstiffened web openings in aluminium sections using numerical and design standard-based approaches.

2.9 Contribution of the Present Study

This thesis aims to address these research gaps by providing a comprehensive investigation into the shear behaviour of aluminium alloy plates with circular edge-stiffened web holes, focusing on two specific shear span ratios (1.0). The study utilizes finite element modelling validated against prior research methods (e.g., [4], [15]), while incorporating material-specific parameters conforming to the ISO 6892-1 (2009) [22] standard for tensile testing of metallic materials.

By exploring a novel combination of variables—material type, hole geometry, stiffener configuration, and loading ratio—this work makes an original contribution to the body of knowledge. The findings can inform future design code enhancements, propose new reduction factor-based equations for aluminium plates with reinforced holes, and ultimately support safer, lighter, and more efficient structural systems across multiple industries, including aerospace, automotive, and civil infrastructure. This research also contributes to the United Nations Sustainable Development Goals (SDGs) by aligning its outcomes with key sustainability objectives. Specifically, it supports SDG 9 (Industry, Innovation, and Infrastructure) by providing improved design rules for aluminium members with stiffened openings, enhancing resilient and innovative infrastructure solutions [31]. It advances SDG 11 (Sustainable Cities and Communities) by enabling modular and lightweight aluminium systems that are safer and more resource-efficient for urban applications as per shown in Fig: 8. Through the optimization

of stiffener geometry, the study also addresses SDG 12 (Responsible Consumption and Production) by reducing excessive material use and promoting sustainable fabrication practices. Finally, the adoption of lightweight and durable aluminium designs directly contributes to SDG 13 (Climate Action) by lowering embodied carbon and minimizing long-term maintenance requirements. Collectively, these contributions demonstrate how structural engineering research can converge with global sustainability agendas.

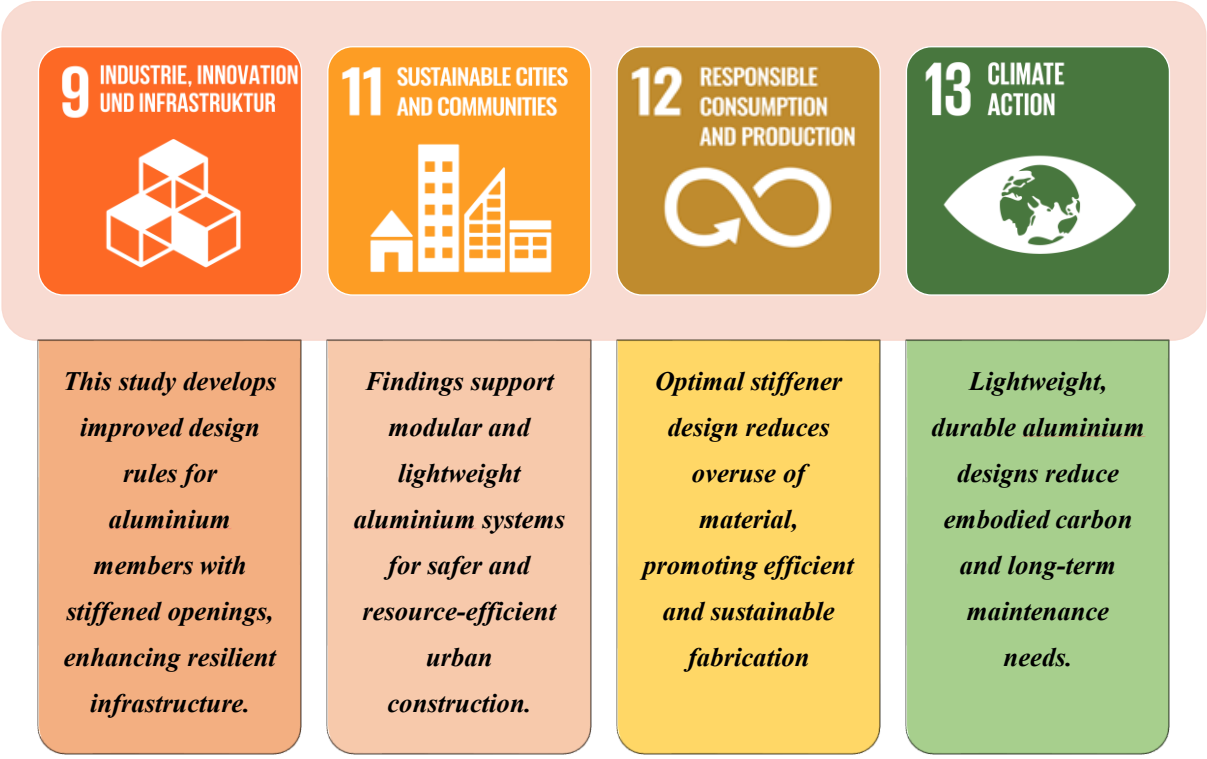

Fig: 8 Convergence of this study with relevant United Nations Sustainable Development Goals.

Chapter 3. Summary of experimental investigation

experimental part consisted of seventeen three-point shear tests on Cold-formed aluminium lipped channel beams (LCBs), which had a circle-shaped web opening of various sizes, an aspect ratio of 1.0 and varied aluminium tempers. There were varied section depths and values of web slenderness included in the test specimens and the material characteristic were gained based on tensile coupon tests. The effects of opening size, section slenderness, and material on the shear capacity of LCBs, determining failure modes, load deflection behaviour, and capacity reduction trends were studied using the experiments.

To conduct the numerical study, nonlinear elasto-plastic finite element (FE) models were prepared in ABAQUS to model the shear behaviour of LCBs by using plain-webbed LCBs, unstiffened/circular web openings and edge-stiffened/circular web openings. FE models consisted of S4R shell elements with a mesh density of 5-10mm refined near openings and lips, as well as real measured cross section competing dimensions, material stress-strain curves and initial geometric imperfections. Boundary conditions, the set-up of the three-point shear test, was simulated and the loading was displacement controlled at the top flange and simple supported at the ends.

The validation process involved comparing FE against the 17 test results with outstanding agreement with the mean V test/VFE ratio near to 1.0 with coefficient of variation (COV) less than 0.05 which optimises the accuracy of the model used against the ultimate shear strength and buckling behaviour.

Following validation, a parametric study was carried out using 204 FE models, systematically varying:

- Section depth and web slenderness ratio (d_1/t_w).
- Hole diameter ratio (d_{wh}/d_1) from 0.1 to 0.7.
- Material temper and yield strength.

The FE solution measured the factors of reduced shear capacities of each configuration and indicated that the bigger the openings, the more the shear capacity was decreased considerably in case of slender webs and edge stiffeners partially compensated the loss. Test and FE reduction factors were then compared to existing shear capacity design rules developed by Shan et al., AS/NZS 4600 [2], McMahon et al., and Keerthan and Mahendran, in which it was found out that the cold-steel-based shear capacity design provisions, coupled with the authors of aluminium shear capacity design provisions, were accurate, whereas existing aluminium standards were more on the conservative side.

A study by Howick Ltd. (2013), shear capacity of cold-formed steel (CFS) channels with plain webs (NH), unstiffened web holes (UH), and edge-stiffened web holes (EH) configurations of webs are researched. EH sections, developed by Howick Ltd. (2013) [32], are becoming more common in NZ to be used as floor joists and bearers, but no research and no provision in the design code have been found so far on their shear performance (AISI 2016 [1]; AS/NZS 2018 [2]).

An experiment program comprised 30 tests that were performed on 2 section sizes (240 mm and 290 mm web depth) 2-hole diameters (90 mm, 140 mm) and two aspect ratios a/d 1.0 and 1. An EH hole was designed better at 13 mm lip to enhance stiffness. Based on material properties measured in tensile tests the yield strength was 301.6 MPa (section 240) and 308.5 MPa (section 290). Back-to-back channels were merely tested under concentrated loading conditions under which the shear capacity is found as total weight/4.

The findings revealed 14.5 increase in the capacity of EH specimens compared to UH. Flange restraint added capacity by ~ 11O and smaller aspect ratios (1.0) by ~ 25O as compared to 1.5. Holes that were bigger minimized capacity. These failure modes were a shear buckling (global in NH, local around holes in UH/ EH) and flange distortion in cases of FU.

The A plane simulated stress of plane AB = 1.01 and the mean of this plane was 0.07. A 224-parametric test with a/d 1 =1.0 tested web slenderness (96290), hole ratio (0.10.7), and stiffener length ratio (0.040.12). Capacity went up ~11.6% with longer stiffeners, dropped by nearly 53% with perimeter of holes (considering only area) and went large with thicker ones.

The comparisons of the CAD to the design rules indicated DSM to be conservative in the absence of tension field action; DSM with tension field action matched quite well. Long-established UH reduction formulae tended to be overconservative or unconservative when they were applied to EH. A composite test FEA-based factor of reduction, EH, is suggested to be used in safe and precise design.

Conclusively, EH increases shear capacity, flange restraint, and smaller aspect ratios expand their performance, and UH-based formulas presently used are potentially unsafe with EH. The validated FE analysis program makes forecasting and code development predictable, and the new EH reduction factor is solving an exceptional gap in terms of the modern CFS construction.

3.1 Bibliometric Analysis of Cold-Formed Aluminium Studies

To better understand the research focus in this domain, a bibliometric analysis was conducted using the Scopus database with the keyword “cold-formed aluminium”. A total of 2,116

publications were retrieved, comprising 14,779 keywords. Using VOSviewer, a co-occurrence network was generated by applying a threshold of 100 minimum occurrences, resulting in 1,295 keywords meeting the criteria. The visualization (Fig: 9) reveals distinct clusters, where “aluminium alloys” and “microstructure” dominate the central research themes, while related topics such as mechanical properties, cold rolling, corrosion resistance, and coatings form strong peripheral connections. This mapping indicates that while significant attention has been devoted to the material science aspects of aluminium alloys, fewer studies address their structural performance under shear with web openings — thereby underscoring the relevance and novelty of the present research.

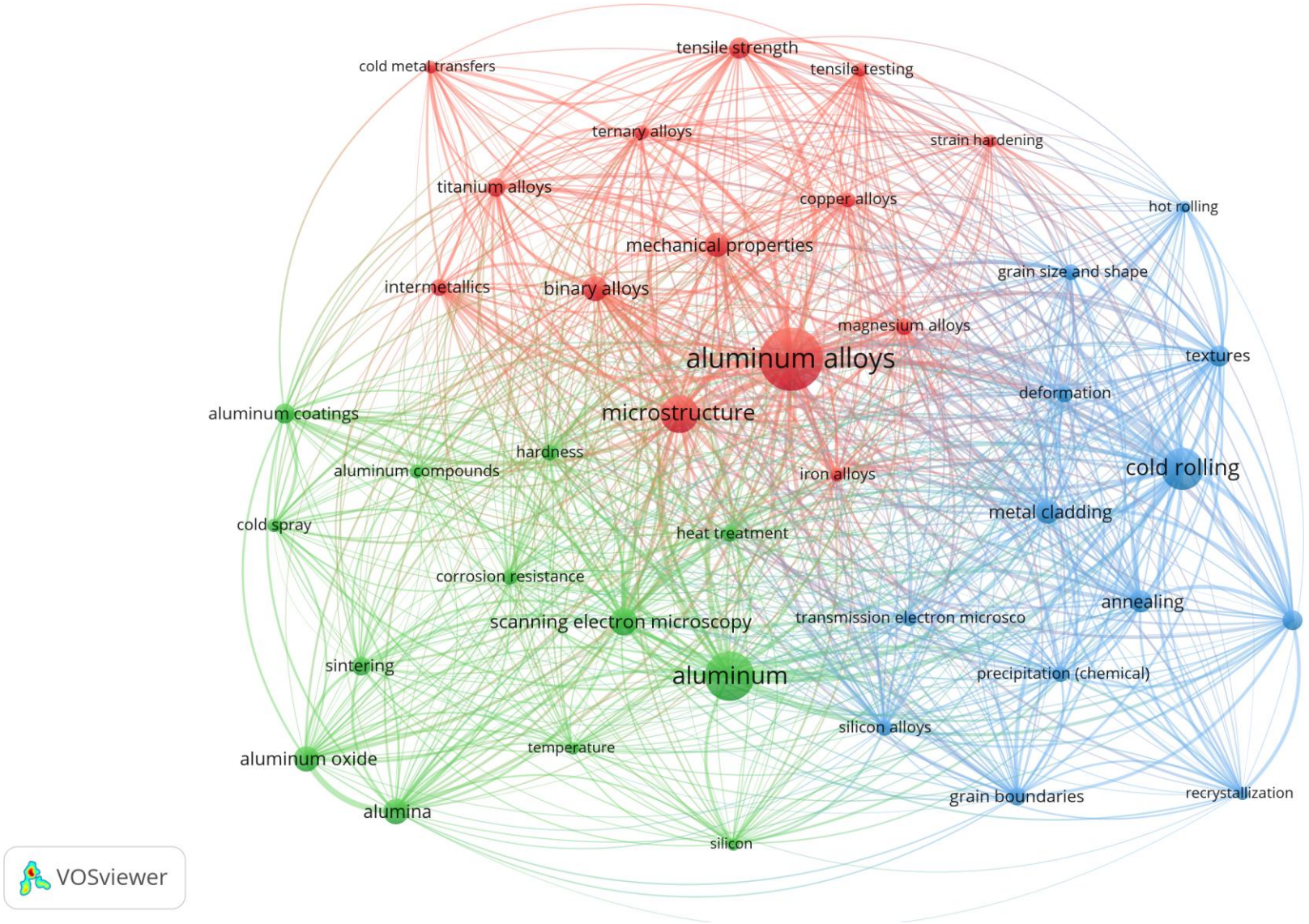

Fig: 9 Co-occurrence network of research on cold-formed aluminium based on Scopus database.

Chapter 4. Numerical investigation

4.1 General

Nonlinear elasto-plastic FE models were developed using ABAQUS software [33] to simulate the shear behaviour of CFS channel sections with plain webs, unstiffened elongated web holes and edge-stiffened elongated web holes. In the FE modelling, the centreline cross-section dimensions as well as the initial geometric imperfections for CFS channel sections were considered. The following subsections provide a detailed description of the modelling techniques.

4.2 Material properties

Summary of the material properties used in the parametric study as shown in Table 2**.** The aluminium alloys used in this study are 5052-H36 and 5052-H38, which differ mainly in their strength and ductility. H38 exhibits higher yield stress (250 MPa) and ultimate strength (300 MPa) compared to H36 (232 MPa and 272 MPa, respectively), indicating greater load resistance before yielding and failure (see Fig: 10). The Young's modulus is nearly identical for both tempers (≈ 68,000–69,400 MPa), showing comparable stiffness in the elastic range. However, H38 demonstrates slightly higher strain at yield and ultimate strain (0.57% and 7.69%) relative to H36 (0.54% and 6.1%), meaning that it combines higher strength with improved ductility. These differences make H38 more suitable for applications requiring both strength and deformation capacity, while H36 remains a slightly lower-strength alternative.

Table 2 Material Properties for finite element analysis [34]**.**

Temper	**Alloy Series of aluminium**	**Yield Stress (f_y) MPa**	**Ultimate Stress (f_u) MPa**	**Young's Modulus (E) MPa**	**ε_y %**	**ε_u %**
H36	5052	232	272	69,400	0.54	6.1
H38	5052	250	300	68,000	0.57	7.69

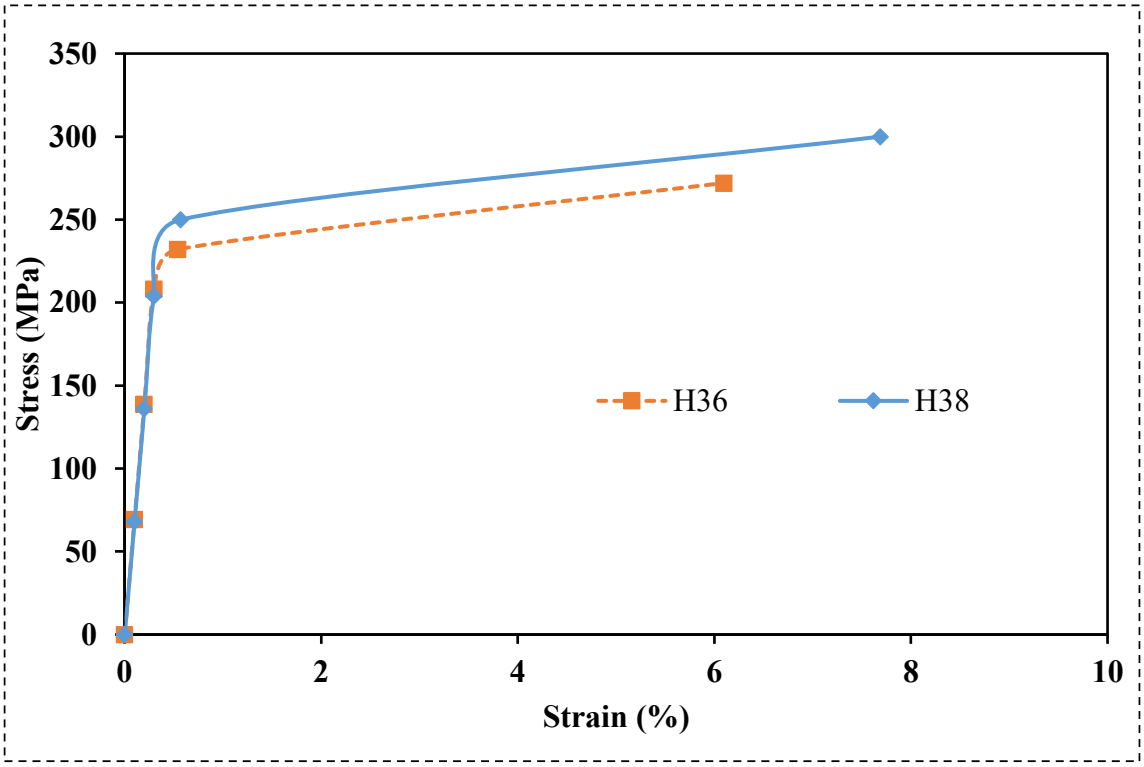

Fig: 10 Stress and stress curve of both materials (H36, H38) [34].

4.3 Meshing details

S4R shell elements were used to model the CFS channel sections, while C3D4 solid elements were chosen to model the loading plates. The mesh details for the C400T2.0-D0.2 section are shown in Fig: 11, where three different element types were used: R3D4 for 3D solid elements, RNODE3D for 3D nodal elements, and S4R for 4-node shell elements. The mesh consists of 40,918 nodes and 40,284 elements, ensuring sufficient refinement for accurate analysis. A 10 mm × 10 mm mesh size was used for the loading plates, while a 5 mm × 5 mm mesh was applied to the channel sections. Specific regions requiring more detailed analysis, such as the web-flange junction, flange-lip junction, and edge-stiffener-web region, were meshed with finer elements to improve the simulation accuracy.

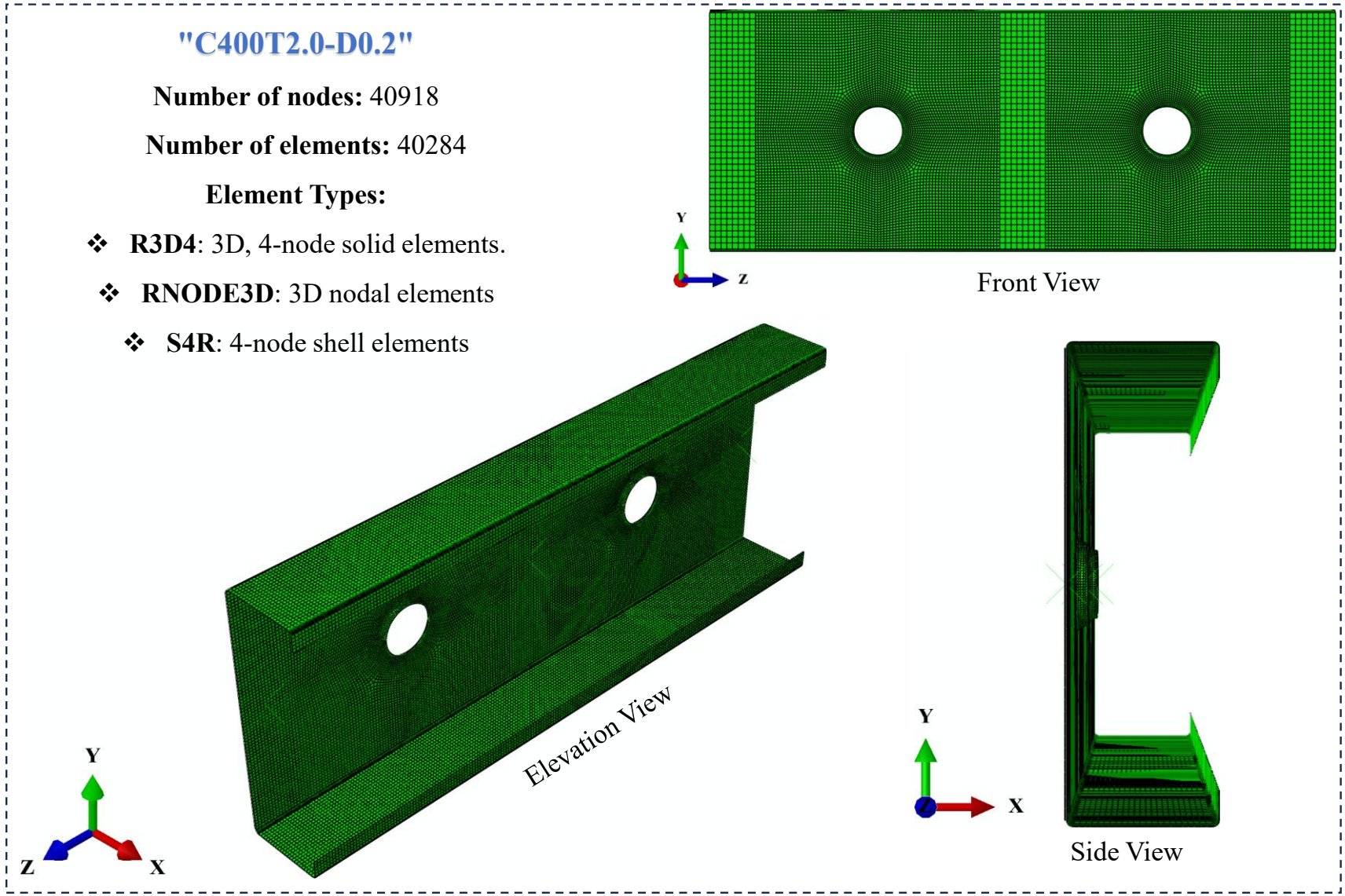

Fig: 11 Mesh detail of the C400T2.0-D0.2 section showing front, side, and elevation views.

4.4 Loading and boundary conditions

The loading and boundary conditions in the FE models were designed to replicate the experimental setup. The models assumed simply supported boundary conditions and applied loads at mid-span, consistent with the three-point loading arrangement used in the tests. Initial geometric imperfections were included in the models to simulate real-world conditions and to ensure accurate failure predictions. As shown in Fig: 12, the loading and boundary conditions are clearly depicted.

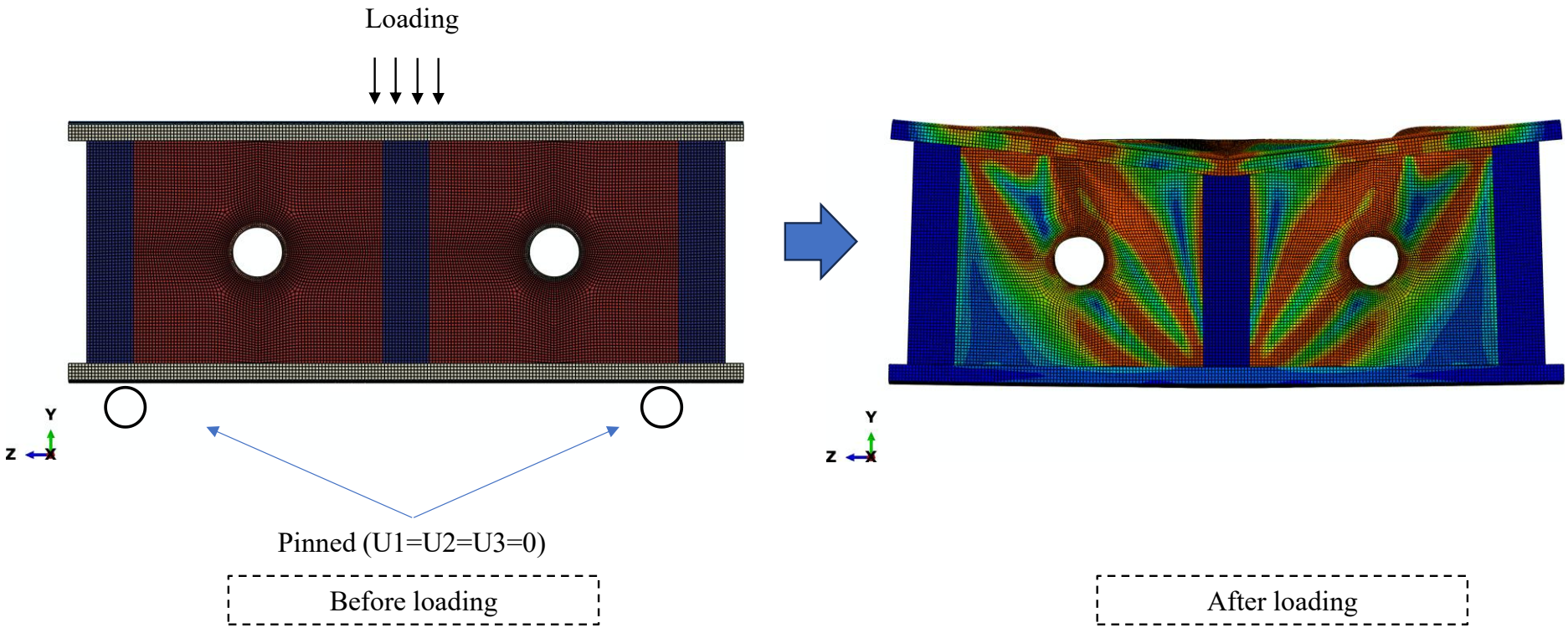

Fig: 12 loading and boundary conditions for C400T2.0-D0.2 section.

4.5 Geometrical imperfections

In the FE modelling, initial geometrical imperfections were considered. The magnitude of local imperfections was taken as 0.64 t for the CFS channel sections [33]. The ABAQUS library's *IMPERFECTION option was used to model the imperfect initial geometries of CFS channel sections in the current study. The FE models included the critical buckling mode obtained from the eigenvalue buckling analysis as the imperfect geometries.

4.6 Validation of the FE model

A comparison between shear capacities experimentally obtained V(EXP) of Rouholamin et al. and Chen et al. and the values calculated V (FEA) in the present research is presented in Table 3 [21]. This data includes a variety of differently shaped aluminium and cold-formed steel channel section samples, including different depth, the flange width, lip size, thickness web hole pattern. In the aluminium specimens of Rouholamin et al. [21], FE-predicted ratios of the actual and the measured shear capacities ranged between 0.84 and 1.08 with cumulative average ratio of approximately 1.02, which is a great confirmation of the lesser difference in the models and the actual tests. In the same way, the mean ratio of cold-formed steel edge-stiffened specimen of Chen et al was 1.07 with low coefficient of variation (CoV) of 0.03 indicating consistent accuracy. The fact that the experimental results correlate closely with FE results proves that the developed model has been able to capture the nature of elastic/post-buckling behaviour in this study as well as ultimate shear strength in sections with and without 24in. stiffened web openings. Such a close agreement confirms the modelling strategy, boundary conditions, material properties, and imperfection assumptions on the geometric imperfection applied to the study so that the FE model is trustworthy to carry out the large-scale parametric studies.

4.7 Comparison of shear obtained from experimental tests in the literature and FEA results from this study

Table 3 Comparison of shear obtained from experimental tests in the literature and FEA results from this study.

Specimen label	Experimental tests	Overall Depth	Width of flange	Lip	Thickness	Web hole depth	Web hole length	Aspect ratio	Test V_{EXP} (kN)	FEA V_{FEA} (kN)	
		d (mm)	bt (mm)	L (mm)	T (mm)	dw (mm)	bw				
SO1	[21]	155.3	64.5	22.5	2.97	49.43		1	49.43	46.78	1.06
SO2		155.8	63.9	22.4	2.96	37.52		1	37.52	34.81	1.08
SO3		155.5	63.8	22.6	2.97	18.99		1	18.99	20.35	0.93
SO4		206.1	77.5	23.2	2.98	57.55		1	58.51	58.32	1.00
SO5		206.3	77.1	23.2	2.98	40.13		1	40.13	37.34	1.07
SO6		206.1	77	23.2	2.97	19.75		1	19.75	19.18	1.03
SO7		255.1	75.4	25.2	2.46	46.29		1	46.29	55.11	0.84
SO8		255.4	75.9	25.2	2.46	33.99		1	33.99	33.56	1.01
SO9		255.4	75.6	25.2	2.47	15.1		1	15.10	14.37	1.05
SO10		255.4	76.7	24.9	2.97	60.44		1	60.44	68.167	0.89
SO11		255.2	76.5	24.9	2.98	44.02		1	44.02	44.11	1.00
SO12		255.2	76.6	25.1	2.97	20.07		1	20.07	19.48	1.03

Specimen label	Experimental tests	Overall Depth	Width of flange	Lip	Thickness	Web hole depth	Web hole length	Aspect ratio	Test V_{EXP} (kN)	FEA V_{FEA} (kN)	
		d (mm)	bt (mm)	L (mm)	T (mm)	dw (mm)	bw				
SO13		401.9	126.4	29.4	2.98	72.28		1	72.88	86.62	0.84
SO14		401.8	126.2	28.4	2.97	47.73		1	47.73	48.10	0.99
SO15		401.7	126	28.4	2.97	21.28		1	21.18	21.15	1.01
										Mean	0.987
										CoV	0.07
SO1	[4]	237.3	45	15	1.86	96.5		1	31.7	33.0	1.04
SO2		238.3	45	15	1.85	93.5		1	28.7	30.4	1.06
SO3		235.5	45	15	1.87	148.9		1	41.0	45.3	1.10
SO4		237.3	45	15	1.85	147.5		1	35.2	38.6	1.09
										Mean	1.07
										CoV	0.03

Table 4 Comparison of FEA results against test results [34].

Experimental	Finite Element Analysis
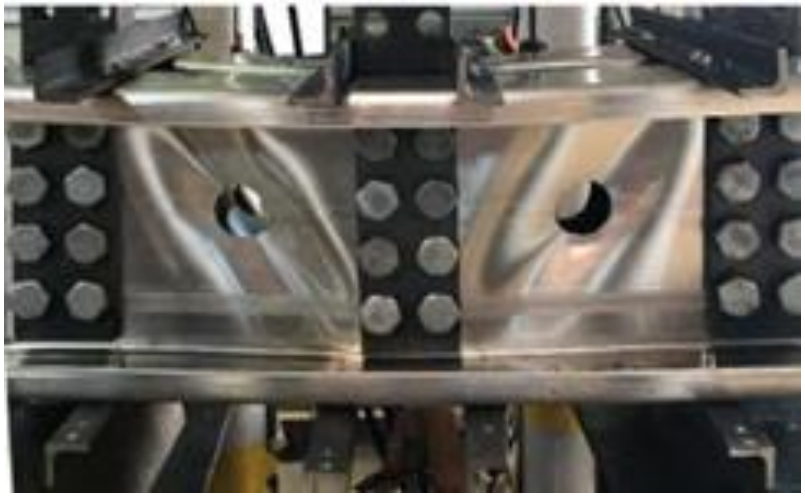	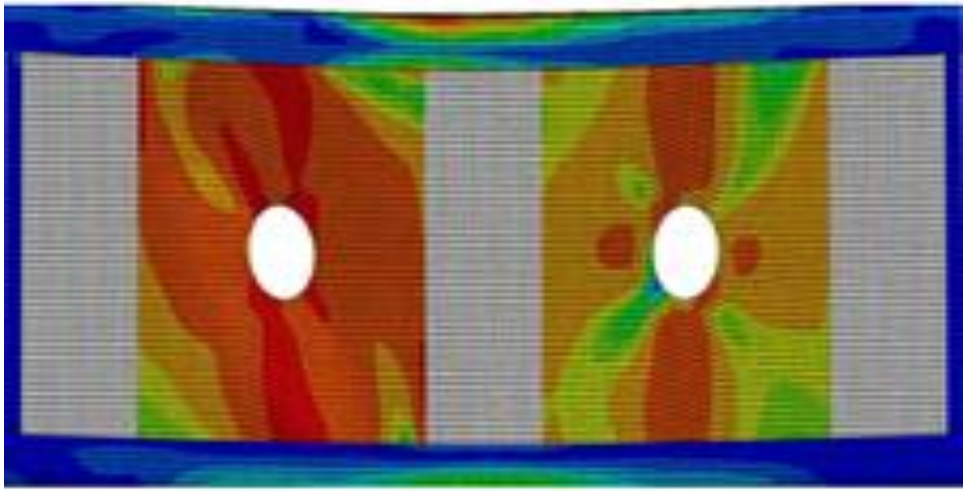
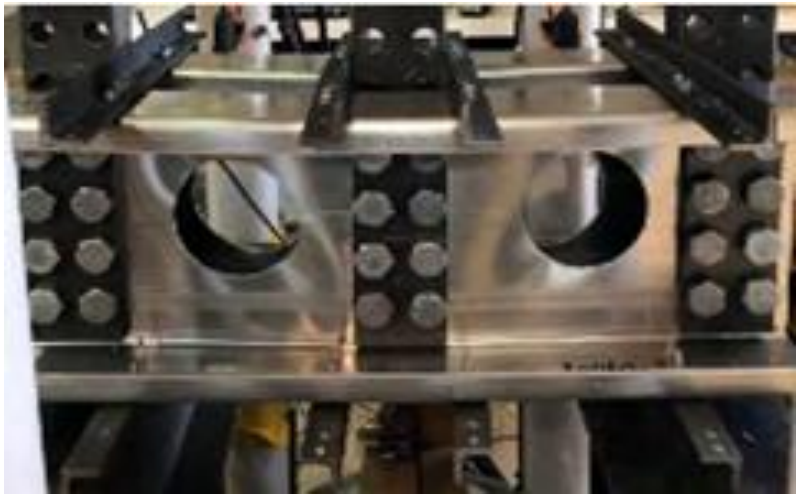	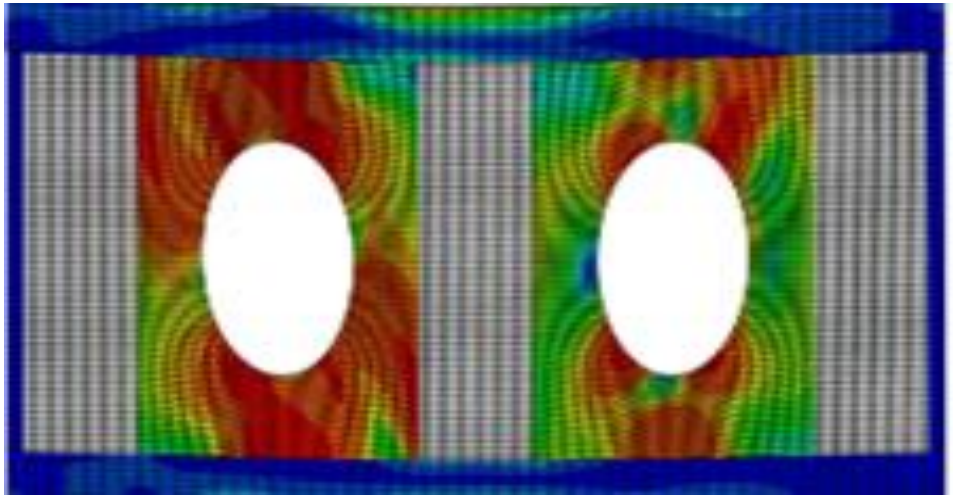

Experimental	Finite Element Analysis
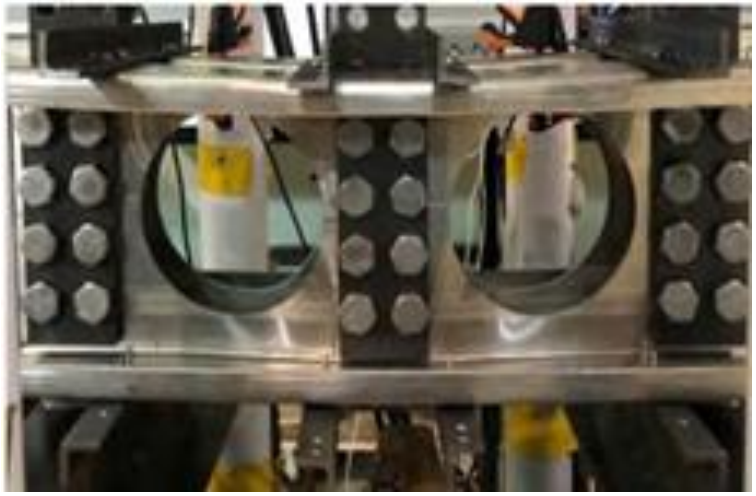	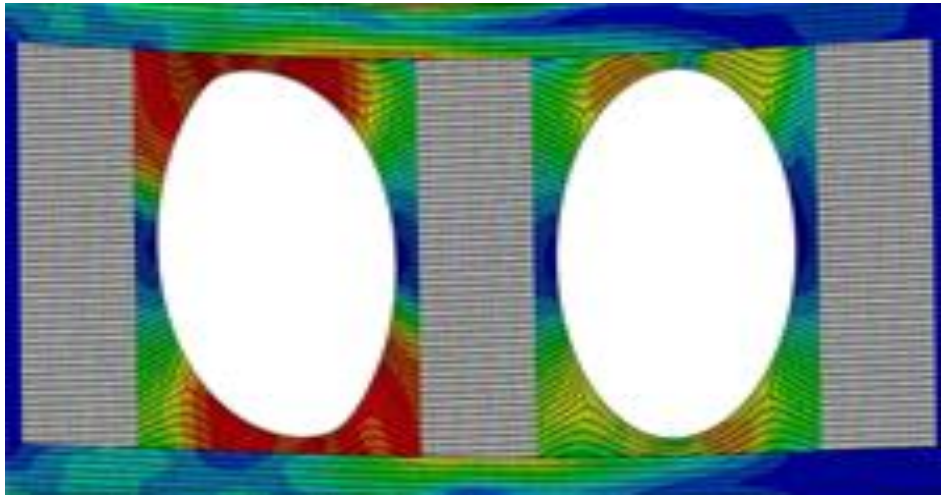
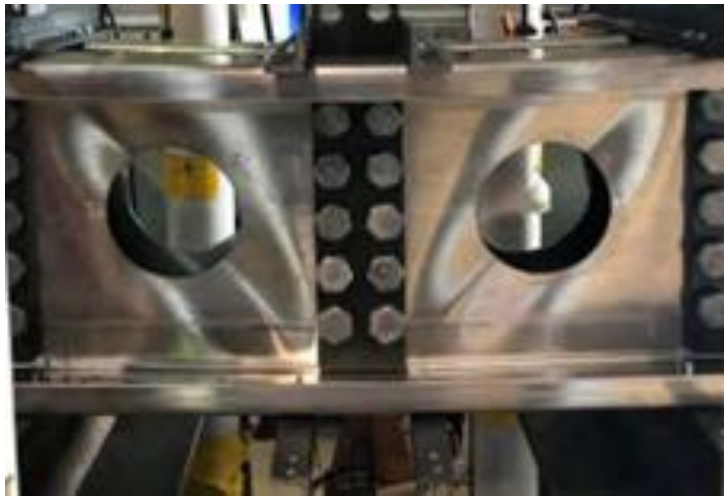	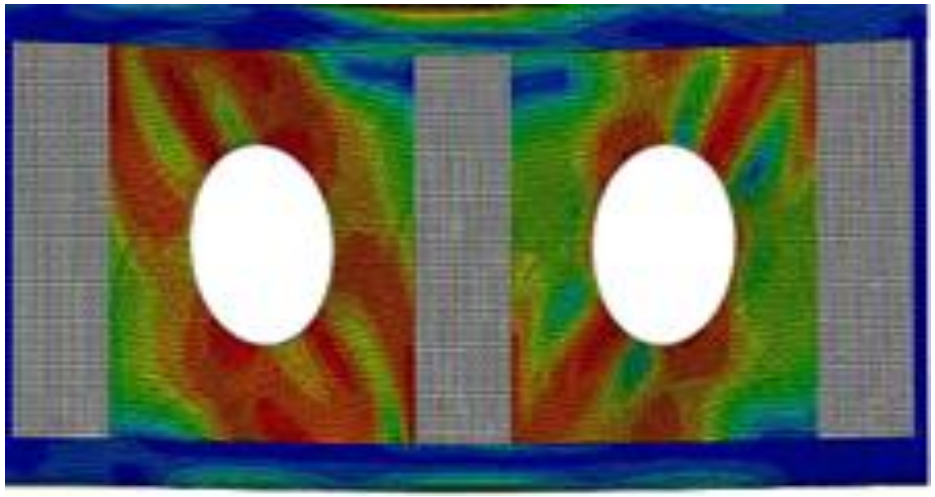

Experimental	Finite Element Analysis
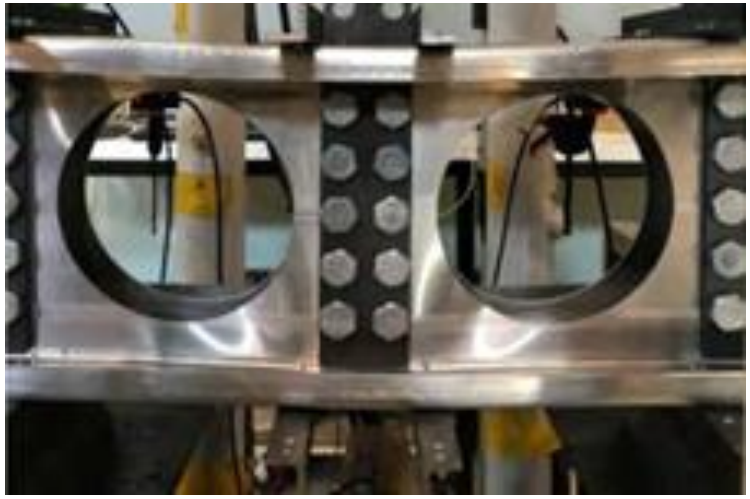	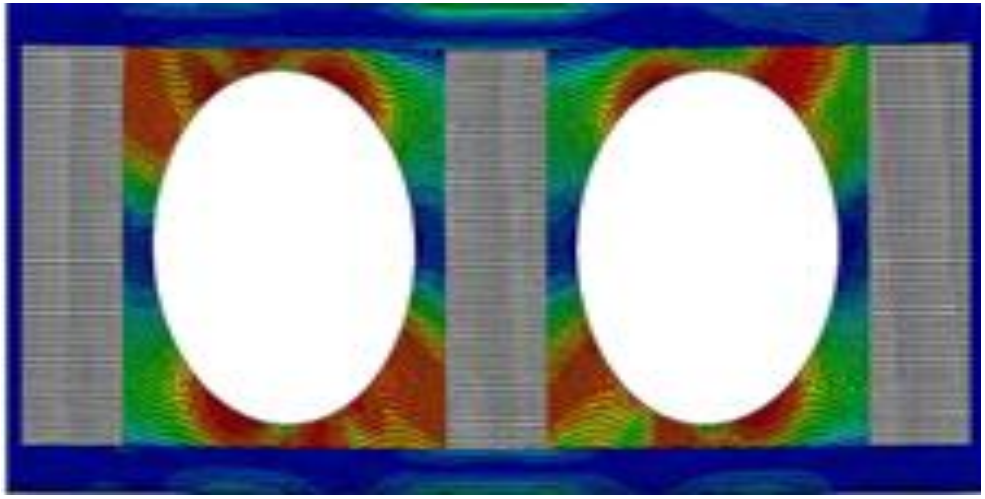
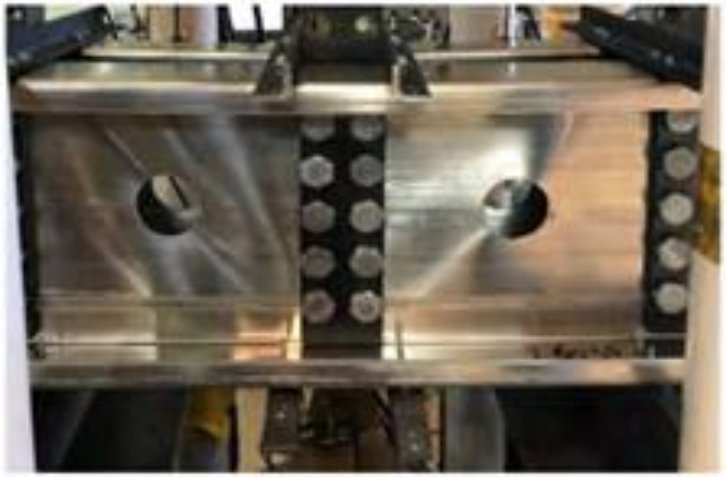	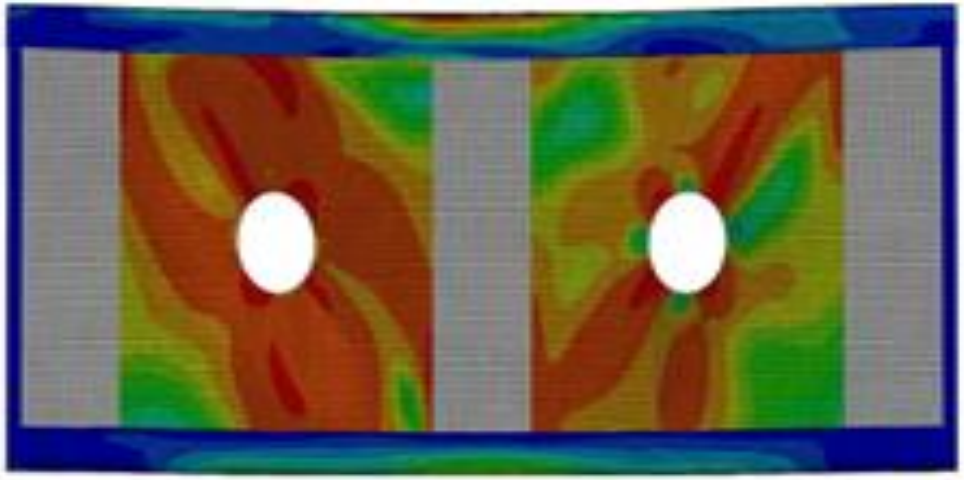

Experimental	Finite Element Analysis
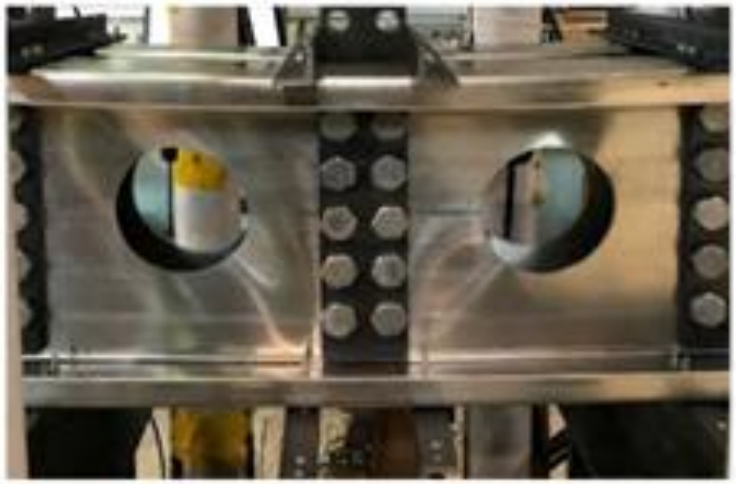	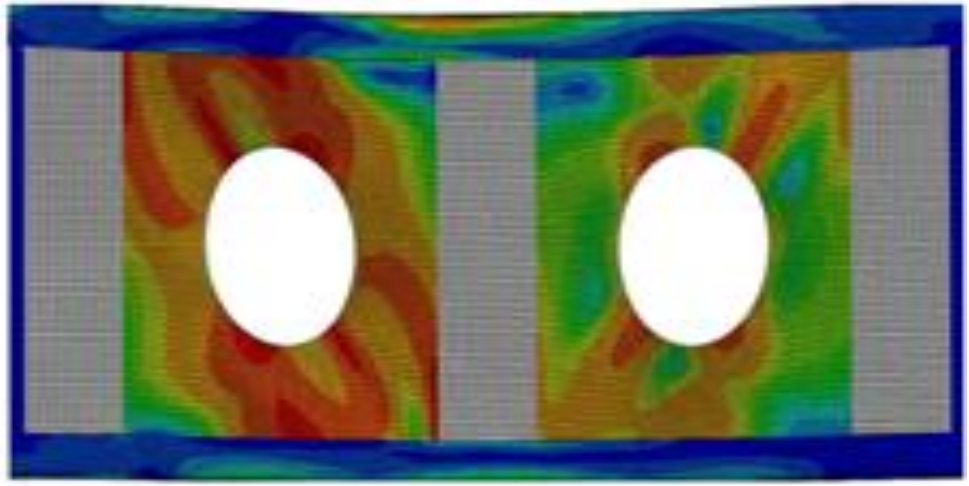
	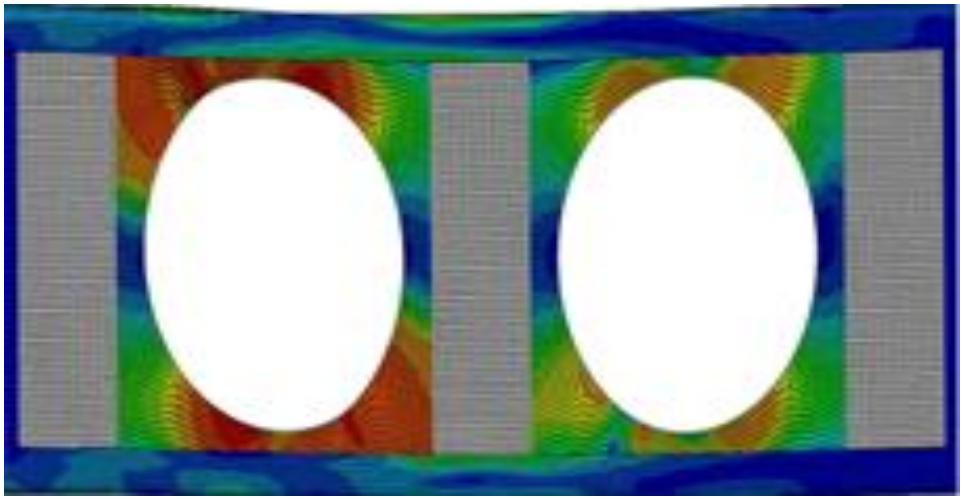

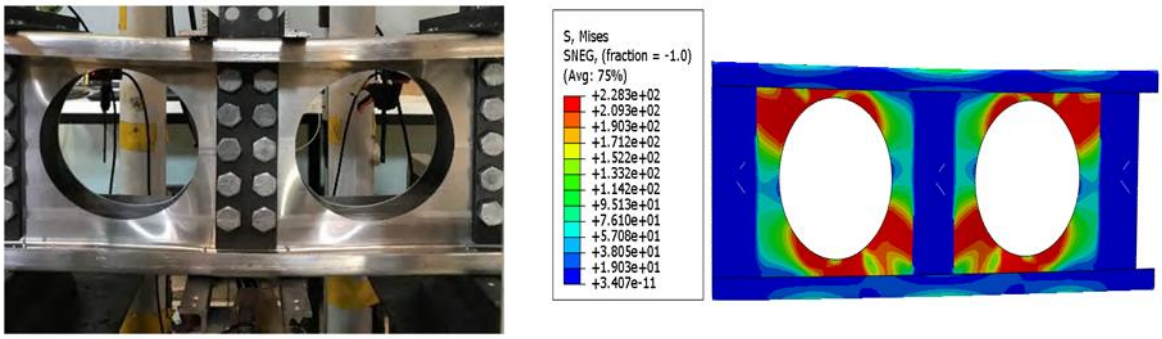

Fig: 13 CFA channels with unstiffened circular web hole [34]

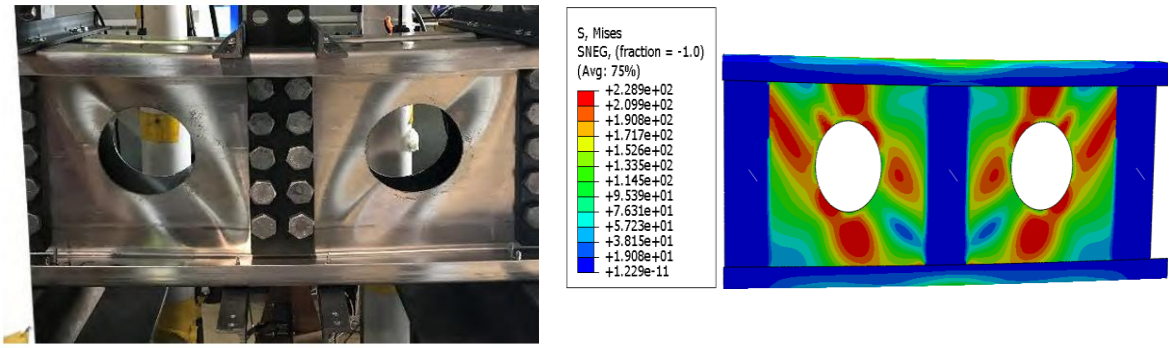

Fig: 14 CFA channels with unstiffened circular web hole [34].

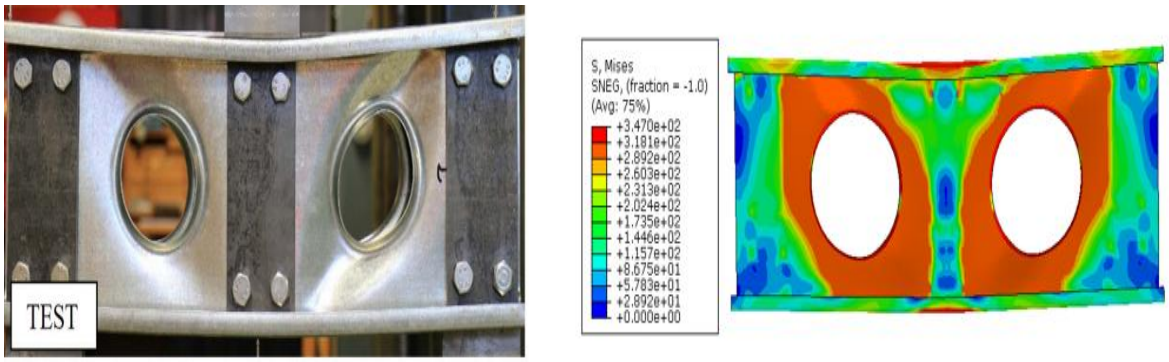

Fig: 15 CFS channels with stiffened circular web holes [34]

The validation of the finite element analysis (FEA) models was carried out by comparing predicted shear capacities with experimental results reported in the literature. Table 3 summarizes the comparison of shear strengths for a series of cold-formed aluminium (CFA) and cold-formed steel (CFS) specimens, highlighting the close agreement between experimental test values (VEXP) and FEA predictions (VFEA). For aluminium specimens tested by Rouholamin et al. and steel specimens tested by Chen et al., the mean ratio of FEA to test results was 0.987 and 1.07 respectively, with low coefficients of variation (0.07 and 0.03). This indicates that the developed FEA models can reliably capture the load-carrying

behaviour of members with circular web openings. A qualitative comparison of failure modes further supports the validity of the FEA model. Table 4 presents side-by-side comparisons of physical test setups with their corresponding FEA contour plots. The distribution of stresses and the initiation of local buckling around the web openings were closely reproduced in the numerical simulations, reflecting the same deformation patterns observed in the experimental specimens. The visual comparisons are extended in Fig: 13, Fig: 14 and Fig: 15, which present CFA and CFS channel sections with unstiffened and stiffened circular web holes. The experimental photographs (left) and the corresponding FEA contour plots (right) show very similar patterns of stress concentration around hole edges and progression of web buckling. For instance, in Fig: 13 and Fig: 14, unstiffened CFA channels displayed early web distortion and buckling at the hole periphery, a behaviour that was accurately replicated by the FEA simulations. Similarly, Fig: 15 shows that stiffened CFS channels exhibited delayed buckling and enhanced load-carrying capacity, again well captured by the FEA model. Together, the quantitative results (Table 3) and visual evidence (Table 4, Fig: 13, Fig: 14 and Fig: 15) confirm that the developed finite element framework is robust and capable of predicting not only the ultimate shear capacity but also the corresponding failure modes of perforated aluminium and steel sections.

4.8 Statistical Error Metrics for comparison

To validate the finite element analysis (FEA) results against experimental data, several statistical error metrics were employed. These include Mean Bias Error (MBE), Mean Absolute Error (MAE), Mean Squared Error (MSE), Root Mean Square Error (RMSE), Normalized Root Mean Square Error (NRMSE), Pearson Correlation Coefficient (PCC), and the Coefficient of Determination (R^2). The following section presents the theory, formulas, and interpretation for each metric.

Let $i = 1, \dots, n$ index paired results from experiment and prediction.

y_i : measured (experimental) value (e.g., V_{EXP} in kN)

$\hat{y}_i$: predicted value (e.g., V_{FEA} or design equation)

$e_i = y_i - \hat{y}_i$: residual (error)

$\bar{y} = \frac{1}{n}\sum_{i=1}^{n} y_i$: mean of measurements

$\overline{\hat{y}} = \frac{1}{n}\sum_{i=1}^{n} \hat{y}_i$: mean of predictions

All formulas below use these definitions.

4.8.1 Mean Bias Error (MBE)

MBE measures the average systematic error (bias) as per shown in Equation 1. Positive values indicate under-prediction, while negative values indicate over-prediction.

Formula:

$$\mathbf{MBE} = \frac{\mathbf{1}}{\boldsymbol{n}}\sum_{\boldsymbol{i=1}}^{\boldsymbol{n}} \boldsymbol{e_i} = \frac{\mathbf{1}}{\boldsymbol{n}}\sum_{\boldsymbol{i=1}}^{\boldsymbol{n}} (\boldsymbol{y_i} - \boldsymbol{\hat{y}_i})$$

Equation 1

4.8.2 Mean Absolute Error (MAE)

MAE gives the average magnitude of errors without considering direction as per shown in Equation 2. It is simple to interpret as the typical absolute deviation.

$$\mathrm{MAE} = \frac{1}{n}\sum_{i=1}^{n} |e_i|$$

Equation 2

4.8.3 Mean Squared Error (MSE)

MSE averages the squared errors, penalizing larger deviations more strongly as per shown in Equation 3.

$$\mathrm{MSE} = \frac{1}{n}\sum_{i=1}^{n} e_i^2$$

Equation 3

4.8.4 Root Mean Square Error (RMSE)

RMSE is the square root of MSE. It emphasizes larger errors and is expressed in the same units as the data as per shown in Equation 4.

$$\mathrm{RMSE} = \sqrt{\mathrm{MSE}} - \sqrt{\frac{1}{n}\sum_{i=1}^{n} (y_i - \hat{y}_i)^2}$$

Equation 4

Interpretation. Larger than (or equal to) MAE; emphasises big misses.

Units. Same as y.

Relationship. RMSE ≥ MAE with equality only if all $|e_i|$ are equal.

4.8.5 Normalized Root Mean Square Error (NRMSE)

NRMSE expresses RMSE as a percentage relative to a reference (mean, range, or standard deviation).

1. By mean of observations

$$\mathrm{NRMSE}_{\mu} = \frac{\mathrm{RMSE}}{\bar{y}} \times 100\%$$

Equation 5

2. By range of observations

$$\mathrm{NRMSE}_{\mathrm{range}} = \frac{\mathrm{RMSE}}{y_{\max} - y_{\min}} \times 100\%$$

Equation 6

3. By standard deviation of observations

$$\mathrm{NRMSE}_{\sigma} = \frac{\mathrm{RMSE}}{s_y} \times 100\%, s_y = \sqrt{\frac{1}{n-1}\sum_{i=1}^{n} (y_i - \bar{y})^2}$$

Equation 7

Interpretation. Smaller is better. Mean-based NRMSE_{μ} is common in structural mechanics; range-based works when the operating range is well defined; stdev-based reflects variability.

4.8.6 Pearson Correlation Coefficient (PCC)

PCC measures the linear correlation between measured and predicted values. It ranges from -1 (perfect negative) to +1 (perfect positive) as per shown in Equation 8.

$$r = \frac{\sum_{i=1}^{n} (y_i - \bar{y})\left(\hat{y}_i - \overline{\hat{y}}\right)}{\sqrt{\sum_{i=1}^{n} (y_i - \bar{y})^2}\sqrt{\sum_{i=1}^{n} \left(\hat{y}_i - \overline{\hat{y}}\right)^2}}$$

Equation 8

Range. -1 to +1. Values near +1 indicate very strong positive linear agreement.

Notes. High r does not guarantee small errors (a line can be well aligned but offset); always report with an error metric.

4.8.7 Coefficient of Determination (R^2)

R^2 shows the proportion of variance in measured values explained by predictions. Values close to 1 indicate excellent agreement as per shown in Equation 9.

$$R^2 = 1 - \frac{\mathrm{SS_{res}}}{\mathrm{SS_{tot}}}, \mathrm{SS_{res}} = \sum_{i=1}^{n} (y_i - \hat{y}_i)^2, \mathrm{SS_{tot}} = \sum_{i=1}^{n} (y_i - \bar{y})^2$$

Equation 9

Range. $(-\infty, 1]$. Values close to 1 indicate excellent agreement; negative values can occur when the model performs worse than using the mean $\bar{y}$.

Relationship. For simple linear fits with an intercept, $R^2 = r^2$. Without an intercept, this equivalence does not hold.

4.9 Comparison graph of CFA

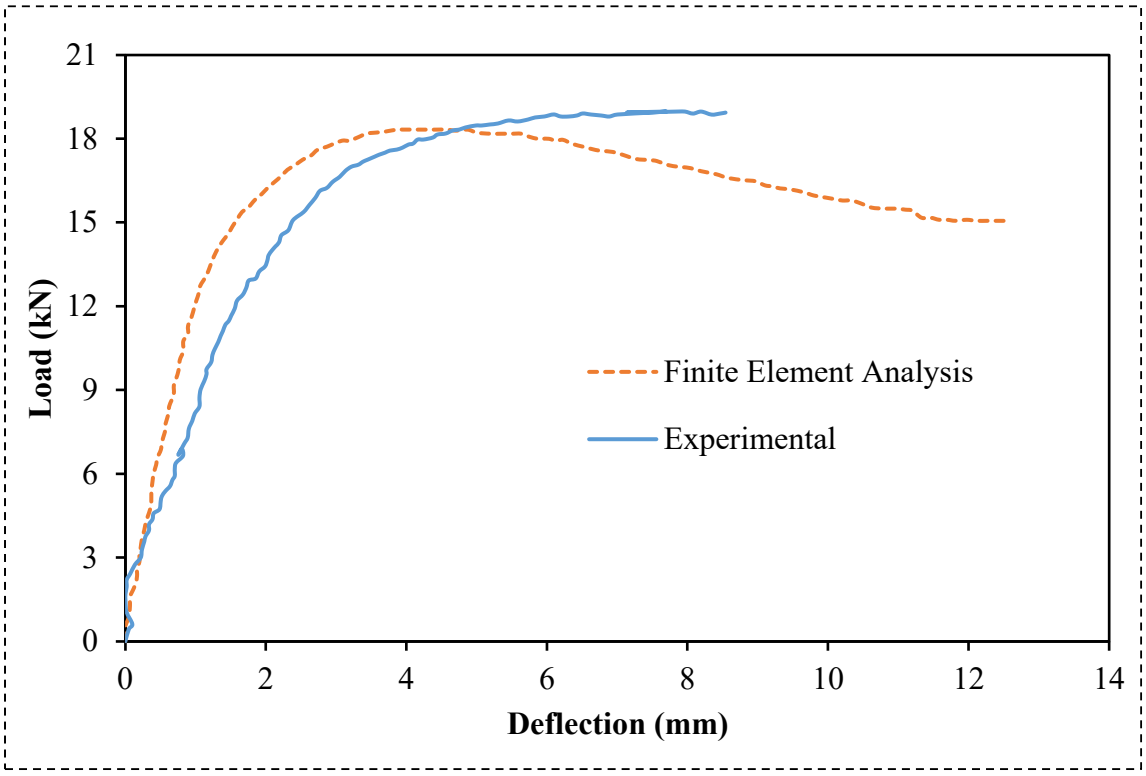

Fig: 16 Comparison of experiment and Finite element analysis.

The accuracy of the finite element analysis (FEA) models was assessed by comparing the predicted load–deflection responses with experimental results for both cold-formed aluminium (CFA) and cold-formed steel (CFS) channel sections. As shown in Fig: 16, the FEA curve for CFA follows the experimental trend closely, particularly in the elastic region, with only slight deviations in the post-yield stage where the simulation marginally underestimates stiffness at higher deflections. A similar consistency is observed in Fig: 17 for CFS specimens, where the

FEA predictions capture both the peak load and the overall shape of the load–displacement curve, although minor discrepancies appear in the descending branch due to simplifications in modelling imperfections and material nonlinearities. The quantitative assessment using statistical validation metrics further reinforces these observations (Table 4). For CFA, the error measures are relatively low (RMSE = 1.74, MAE = 1.19, MBE = 0.63) with a high Pearson correlation coefficient (PCC = 0.95), indicating excellent agreement between numerical and experimental results. Likewise, for CFS, the correlation is perfect (PCC = 1.00) with acceptable error values (RMSE = 2.97, MAE = 1.68, MBE = 1.68), reflecting the robustness of the developed FEA model. The coefficient of determination (R^2) values of 0.68 for CFA and 0.77 for CFS demonstrate that a significant proportion of the variance in experimental data is explained by the simulations. Overall, the combined graphical (Fig: 16 & Fig: 17) and statistical (Table 5) evidence validates the reliability of the FEA models for predicting shear behaviour and load–deflection characteristics of perforated channel sections.

4.10 *Comparison graph of CFS*

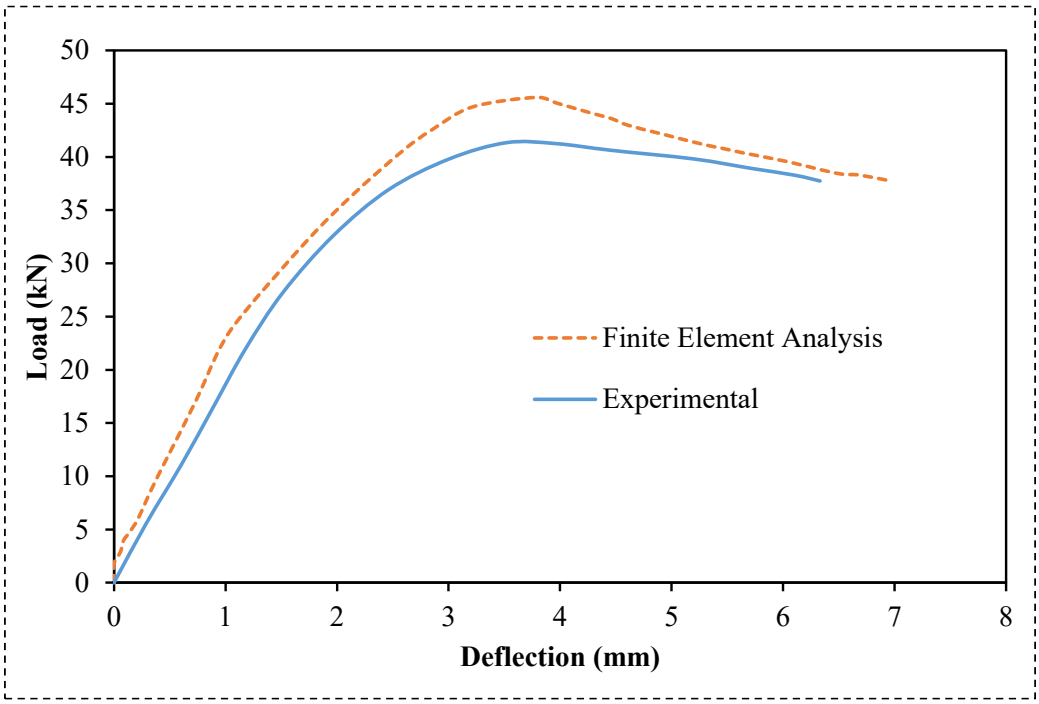

Fig: 17 Comparison of load-displacement curves for the specimen.

Table 5 Statistical Validation Metrics for Experimental test and FEM Results.

	RMSE	MSE	MAE	MBE	R^2	NRMSE	PCC

CFA	1.74	1.74	1.19	0.63	0.68	0.09	0.95
CFS	2.97	2.97	1.68	1.68	0.77	0.07	1.00

RMSE (Root Mean Square Error), MSE (Mean Square Error), MAE (Mean Absolute Error), MBE (Mean Bias Error), R^2 (Coefficient of Determination), NRMSE (Normalized Root Mean Square Error), and PCC (Pearson Correlation Coefficient).

Chapter 5. Parametric study

5.1 Parametric design

Stiffening Loop Effect An extensive parametric study to investigate how the geometric parameters, material grades, and stiffening configurations affect the shear performance of cold-formed aluminium (CFA) channel sections was performed on the verified finite element (FE) models after comparing them with the experimental results by Rouholamin and et al. and Chen and et al. This analysis was conducted in order to produce an all-inclusive data that could sufficiently state interaction effects based on hole shape and length of metal stiffeners, the thickness of the member section and the type of alloy used in producing the member and along this line the experiment provided a higher guide to a better design ideal of an aluminium member with a perforated web.

An analysis of numerous FE models was undertaken and three web designs (plain webs, unstiffened circular web holes (CUH), circular web holes reinforced with edge stiffeners (CEH)) were investigated. Two section sizes have been studied namely C250x 75x 25 mm and C400x 125x 30 mm which was modelled again using four different web thicknesses that are 2.0 mm, 2.5 mm, 3.0 mm and 3.5 mm (see Table 6). Hole depth-to-web depth ratio (dw/d1) varied by 0.2, 0.3, 0.4, 0.5, and 0.6 and stiffener length, to- web depth ratio (q/d 1) was 0.04, 0.06, and 0.08. In the case of stiffened holes, the radius of bend between the web flat and stiffener (Rq) was kept constant (=4 mm). The ratio between the hole length and the hole depth (bw/dw) was kept within 2 to 3 ratio to reflect the practicable proportions of the fabrication (see Table 6).

The study has taken into consideration two of the more commonly utilized structural grades of aluminium; H36, a 5052 structural grade (yield strength of 232 MPa and ultimate tensile strength of 272 MPa) and H38, also a 5052 structural grade (this one with a yield of 250 MPa and an ultimate tensile strength of 300 MPa). The nonlinear stress-strain behaviour was used to model both these materials according to ISO 6892-1 (2009), allowing realistic simulation of elastic plastic as well strain-hardening behaviour [22].

This parametric study measured the loss of capacity due to web holes of various sprung and the recuperation of strength by edge stiffeners, the impact of thickness, grade and web depth on performance. The results give a clear criterion of finding of critical hole dimensions where stiffening is necessary and give a reason to come up with modified shear reduction factors specific to aluminium members.

The specimens used for the parametric study were labelled such that the web depth, thickness, web hole depth ratio, web hole length ratio, stiffener length ratio, and inner bent radius between the web and stiffener were defined. Table 6 illustrates the labelling of the investigated channel sections in the parametric study. For example, the label "C250-T1-D0.3 can be explained as given below.

• "C250" indicates the depth of the section in millimetres i.e., d = 240 mm.

• "T3" defines the thickness of the section in millimetres i.e., t = 3 mm.

• "D0.3" refers to the hole depth to web depth ratio (dw/d1) i.e., dw/d1 = 0.3.

The parametric study systematically examined the effect of section thickness, hole geometry, and stiffener length on the shear strength of CFA channel sections, with results presented in Table 7, Table 8, Table 9, Table 10, Table 11, Table 12, Table 13 and Table 14. For thin sections (2.0 mm), as shown in Table 7, the introduction of circular unstiffened web holes (CUH) significantly reduced shear capacity compared to plain webs, while edge stiffeners (CEH) effectively restored part of the lost strength, particularly at higher stiffener lengths (S = 15). Similar trends were observed for 2.5 mm sections (Table 8), where CEH specimens consistently showed higher shear strengths than CUH, with improvements more pronounced in deeper sections (C400). As thickness increased to 3.0 mm (Table 9) and 3.5 mm (Table 10), overall shear strength improved substantially, with the H38 alloy outperforming H36 due to its higher yield stress. The role of stiffeners remained important, especially for larger hole depth ratios (D0.5–D0.6), where unstiffened webs suffered severe capacity reduction. Complementary results for purely unstiffened cases are summarized in Table 11, Table 12, Table 13 and Table 14, which reinforce that hole presence alone leads to up to 60% reduction in shear strength, depending on hole depth ratio and web thickness. Across all thicknesses, plain web sections always exhibited the highest capacity, followed by CEH and then CUH specimens, while the beneficial effect of stiffeners increased with thickness and hole size. Collectively, these results confirm that web stiffening is an effective strategy to mitigate strength losses from service holes and highlight the combined influence of thickness, alloy grade, and stiffener configuration on shear performance. The parametric ranges were selected to reflect realistic fabrication limits and commonly used aluminium grades. Section sizes (C250 and C400), thicknesses (2.0–3.5 mm), and alloys (H36 and H38) were chosen to represent practical construction applications. Hole depth ratios (0.2–0.6) and stiffener length ratios (0.04–0.08) were varied to capture typical service hole geometries and stiffening practices, while keeping other parameters (e.g., bend radius, hole aspect ratio) within fabrication standards. These ranges ensure that the study not only covers extreme conditions but also

remains relevant to real-world design scenarios, providing meaningful insights into shear performance and code development.

Table 6 Parameters chosen in this study

Section (mm*mm*mm)	**Grade Fy (MPa)**	**Thickness (t) (mm)**	**Aspect ratio A. R**	**Hole depth /web depth dw/d**	**Hole length/web depth bw/dw**	**stiffener length/web depth q/d**	**Type of holes**
Edge-stiffened web holes							
C250x75x25 C400x125x30	H-36 (5052) H-38 (5052)	2,2.5, 3 and 3.5	1.0	0.2,0.3,0.4,0.5 and 0.6	-	0.04, 0.06 and 0.08	Circular
Unstiffened web holes							
C250x75x25 C400x125x30	H-36 (5052) H-38 (5052)	2,2.5, 3 and 3.5	1.0	0.2,0.3,0.4,0.5 and 0.6	-	-	Circular
Plain webs							
250x75x25 C400x125x30	H-36 (5052) H-38 (5052)	2,2.5, 3 and 3.5	1.0	-	-	-	No holes

5.2 Shear strength obtained from the parametric study for thickness 2 mm

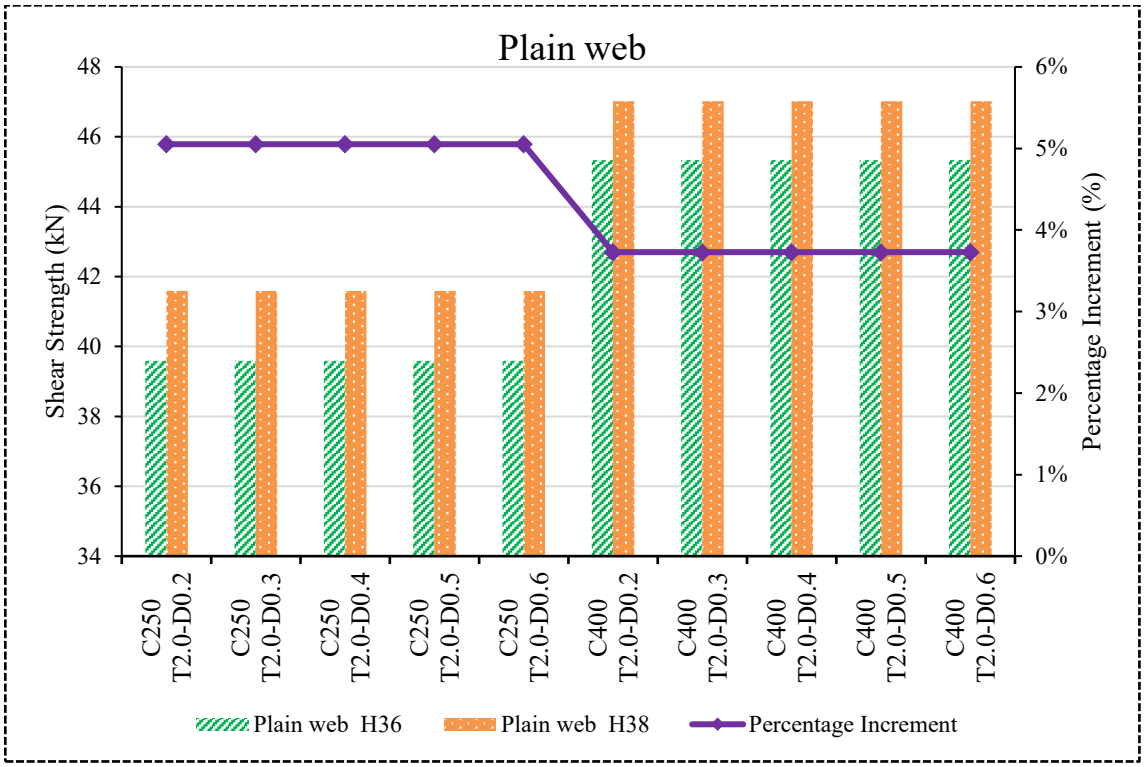

Fig: 18 Shear capacity of plain web aluminium sections (stiffened) at 2.0 mm thickness.

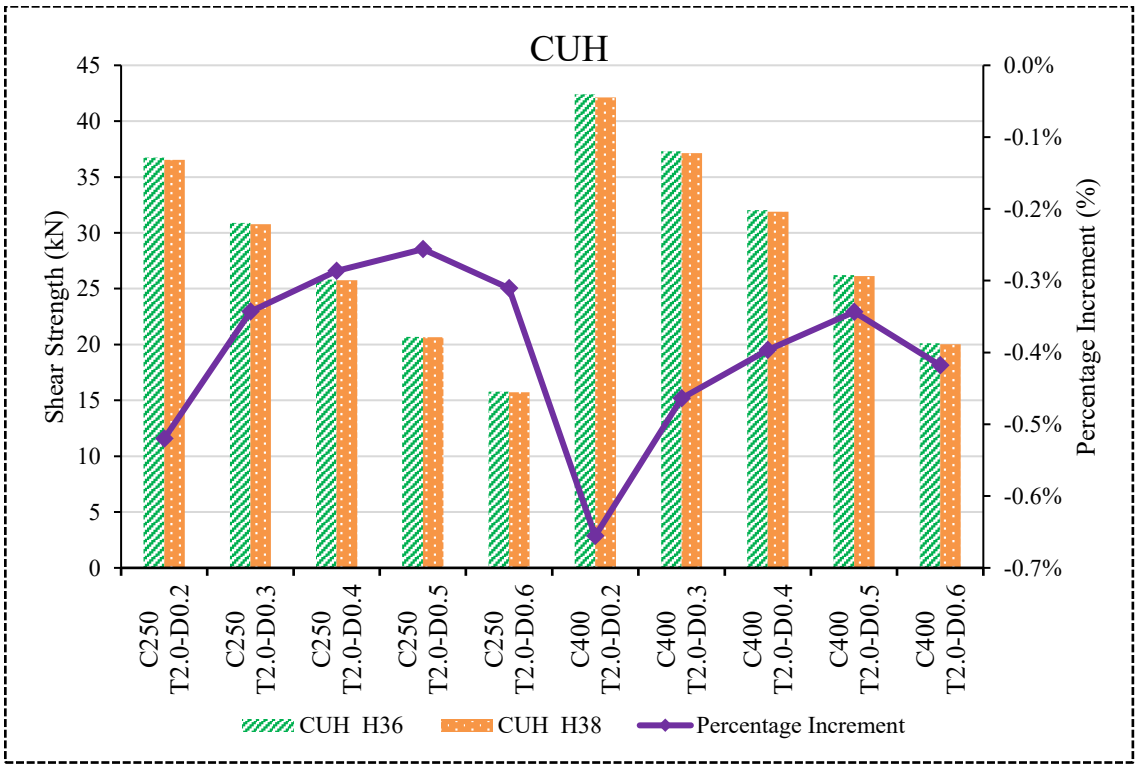

Fig: 19 Shear capacity of CUH aluminium sections (stiffened) at 2.0 mm thickness.

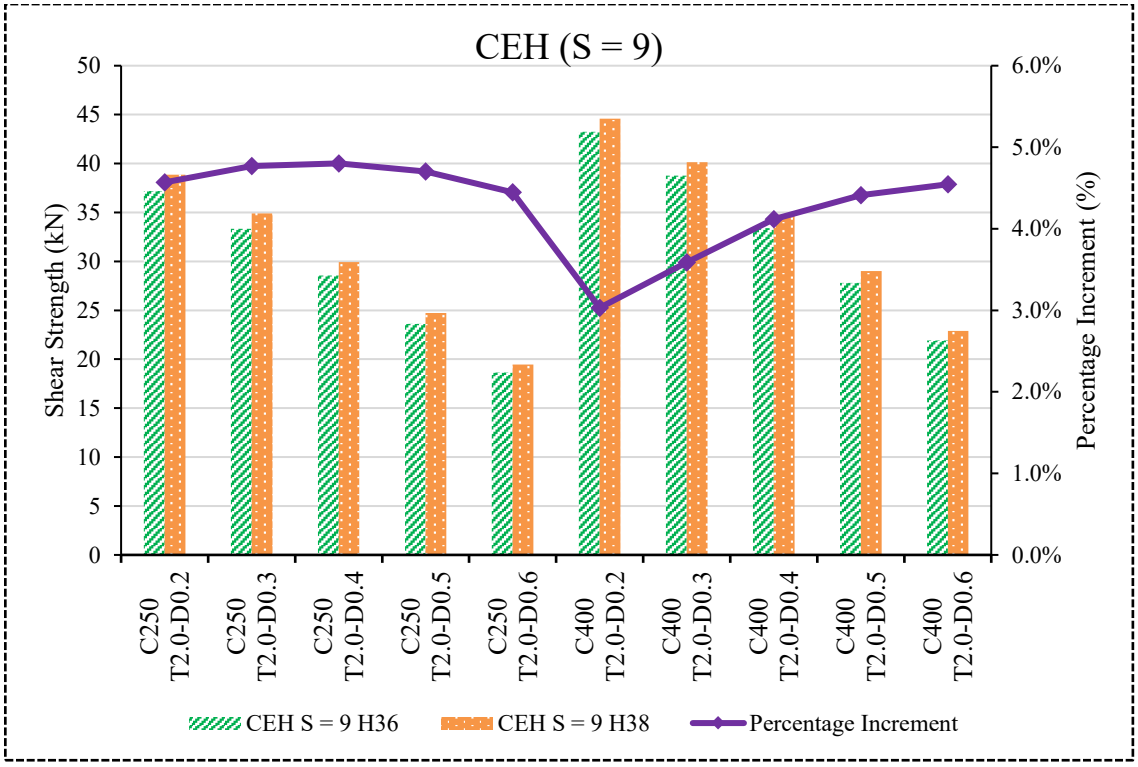

Fig: 20 Shear capacity of CEH (S=9) aluminium sections (stiffened) at 2.0 mm thickness.

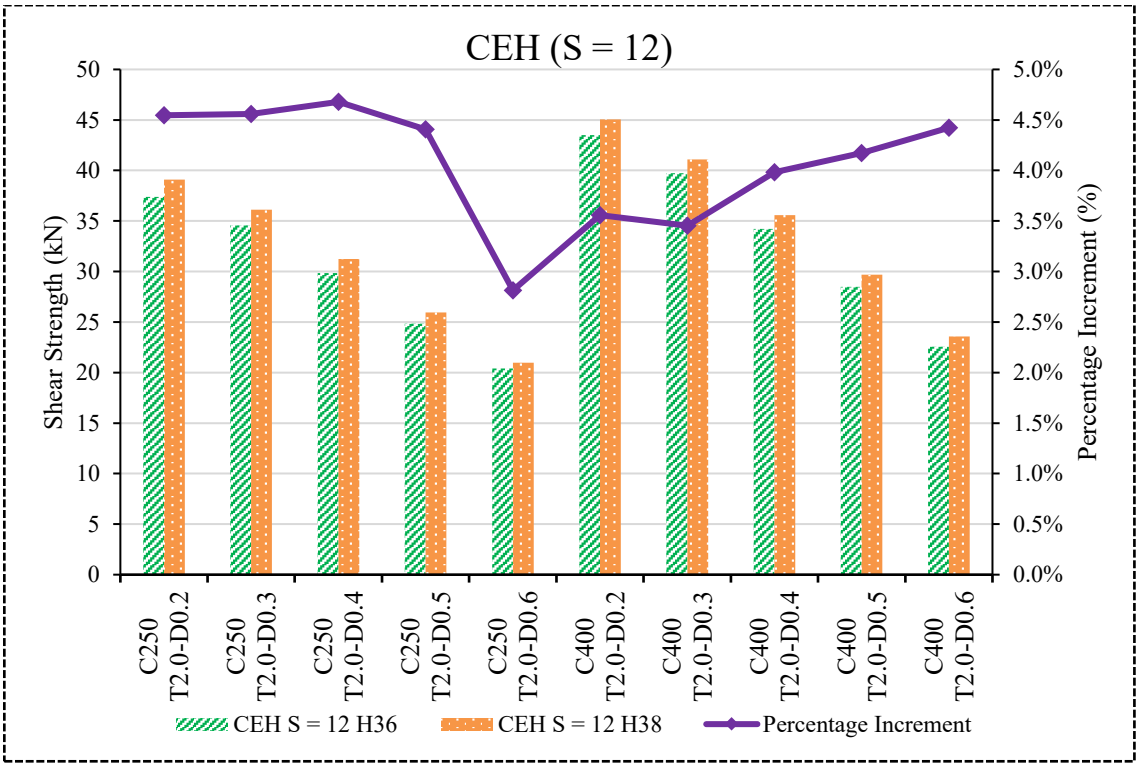

Fig: 21 Shear capacity of CEH (S=12) aluminium sections (stiffened) at 2.0 mm thickness.

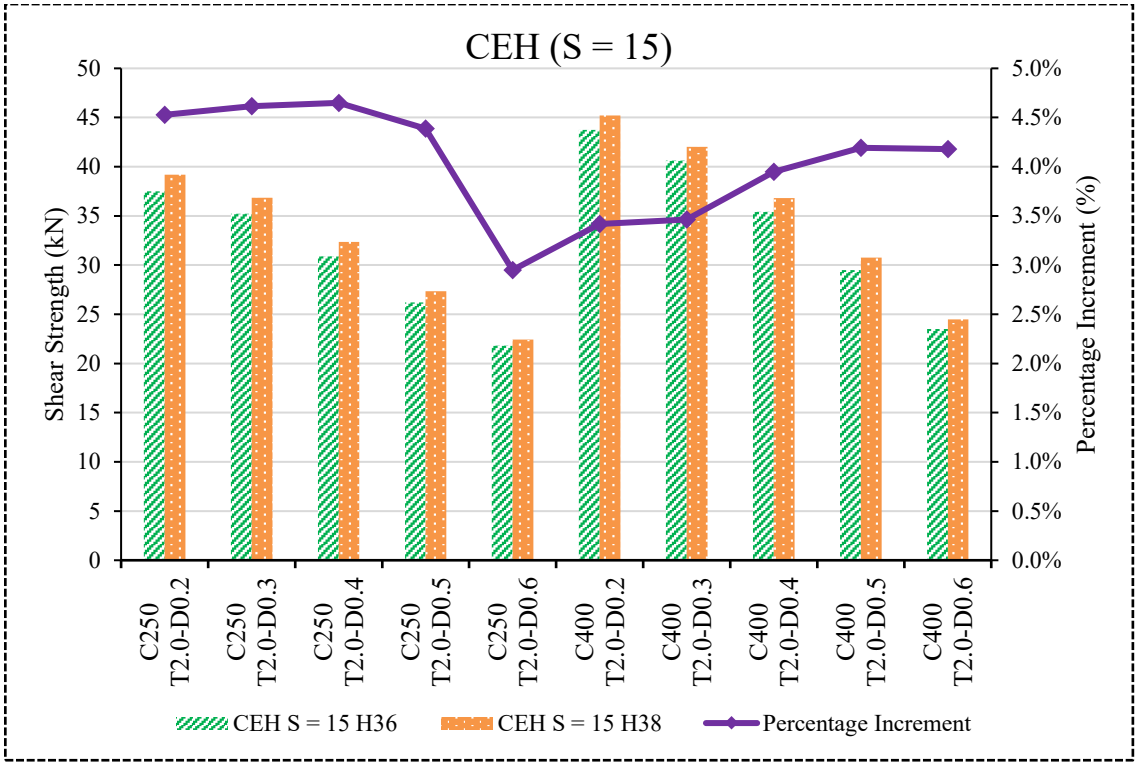

Fig: 22 Shear capacity of CEH (S=15) aluminium sections (stiffened) at 2.0 mm thickness.

For the 2 mm thickness case, the results of shear strength for plain web, unstiffened (CUH), and stiffened (CEH) specimens with varying stiffener lengths are presented in (Fig: 18, Fig: 19, Fig: 20, Fig: 21, & Fig: 22). As shown in Fig: 18, plain web sections provide the baseline, with H38 consistently outperforming H36 by about 5% (C250) and 3.7% (C400) across all hole ratios, reflecting the effect of higher yield strength. When unstiffened holes were introduced (Fig:13-32), shear strength reduced sharply, and the percentage increment of H38 over H36 became almost negligible or slightly negative (–0.2% to –0.6%), indicating that unstiffened holes eliminate the alloy advantage. The introduction of stiffened holes (CEH) significantly improved performance (Fig: 20,Fig: 21, & Fig: 22), where H38 recovered its advantage with ~4.4–4.8% higher strength than H36 across stiffener lengths S = 9, 12, and 15. The recovery trend was consistent for both C250 and C400 webs, and the effect of increasing stiffener length was positive, with S = 15 showing the highest recovery. Overall, these results demonstrate that while unstiffened holes degrade capacity and neutralize material benefits, stiffeners not only restore part of the lost strength but also re-establish the superior performance of H38 alloy, with the highest gains observed at longer stiffener lengths.

Table 7 Shear strength obtained from the parametric study for thickness 2 mm.

Specimen	Shear strength for circular web holes, VFEA (kN)									
	H36					H38				
	Plain web (kN)	CUH (kN)	CEH S = 9 (mm)	CEH S = 12 (mm)	CEH S = 15 (mm)	Plain web (kN)	CUH (kN)	CEH S = 9 (mm)	CEH S = 12 (mm)	CEH S = 15 (mm)
C250-T2.0-D0.2	39.59	36.734	37.175	37.393	37.498	41.59	36.543	38.873	39.093	39.196
C250-T2.0-D0.3	39.59	30.881	33.322	34.557	35.213	41.59	30.775	34.911	36.133	36.838
C250-T2.0-D0.4	39.59	25.826	28.552	29.836	30.908	41.59	25.752	29.923	31.232	32.345
C250-T2.0-D0.5	39.59	20.695	23.614	24.851	26.194	41.59	20.642	24.724	25.946	27.343
C250-T2.0-D0.6	39.59	15.78	18.626	20.399	21.8	41.59	15.731	19.454	20.973	22.443
C400-T2.0-D0.2	45.33	42.402	43.258	43.495	43.732	47.02	42.124	44.569	45.042	45.227
C400-T2.0-D0.3	45.33	37.306	38.755	39.731	40.611	47.02	37.133	40.145	41.103	42.018
C400-T2.0-D0.4	45.33	32.029	33.38	34.213	35.41	47.02	31.902	34.755	35.576	36.808
C400-T2.0-D0.5	45.33	26.218	27.788	28.487	29.51	47.02	26.128	29.014	29.676	30.747
C400-T2.0-D0.6	45.33	20.106	21.897	22.564	23.516	47.02	20.022	22.892	23.562	24.499

5.3 Shear strength obtained from the parametric study for thickness 2.5 mm

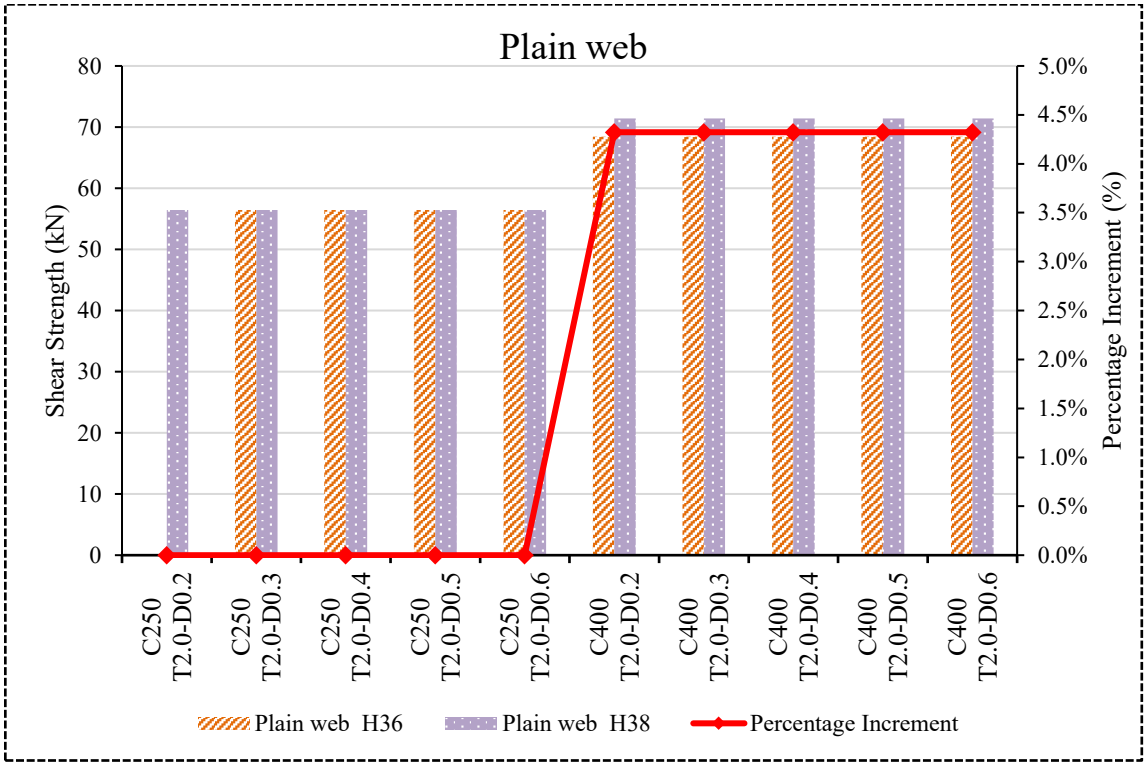

Fig: 23 Shear capacity of plain web aluminium sections (stiffened) at 2.5 mm thickness.

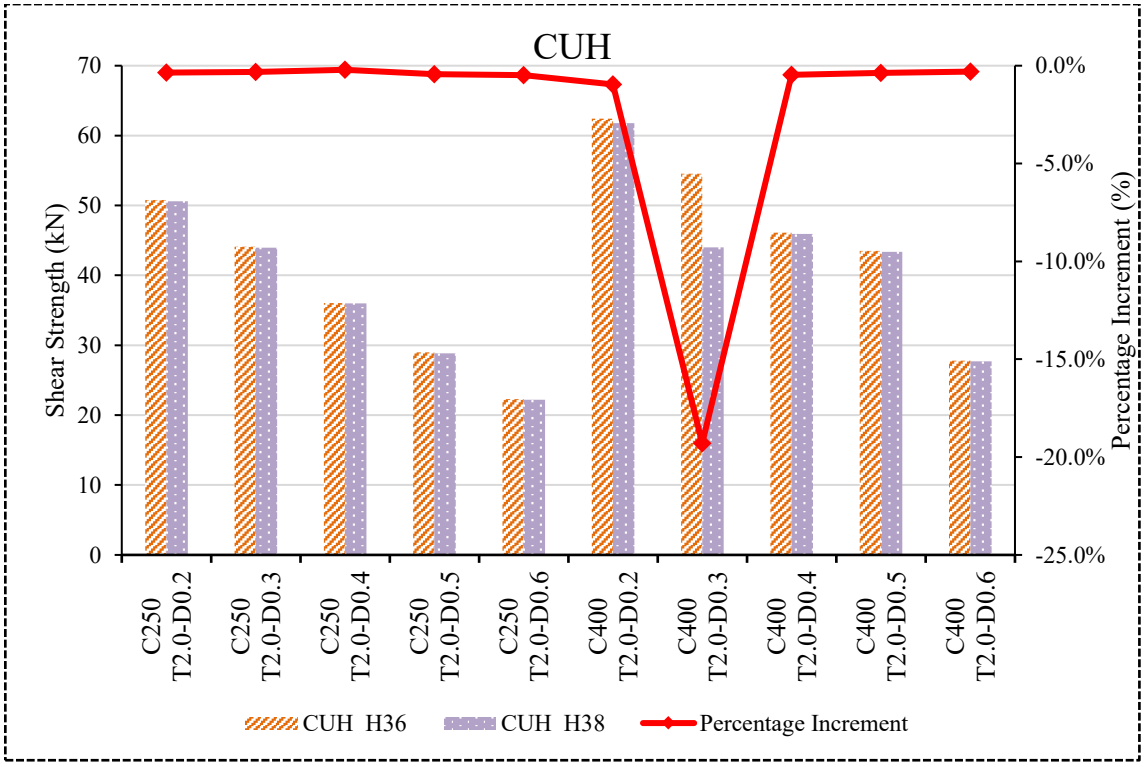

Fig: 24 Shear capacity of CUH aluminium sections (stiffened) at 2.5 mm thickness.

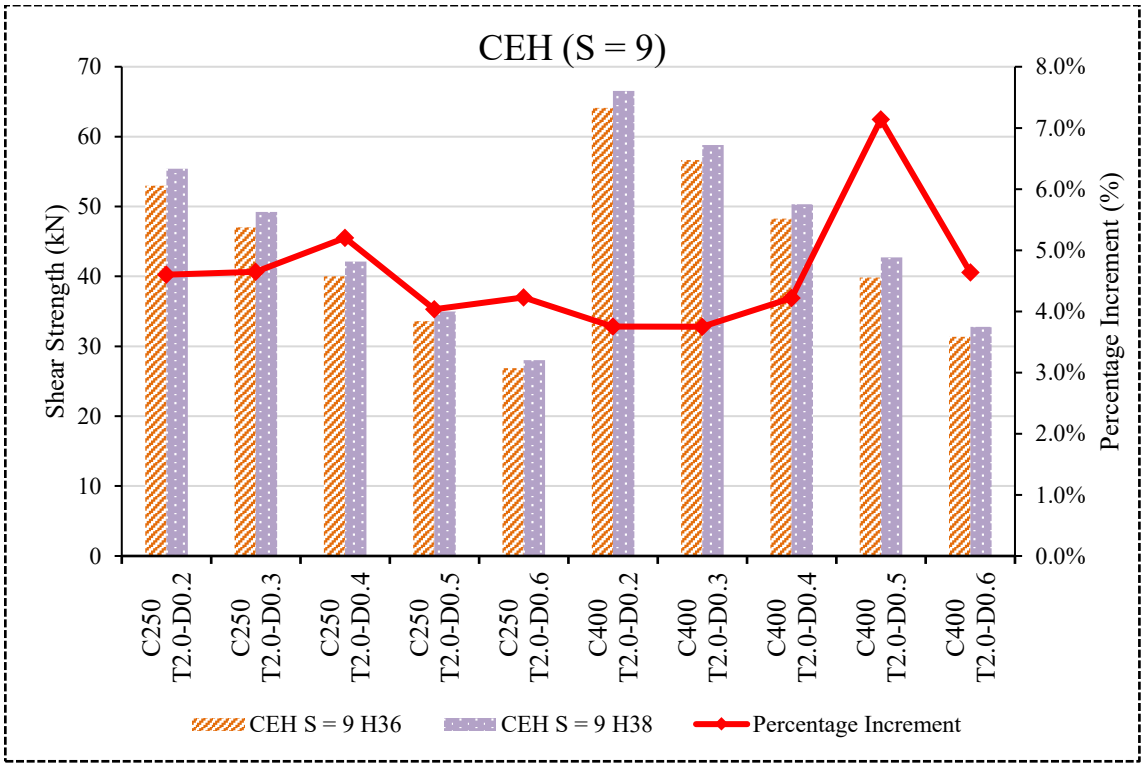

Fig: 25 Shear capacity of CEH (S=9) aluminium sections (stiffened) at 2.5 mm thickness.

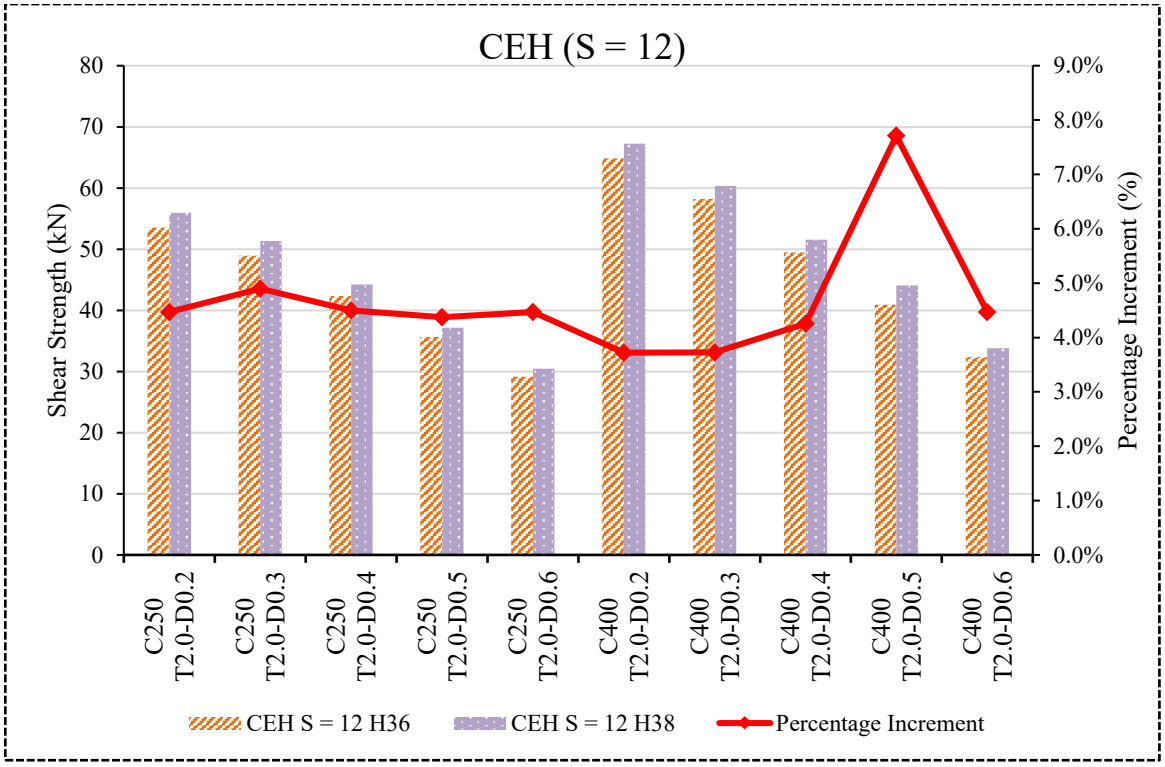

Fig: 26 Shear capacity of CEH (S=12) aluminium sections (stiffened) at 2.5 mm thickness.

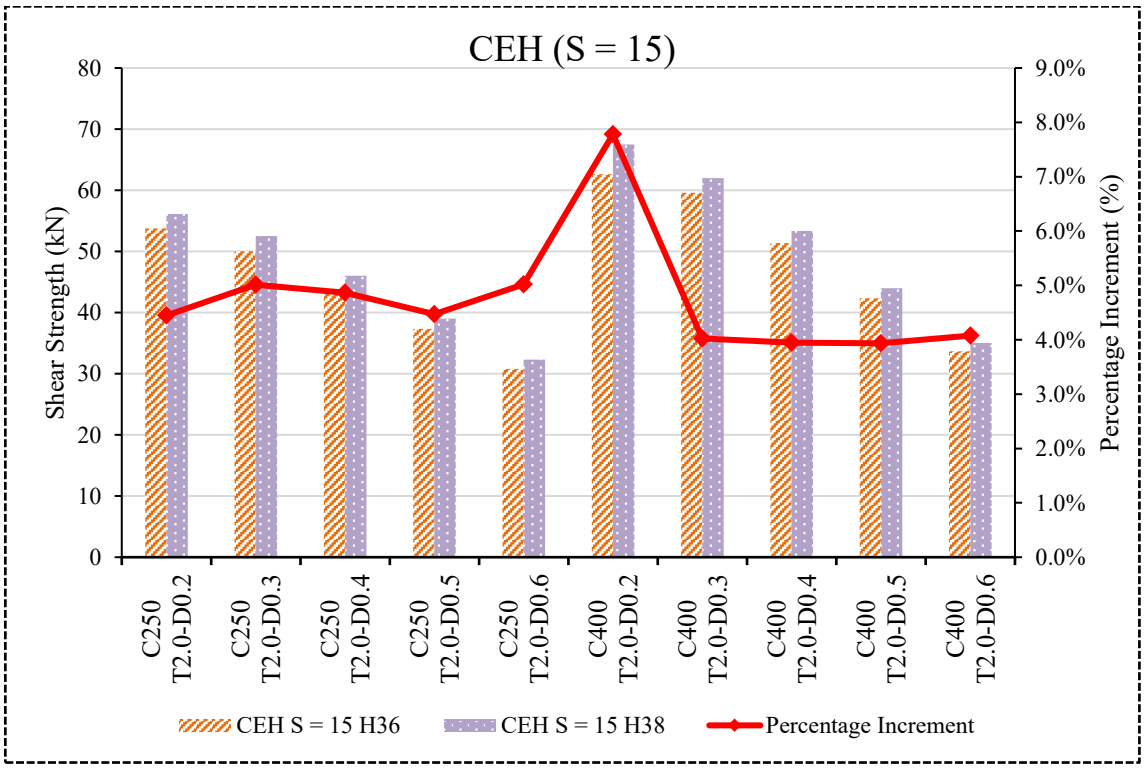

Fig: 27 Shear capacity of CEH (S=15) aluminium sections (stiffened) at 2.5 mm thickness.

For the 2.5 mm thickness specimens, the shear strength behaviour is summarized in Fig: 23, Fig: 24, Fig: 25, Fig: 26, & Fig: 27. As seen in Fig: 23, plain web sections show consistent results, with H38 generally higher than H36 by about 4–5% for C400 and nearly negligible difference (0%) for C250, reflecting the stabilizing influence of increased thickness. The introduction of unstiffened holes Fig: 24 caused a significant reduction in strength, with percentage differences turning slightly negative (–0.2% to –0.9%), and even more severe in the C400-T2.5-D0.3 case, where H38 dropped almost 19% below H36, showing a sensitivity to hole depth. With stiffened holes (Fig: 23, Fig: 24, Fig: 25, Fig: 26, & Fig: 27), performance improved substantially: H38 regained its advantage with ~4–5% higher capacity than H36 for most specimens, and in some cases (e.g., C400-T2.5-D0.5) the increment reached over 7% recovery at S=12. Increasing stiffener length from S=9 to S=15 generally enhanced recovery, particularly for deeper holes, highlighting the effectiveness of stiffeners in restoring the lost strength and re-establishing alloy benefits.

Table 8 Shear strength obtained from the parametric study for thickness 2.5 mm.

Specimen	Shear strength for circular web holes, VFEA (kN)									
	H36					H38				
	Plain web (kN)	CUH (kN)	CEH S = 9 (mm)	CEH S = 12 (mm)	CEH S = 15 (mm)	Plain web (kN)	CUH (kN)	CEH S = 9 (mm)	CEH S = 12 (mm)	CEH S = 15 (mm)
C250-T2.5-D0.2	56.45	50.774	52.993	53.535	53.76	56.45	50.595	55.432	55.927	56.151
C250-T2.5-D0.3	56.45	44.112	47.038	48.954	50.004	56.45	43.968	49.223	51.351	52.51
C250-T2.5-D0.4	56.45	36.058	40.038	42.323	43.895	56.45	35.982	42.12	44.227	46.032
C250-T2.5-D0.5	56.45	28.982	33.618	35.609	37.328	56.45	28.858	34.974	37.167	38.998
C250-T2.5-D0.6	56.45	22.309	26.896	29.14	30.785	56.45	22.202	28.033	30.442	32.33
C400-T2.5-D0.2	68.43	62.397	64.122	64.854	62.599	71.388	61.797	66.528	67.267	67.469
C400-T2.5-D0.3	68.43	54.519	56.657	58.171	59.595	71.388	44.002	58.781	60.339	61.993
C400-T2.5-D0.4	68.43	46.131	48.288	49.438	51.343	71.388	45.914	50.326	51.542	53.37
C400-T2.5-D0.5	68.43	43.51	39.859	40.919	42.341	71.388	43.347	42,705	44.074	44.007
C400-T2.5-D0.6	68.43	27.788	31.343	32.356	33.678	71.388	27.705	32.797	33.801	35.051

5.4 Shear strength obtained from the parametric study for thickness 3 mm

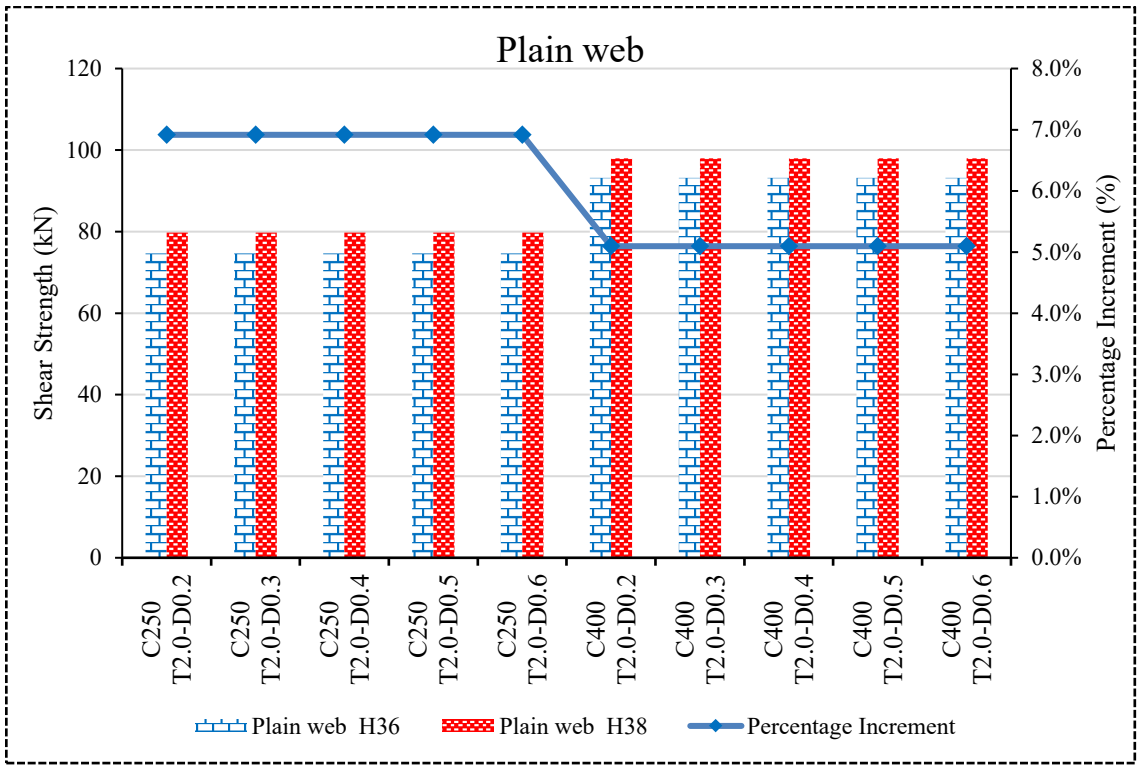

Fig: 28 Shear capacity of plain web aluminium sections (stiffened) at 3 mm thickness.

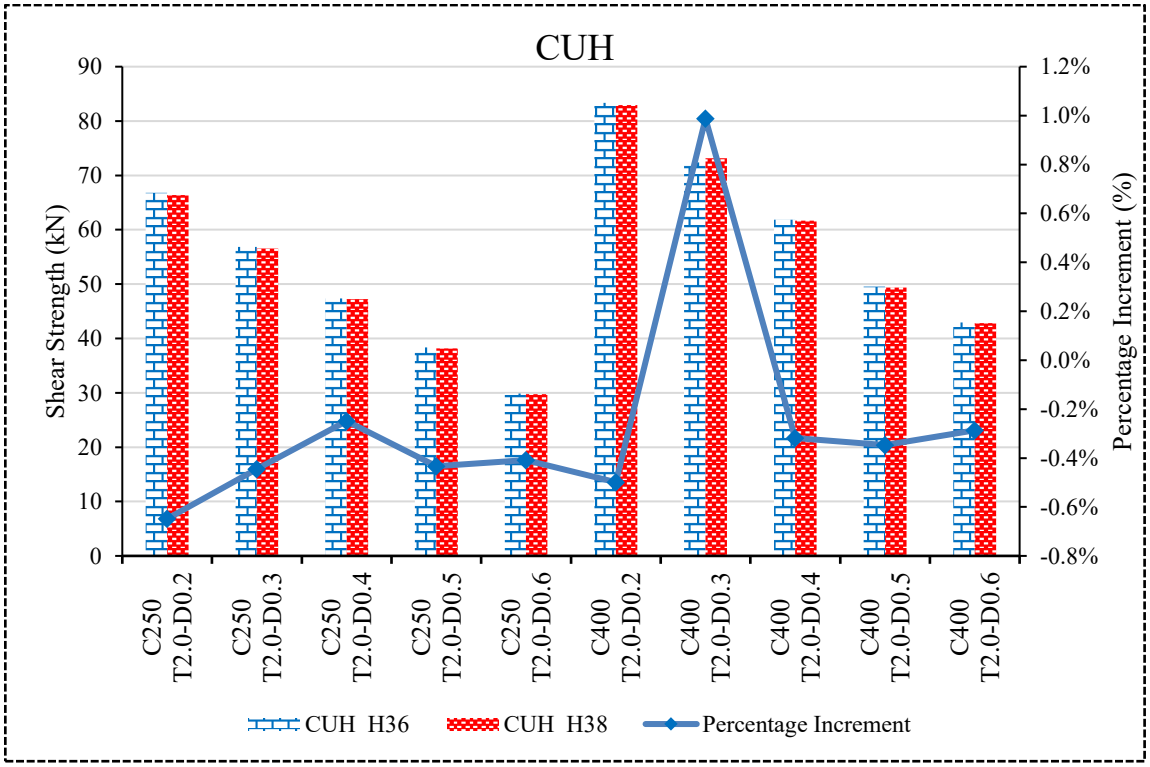

Fig: 29 Shear capacity of CUH aluminium sections (stiffened) at 3 mm thickness.

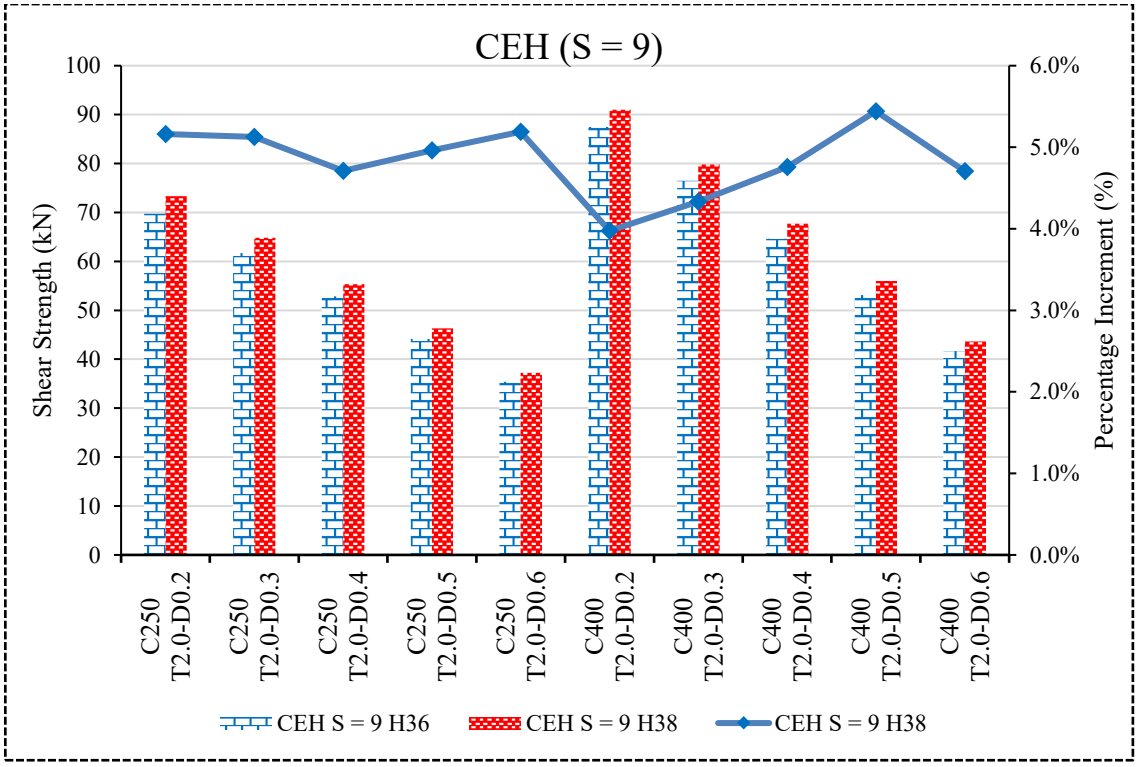

Fig: 30 Shear capacity of CEH (S=9) aluminium sections (stiffened) at 3 mm thickness.

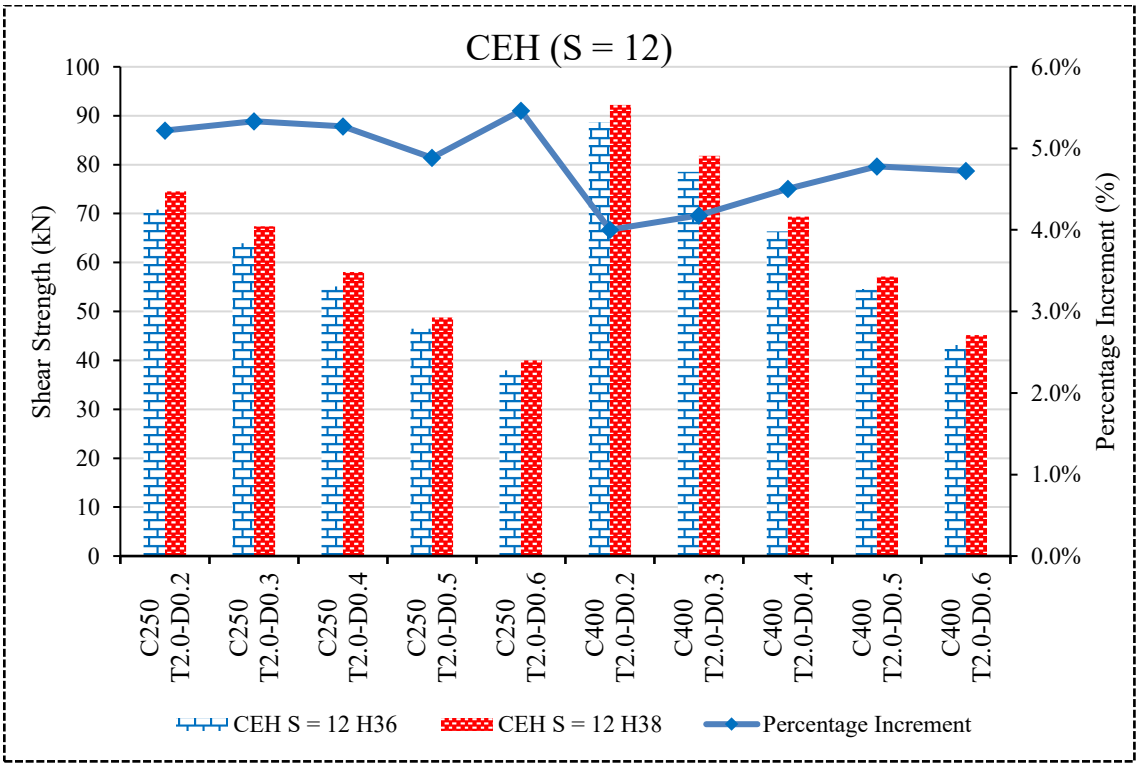

Fig: 31 Shear capacity of CEH (S=12) aluminium sections (stiffened) at 3 mm thickness.

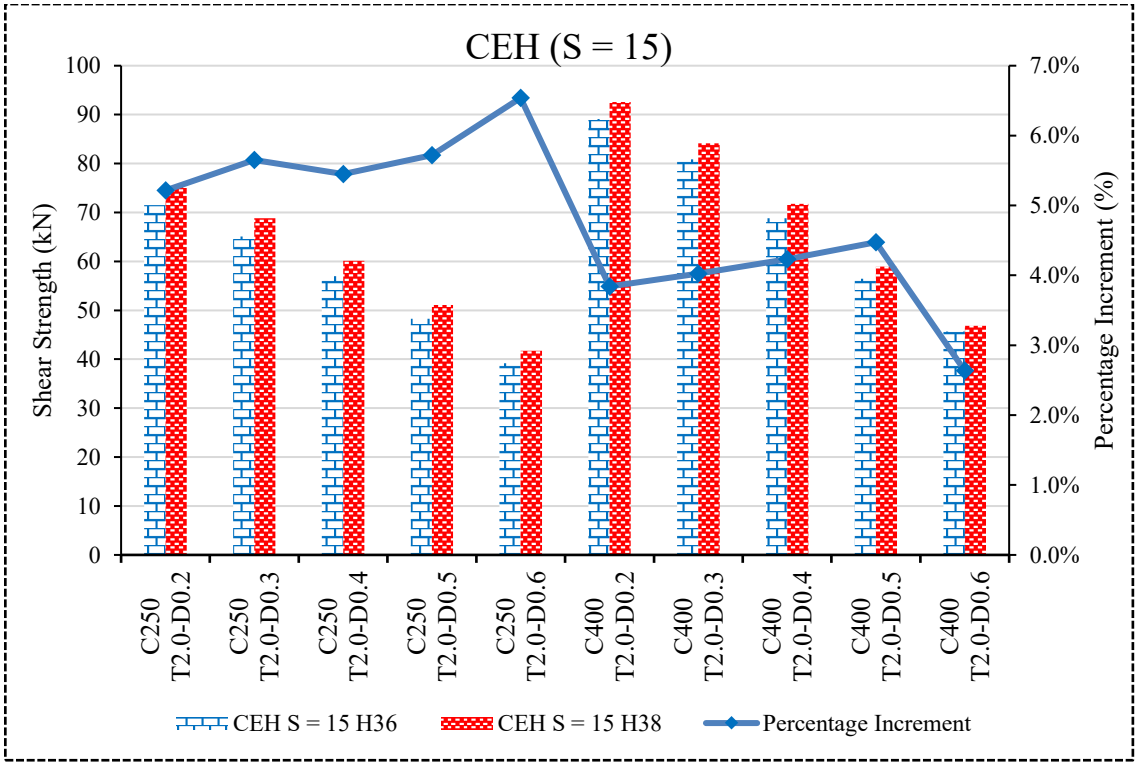

Fig: 32 Shear capacity of CEH (S=15) aluminium sections (stiffened) at 3 mm thickness.

For the 3.0 mm specimens, the comparative shear capacities are presented in Fig: 28, Fig: 29, Fig: 30, Fig: 31, &Fig: 32. As illustrated in Fig: 28, plain web sections consistently showed that H38 outperformed H36, with increments of about 6.9% for C250 and ~5% for C400, highlighting the strengthening influence of alloy grade at this thickness. The introduction of unstiffened holes (Fig: 29) again reduced shear capacity substantially, and the percentage increment between alloys nearly disappeared, with values close to zero or slightly negative (–0.2% to –0.6%), showing that unstiffened openings nullify the advantage of higher yield strength. When stiffeners were applied (Fig: 28, Fig: 29, Fig: 30, Fig: 31, &Fig: 32), performance improved considerably, and H38 regained its benefit, with percentage increments generally in the range of ~4–6% across stiffener lengths. Recovery was particularly strong for C250 specimens with deeper holes (e.g., D0.6), where increments reached over 6.5% at S = 15. For C400 webs, recovery trends were steady though slightly lower, with increments around 4–5%. Overall, stiffened holes at 3.0 mm thickness not only restored the lost strength but consistently reinforced the alloy advantage of H38, especially for deeper web openings and longer stiffeners.

Table 9 Shear strength obtained from the parametric study for thickness 3 mm.

Specimen	Shear strength for circular web holes, VFEA (kN)									
	H36					H38				
	Plain web (kN)	CUH (kN)	CEH S = 9 (mm)	CEH S = 12 (mm)	CEH S = 15 (mm)	Plain web (kN)	CUH (kN)	CEH S = 9 (mm)	CEH S = 12 (mm)	CEH S = 15 (mm)
C250-T3.0-D0.2	74.62	66.797	69.71	70.821	71.497	79.781	66.364	73.308	74.516	75.227
C250-T3.0-D0.3	74.62	56.824	61.669	63.974	65.111	79.781	56.571	64.831	67.386	68.79
C250-T3.0-D0.4	74.62	47.346	52.862	55.13	56.993	79.781	47.228	55.351	58.035	60.098
C250-T3.0-D0.5	74.62	38.325	44.125	46.485	48.305	79.781	38.159	46.315	48.756	51.068
C250-T3.0-D0.6	74.62	29.854	35.408	37.948	39.182	79.781	29.732	37.246	40.021	41.744
C400-T3.0-D0.2	93.19	83.349	87.493	88.655	89.137	97.938	82.933	90.971	92.203	92.56
C400-T3.0-D0.3	93.19	72.419	76.494	78.553	80.88	97.938	73.134	79.809	81.835	84.135
C400-T3.0-D0.4	93.19	61.871	64.656	66.358	68.833	97.938	61.674	67.731	69.346	71.745
C400-T3.0-D0.5	93.19	49.554	53.11	54.56	56.438	97.938	49.382	56	57.168	58.963
C400-T3.0-D0.6	93.19	42.935	41.67	43.13	45.637	97.938	42.812	43.631	45.167	46.84

5.5 Shear strength obtained from the parametric study for thickness 3.5 mm

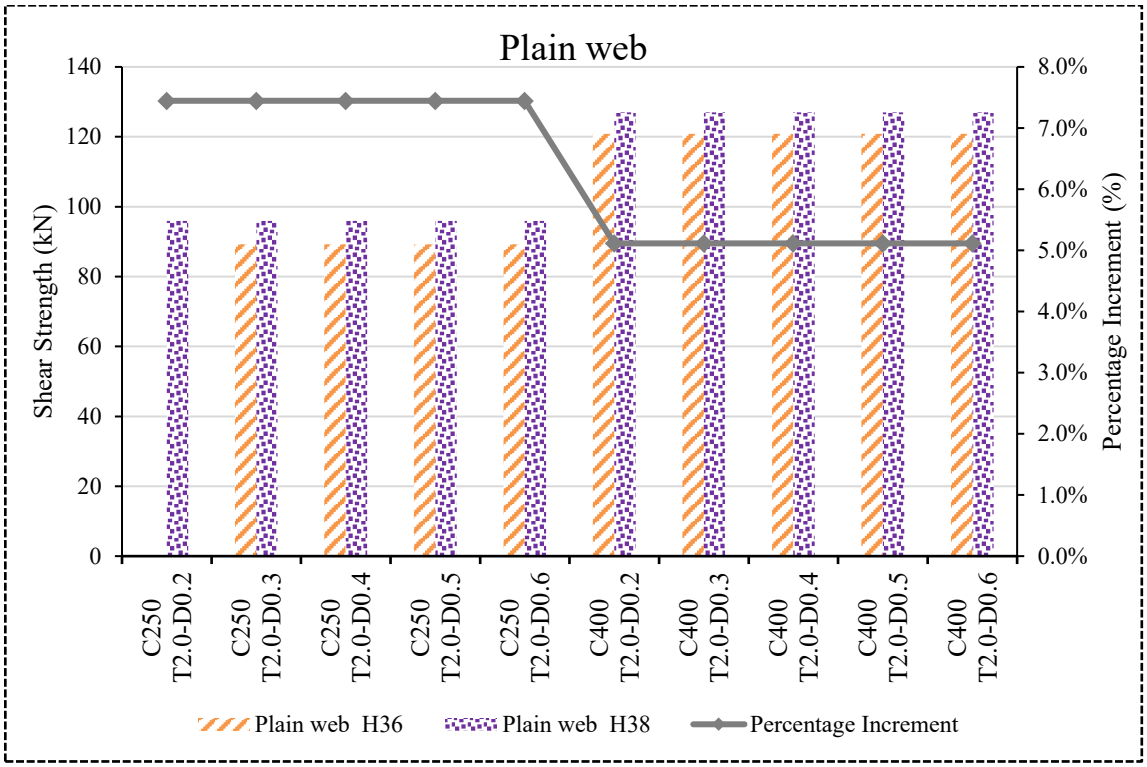

Fig: 33 Shear capacity of plain web aluminium sections (stiffened) at 3.5 mm thickness.

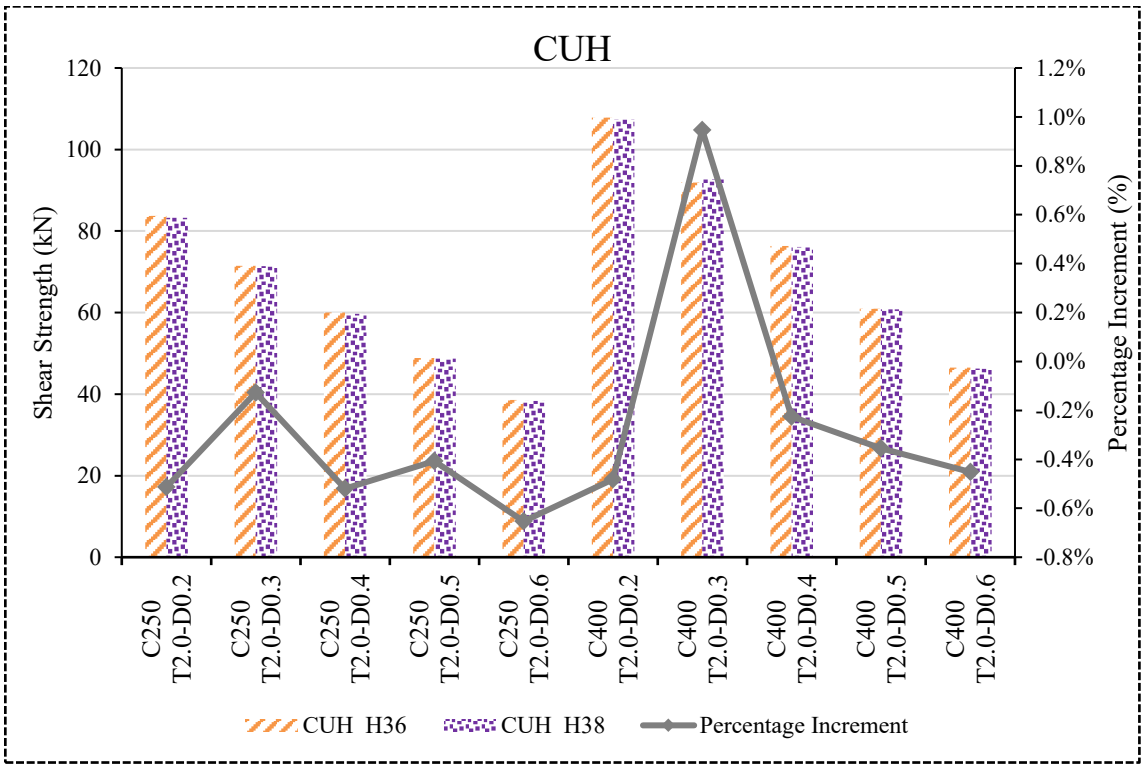

Fig: 34 Shear capacity of CUH aluminium sections (stiffened) at 3.5 mm thickness.

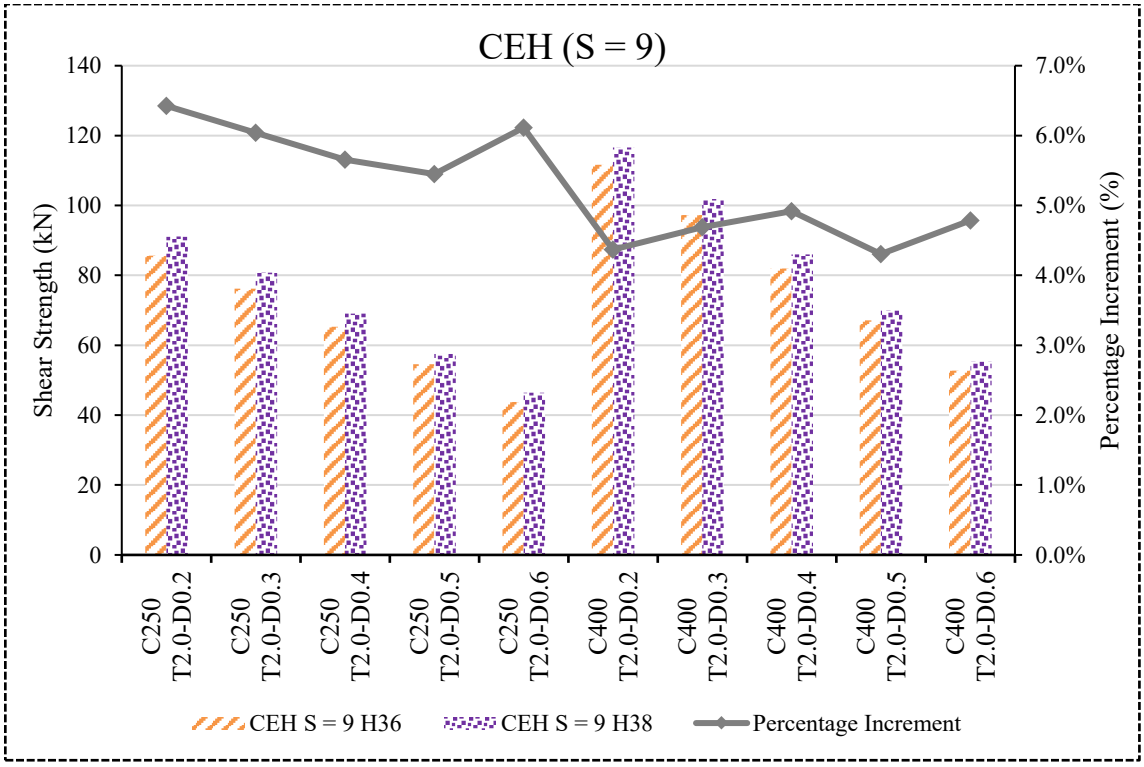

Fig: 35 Shear capacity of CEH (S=9) aluminium sections (stiffened) at 3.5 mm thickness.

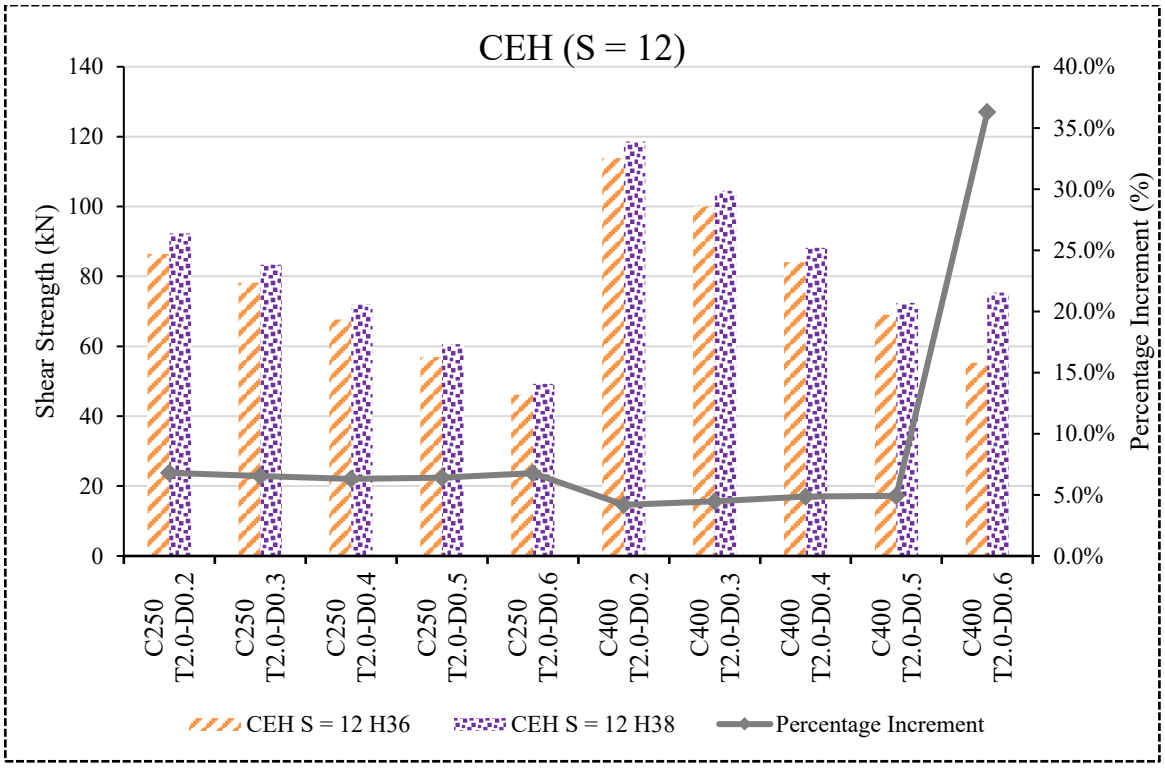

Fig: 36 Shear capacity of CEH (S=12) aluminium sections (stiffened) at 3.5 mm thickness.

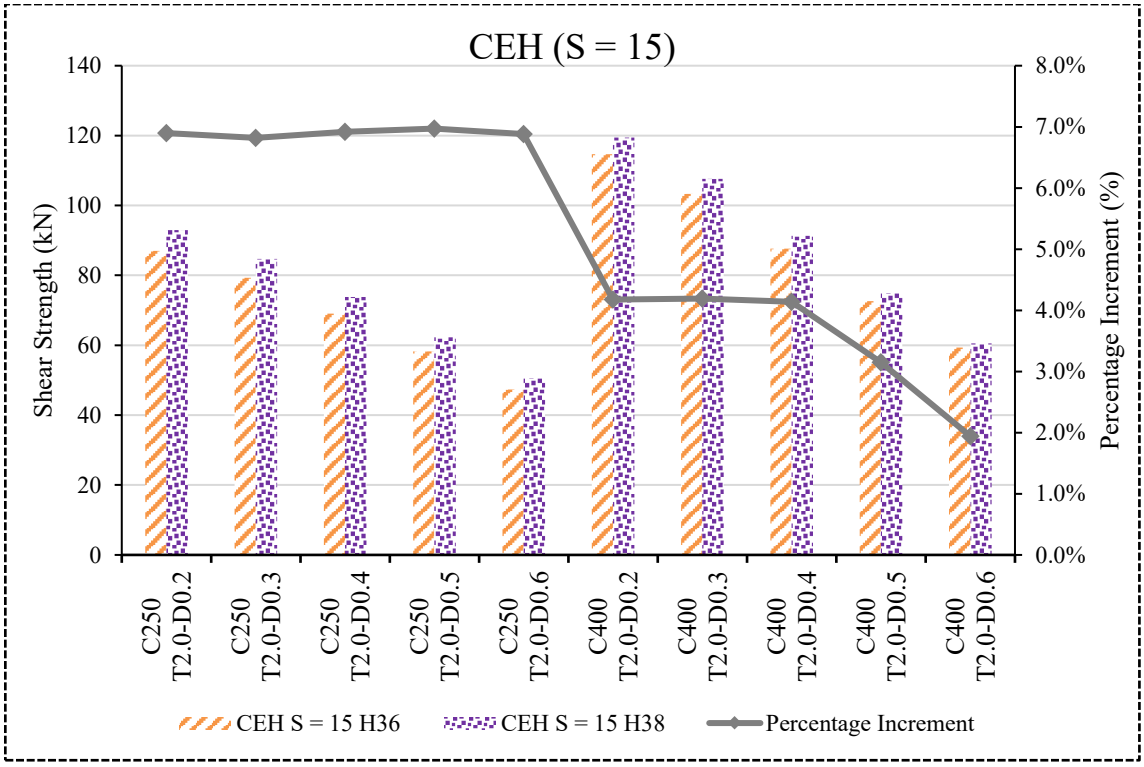

Fig: 37 Shear capacity of CEH (S=15) aluminium sections (stiffened) at 3.5 mm thickness.

For the 3.5 mm thickness specimens, the results are illustrated in Fig: 33, Fig: 34, Fig: 35, Fig: 36, & Fig: 37. As shown in Fig: 33, plain web sections consistently demonstrated the superiority of H38 over H36, with increments of about 7.5% in C250 and ~5% in C400, representing the strongest alloy advantage among all thicknesses studied. When unstiffened holes were introduced (Fig: 34), the increments were again neutralized, with values close to zero or slightly negative (–0.2% to –0.6%), confirming that CUH negates the benefit of higher yield strength. With stiffened holes (Fig: 33, Fig: 34, Fig: 35, Fig: 36, &Fig: 37), recovery was significant, with H38 showing ~5–7% higher strength than H36 in most C250 specimens and around 4–5% in C400 webs. In particular, deeper holes (e.g., C250-D0.6) exhibited the largest gains, reaching nearly 6.9% at S = 15, while the C400-D0.6 specimen at S = 12 displayed an anomalous spike (~36% increment), likely influenced by numerical sensitivity or local stiffener–hole interaction. Despite this anomaly, the general trend shows that stiffener length (S = 9–15) systematically enhanced recovery, with S = 15 providing the maximum improvement. Overall, at 3.5 mm thickness, stiffened holes not only restored the lost strength but consistently amplified the alloy advantage of H38, making it the most efficient configuration among all studied thicknesses.

Table 10 Shear strength obtained from the parametric study for thickness 3.5 mm.

Specimen	Shear strength for circular web holes, VFEA (kN)									
	H36					H38				
	Plain web (kN)	CUH (kN)	CEH S = 9 (mm)	CEH S = 12 (mm)	CEH S = 15 (mm)	Plain web (kN)	CUH (kN)	CEH S = 9 (mm)	CEH S = 12 (mm)	CEH S = 15 (mm)
C250-T3.5-D0.2	89.28	83.687	85.659	86.489	86.971	95.928	83.258	91.163	92.364	92.97
C250-T3.5-D0.3	89.28	71.507	76.161	78.232	79.342	95.928	71.416	80.763	83.337	84.753
C250-T3.5-D0.4	89.28	59.997	65.313	67.67	69.062	95.928	59.685	69.007	71.94	73.839
C250-T3.5-D0.5	89.28	48.892	54.548	56.969	58.223	95.928	48.693	57.521	60.622	62.282
C250-T3.5-D0.6	89.28	38.572	43.738	46.157	47.31	95.928	38.32	46.411	49.279	50.567
C400-T3.5-D0.2	120.84	107.85	111.68	113.85	114.64	127.02	107.33	116.56	118.61	119.43
C400-T3.5-D0.3	120.84	91.914	97.268	100.03	103.28	127.02	92.784	101.83	104.49	107.61
C400-T3.5-D0.4	120.84	76.311	81.965	84.099	87.652	127.02	76.139	85.997	88.177	91.282
C400-T3.0-D0.5	120.84	60.978	67.111	69.067	72.667	127.02	60.762	70	72.47	74.957
C400-T3.0-D0.6	120.84	46.484	52.778	55.329	59.373	127.02	46.274	55.304	75.409	60.526

5.6 Unstiffened Holes

This section focuses on the shear strength of CFA sections with unstiffened circular web holes, evaluated across four different thicknesses (2.0 mm, 2.5 mm, 3.0 mm, and 3.5 mm). The impact of hole geometry (depth-to-web depth ratio, dw/d1), the effect of increasing hole size, and the subsequent shear strength degradation are discussed. The parametric study examines the performance of these sections under shear loading and provides valuable insights into the magnitude of strength loss associated with unstiffened holes.

5.6.1 Shear strength obtained from the parametric study for thickness 2.0 mm (Unstiffened Holes)

For the 2 mm thickness specimens, the comparison between plain web sections and unstiffened holes (CUH) is illustrated in Fig: 38, Fig: 39. As shown in Fig: 38, plain webs establish the baseline capacity, with H38 consistently outperforming H36 by about 5.0% in C250 and 3.7% in C400 sections, reflecting the higher yield strength of the alloy. However, when unstiffened holes were introduced (Fig: 39), the alloy advantage nearly disappeared and even became slightly negative, with differences ranging from –0.3% to –0.7% across all hole depth ratios. This indicates that CUH not only reduces the absolute shear strength but also eliminates the benefit of using higher grade aluminium (H38), making both alloys perform almost identically. Overall, the results highlight that unstiffened holes are highly detrimental, causing a double penalty of capacity reduction and loss of material advantage.

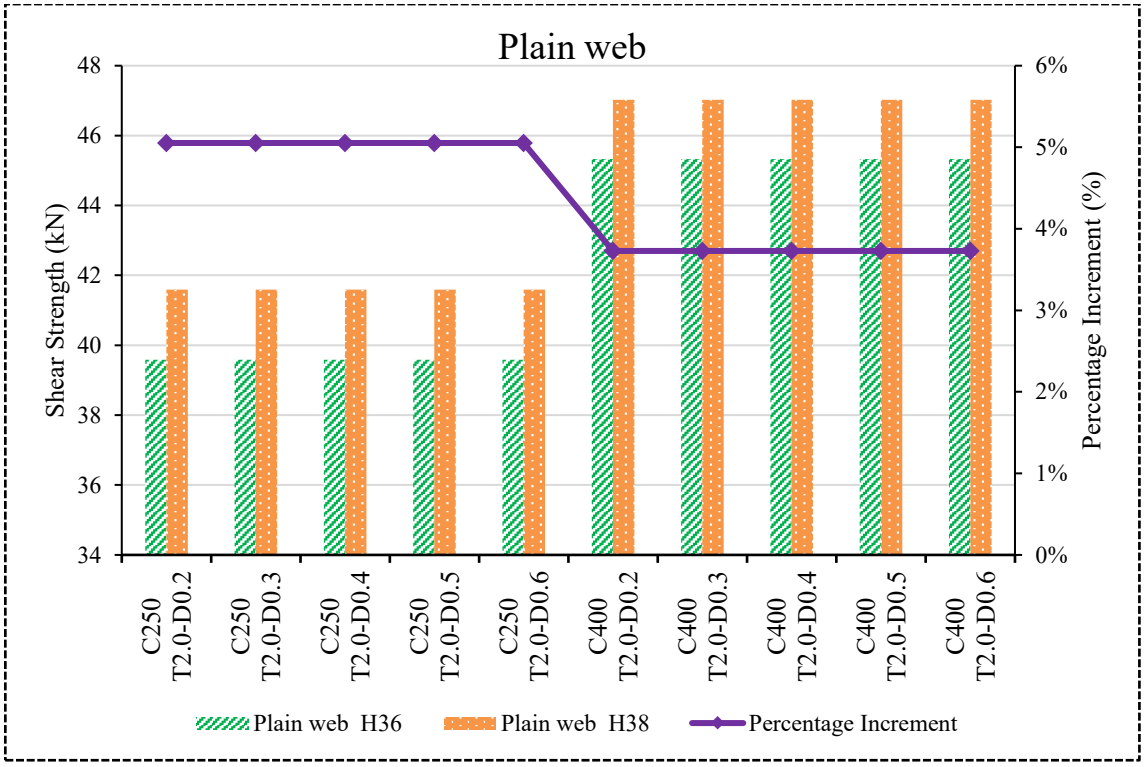

Fig: 38 Shear capacity of plain web aluminium sections (Unstiffened) at 2.0 mm thickness.

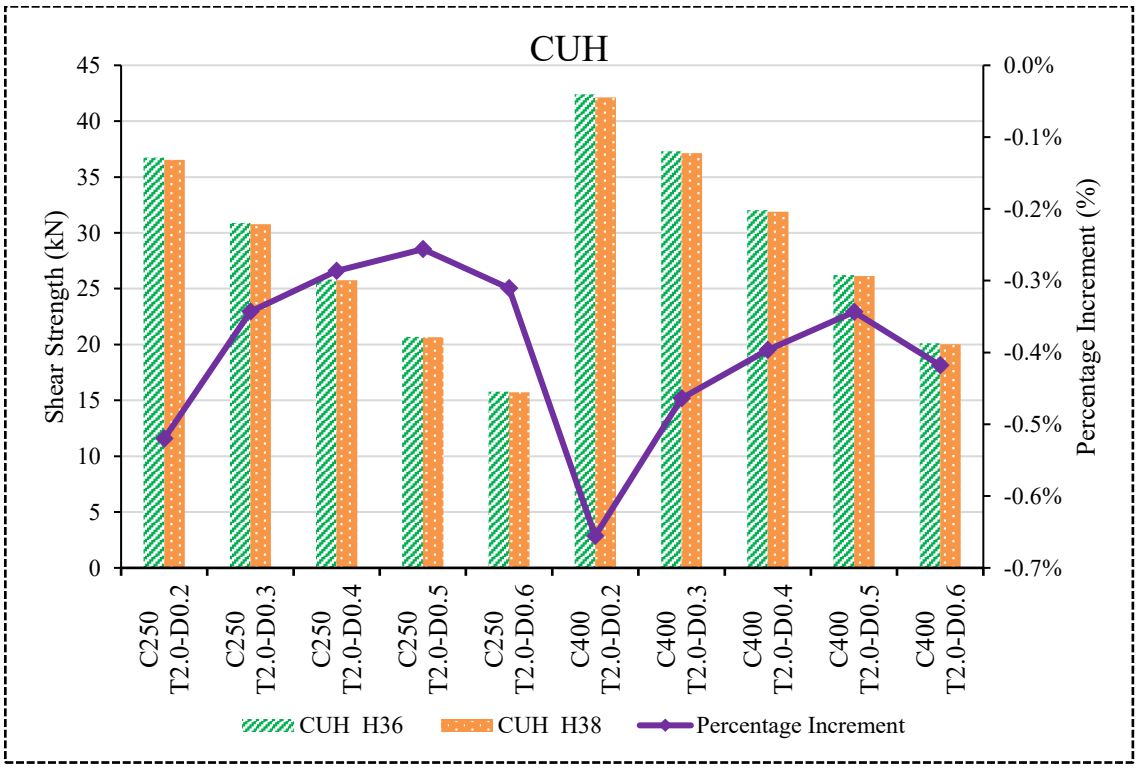

Fig: 39 Shear capacity of CUH aluminium sections (Unstiffened) at 2.0 mm thickness.

Table 11 Shear strength obtained from the parametric study for thickness 2.0 mm.

	H36		H38	
Specimen	**Plain web**	**CUH**	**Plain web**	**CUH**
	(kN)	**(kN)**	**(kN)**	**(kN)**
C250-T2.0-D0.2	39.59	36.734	41.59	36.543
C250-T2.0-D0.3	39.59	30.881	41.59	30.775
C250-T2.0-D0.4	39.59	25.826	41.59	25.752
C250-T2.0-D0.5	39.59	20.695	41.59	20.642
C250-T2.0-D0.6	39.59	15.78	41.59	15.731
C400-T2.0-D0.2	45.33	42.402	47.02	42.124
C400-T2.0-D0.3	45.33	37.306	47.02	37.133
C400-T2.0-D0.4	45.33	32.02	47.02	31.902
C400-T2.0-D0.5	45.33	26.21	47.02	26.128
C400-T2.0-D0.6	45.33	20.106	47.02	20.022

5.6.2 Shear strength obtained from the parametric study for thickness 2.5 mm (Unstiffened Holes)

For the 2.5 mm specimens, the comparison of plain webs and unstiffened holes is presented in Fig: 40, Fig: 41. As shown in Fig. W(a), plain web sections provided consistent baselines, with H38 equal to H36 in the C250 series (0% increment) and about 4.3% higher in C400 sections, reflecting the alloy advantage in deeper webs. When unstiffened holes were introduced (Fig. W(b)), this advantage was neutralized or reversed, with H38 showing slightly lower strengths than H36 by –0.2% to –1.0% across most hole ratios. The trend is consistent for both C250 and C400, where CUH eliminated the benefit of higher yield stress. An outlier occurs in the C250–D0.6 entry, which appears to be a data error (showing –66.7%); aside from this anomaly, the overall pattern demonstrates that unstiffened holes significantly reduce shear strength while cancelling out the alloy advantage. This confirms that CUH sections at 2.5 mm thickness behave similarly to the 2.0 mm case, with weakened capacity and negligible material-grade benefit.

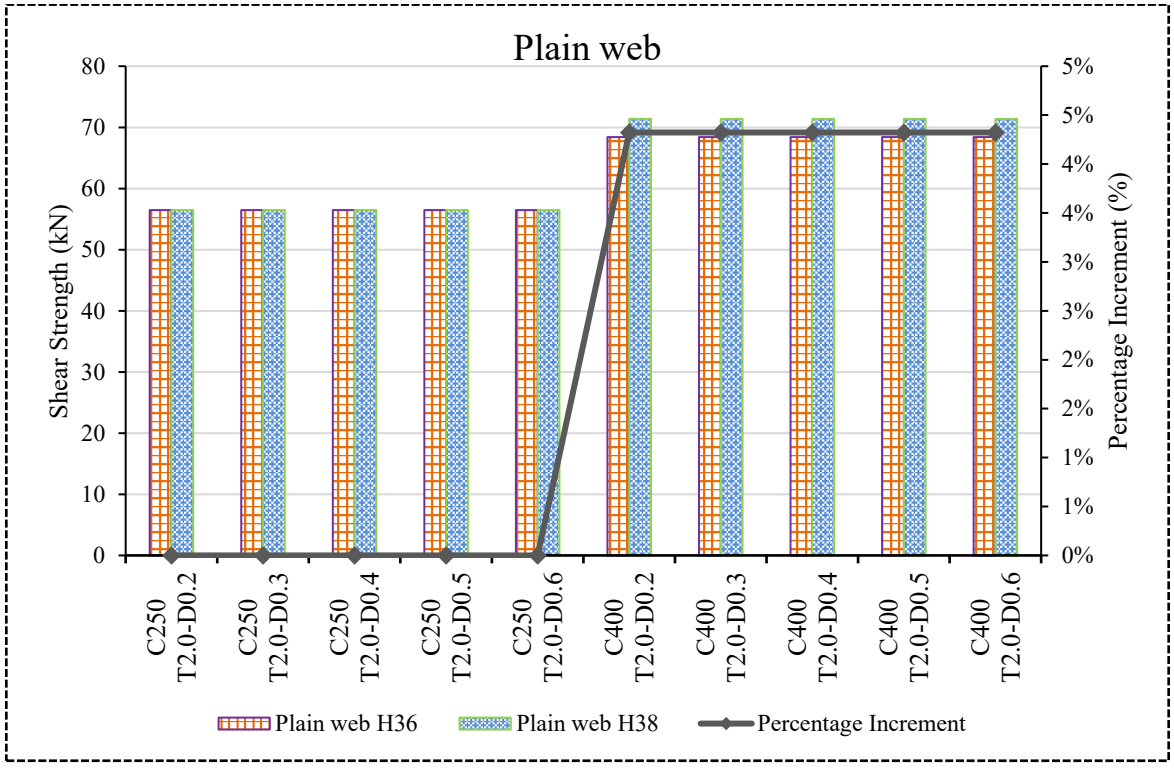

Fig: 40 Shear capacity of plain web aluminium sections (Unstiffened) at 2.5 mm thickness.

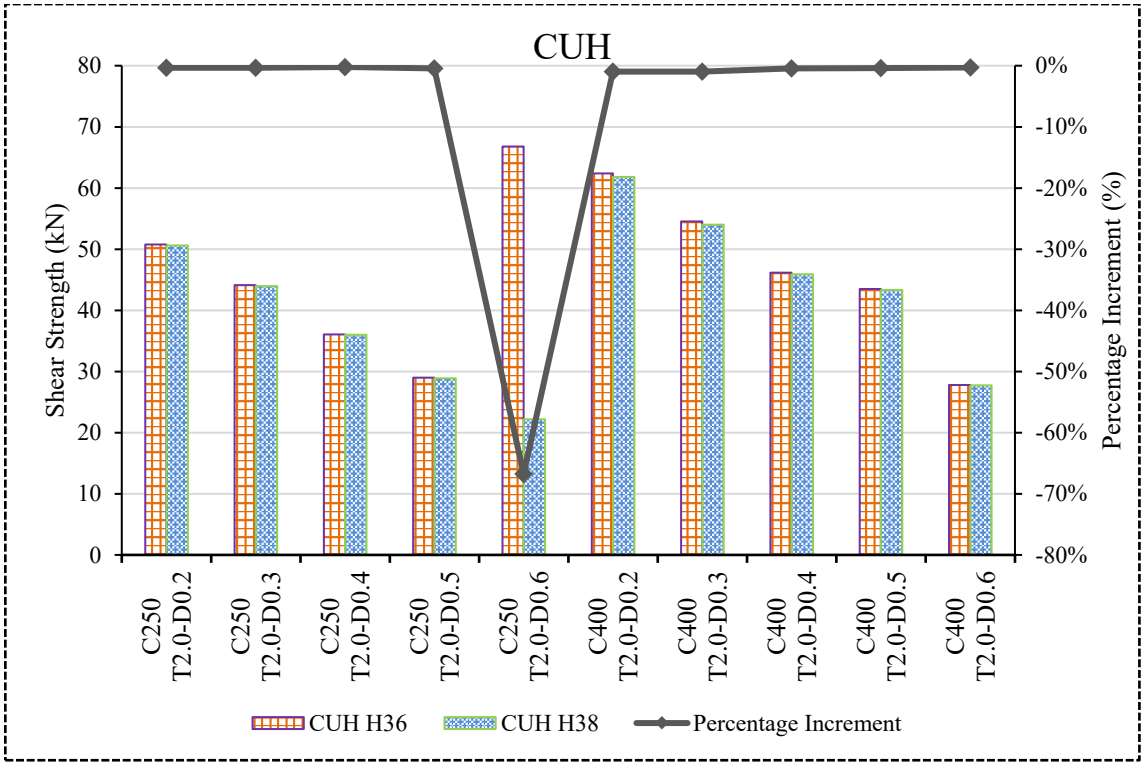

Fig: 41 Shear capacity of CUH aluminium sections (Unstiffened) at 2.5 mm thickness.

Table 12 Shear strength obtained from the parametric study for thickness 2.5 mm.

	H36		H38	
Specimen	**Plain web**	**CUH**	**Plain web**	**Plain web**
	(kN)	**(kN)**	(kN)	**(kN)**
C250-T2.5-D0.2	56.45	50.774	56.45	50.595
C250-T2.5-D.0.3	56.45	44.112	56.45	43.968
C250-T2.5-D0.4	56.45	36.058	56.45	35.982
C250-T2.5-D0.5	56.45	28.982	56.45	28.858
C250-T2.5-D0.6	56.45	66.797	56.45	22.202
C400-T2.5-D0.2	68.43	62.397	71.388	61.797
C400-T2.5-D0.3	68.43	54.519	71.388	54.002
C400-T2.5-D0.4	68.43	46.131	71.388	45.914
C400-T2.5-D0.5	68.43	43.51	71.388	43.347
C400-T2.5-D0.6	68.43	27.788	71.388	27.705

5.6.3 Shear strength obtained from the parametric study for thickness 3.0 mm (Unstiffened Holes)

For the 3.0 mm specimens, the behaviour of plain webs and unstiffened holes is shown in Fig: 42, & Fig: 43. As illustrated in Fig: 42, plain web sections highlight the clear material advantage of H38, which achieved about 6.9% higher capacity in C250 and ~5.1% in C400, reflecting its higher yield strength. However, with the introduction of unstiffened holes (Fig: 43), this advantage diminished almost completely, with percentage increments turning negative in most cases (–0.3% to –0.7%) and only a marginally positive value (+0.99%) observed for the C400–D0.3 specimen. This confirms that CUH not only causes a significant loss of shear strength but also suppresses the material-grade benefits of H38. The trend mirrors the results of thinner specimens, showing that unstiffened openings consistently penalize both strength and alloy advantage across thicknesses.

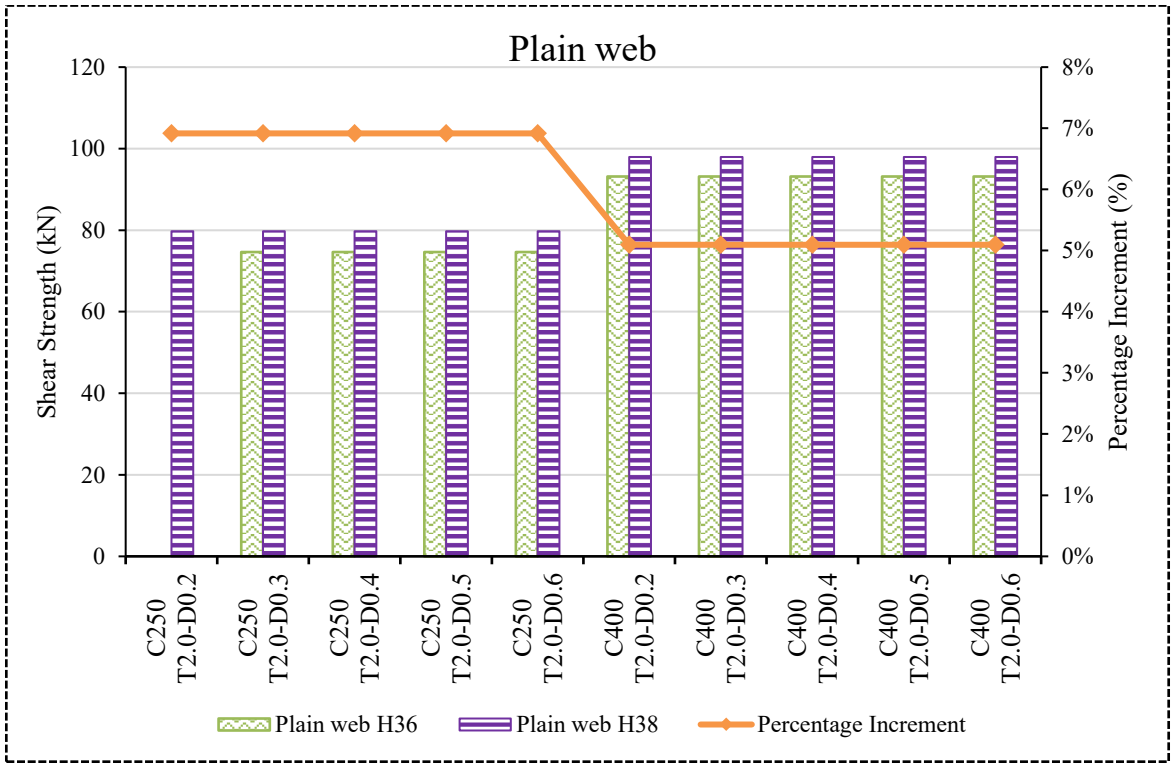

Fig: 42 Shear capacity of plain web aluminium sections (Unstiffened) at 3 mm thickness.

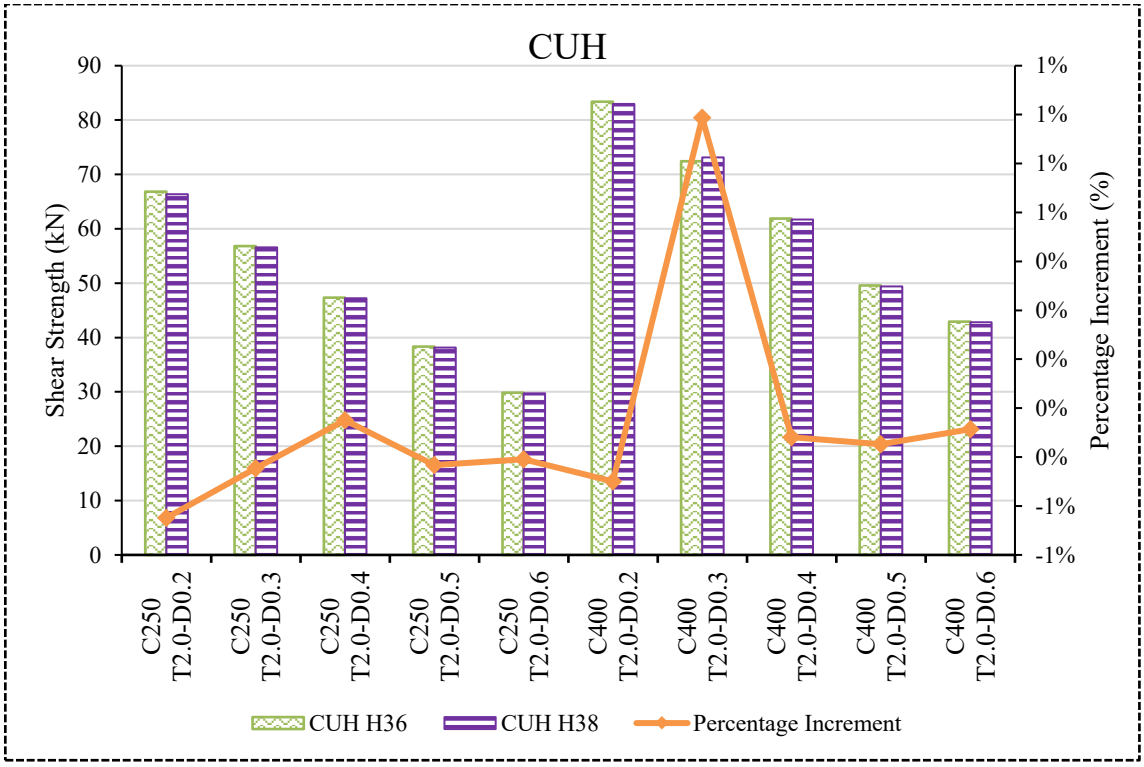

Fig: 43 Shear capacity of CUH aluminium sections (Unstiffened) at 3.0 mm thickness.

Table 13 Shear strength obtained from the parametric study for thickness 3.0 mm.

	H36		H38	
Specimen	**Plain web (kN)**	**CUH (kN)**	**Plain web (kN)**	**Plain web (kN)**
C250-T3.0-D0.2	74.62	66.797	79.781	66.364
C250-T3.0-D0.3	74.62	56.824	79.781	56.571
C250-T3.0-D0.4	74.62	47.346	79.781	47.228
C250-T3.0-D0.5	74.62	38.325	79.781	38.159
C250-T3.0-D0.6	74.62	29.854	79.781	29.732
C400-T3.0-D0.2	93.19	83.349	97.938	82.933
C400-T3.0-D0.3	93.19	72.419	97.938	73.134
C400-T3.0-D0.4	93.19	61.871	97.938	61.674
C400-T3.0-D0.5	93.19	49.554	97.938	49.382
C400-T3.0-D0.6	93.19	42.935	97.938	42.812

5.6.4 Shear strength obtained from the parametric study for thickness 3.5 mm (Unstiffened Holes)

For the 3.5 mm thickness specimens, the shear capacities of plain webs and CUH sections are presented in Fig: 44,.& Fig: 45 As shown in Fig: 44, plain web sections highlight the strongest alloy advantage, with H38 achieving about 7.5% higher capacity in C250 and ~5.1% in C400, confirming the benefit of the higher-grade material at greater thickness. However, the introduction of unstiffened holes (Fig: 45) neutralized this advantage, with H38 performing slightly worse than H36 in most cases (–0.2% to –0.7%) and only a marginally positive increment (+0.95%) observed in the C400–D0.3 specimen. This trend is consistent with thinner sections, showing that CUH drastically reduces capacity and cancels the alloy benefit regardless of thickness. Overall, the 3.5 mm results emphasize that without stiffening, even thicker aluminium webs cannot retain the material advantage of H38 once unstiffened openings are introduced.

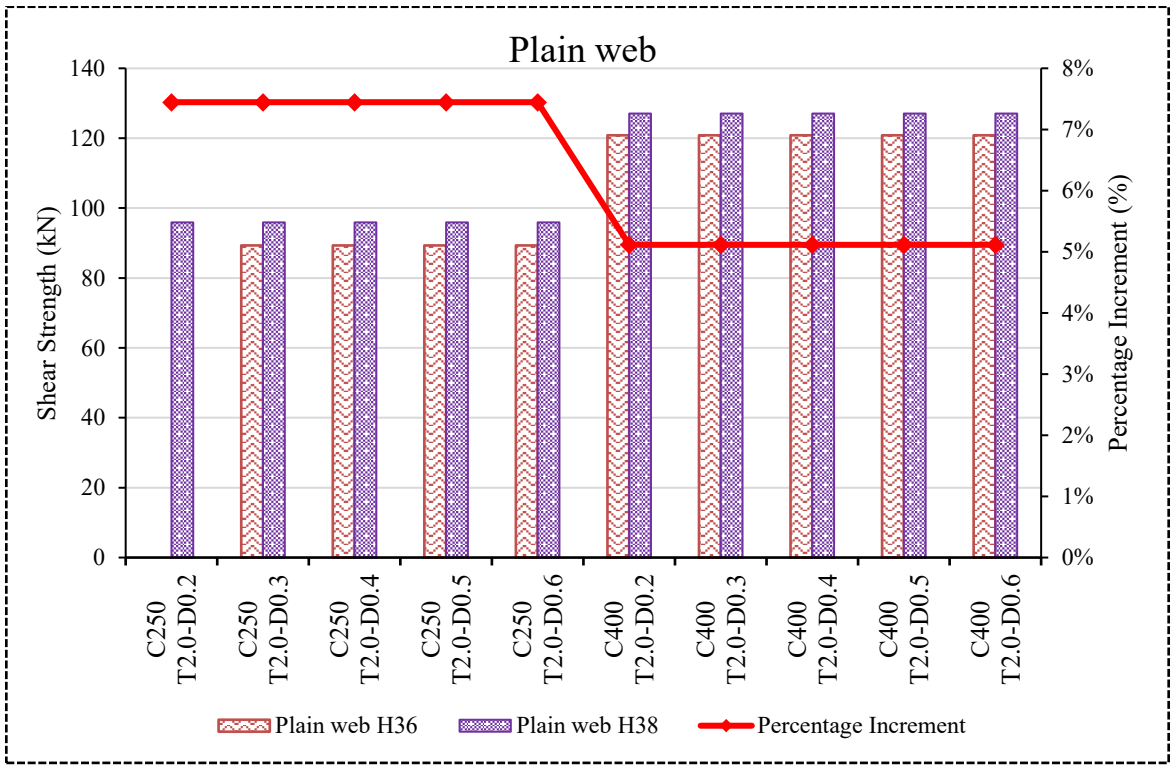

Fig: 44 Shear capacity of plain web aluminium sections (Unstiffened) at 3.5 mm thickness.

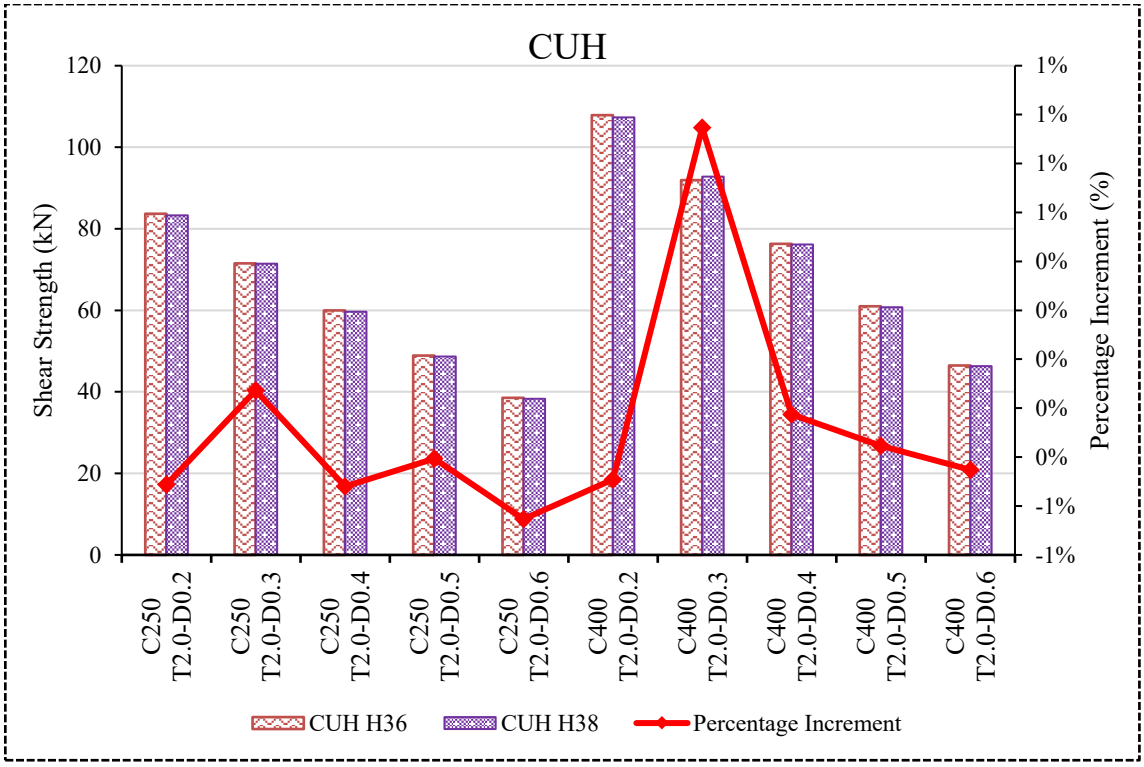

Fig: 45 Shear capacity of CUH aluminium sections (Unstiffened) at 3.5 mm thickness.

Table 14 Shear strength obtained from the parametric study for thickness 3.5 mm.

	H36		H38	
Specimen	**Plain web (kN)**	**CUH (kN)**	**Plain web (kN)**	**Plain web (kN)**
C250-T3.5-D0.2	89.28	83.687	95.928	83.258
C250-T3.5-D0.3	89.28	71.507	95.928	71.416
C250-T3.5-D0.4	89.28	59.997	95.928	59.685
C250-T3.5-D0.5	89.28	48.892	95.928	48.693
C250-T3.5-D0.6	89.28	38.572	95.928	38.32
C400-T3.5-D0.2	120.84	107.86	127.02	107.33
C400-T3.5-D0.3	120.84	91.914	127.02	92.784
C400-T3.5-D0.4	120.84	76.311	127.02	76.139
C400-T3.5-D0.5	120.84	60.978	127.02	60.762
C400-T3.5-D0.6	120.84	46.484	127.02	46.274

Chapter 6. Results and discussion

6.1 Overview of FE Model Validation

The developed finite element (FE) models were validated using experimental data from Rouholamin et al. and Chen et al. for aluminium and cold-formed steel sections, respectively. For the aluminium specimens reported by Rouholamin et al., the FE-predicted shear capacities (V_{FEA}) showed strong agreement with experimental values (V_{EXP}), with the mean ratio V_{FEA}/V_{EXP} ranging between 0.84 and 1.08, and an overall mean of 1.02 with a coefficient of variation (CoV) of less than 0.06.

Similarly, comparison with Chen et al.'s steel-based edge-stiffened data produced a mean ratio of 1.07 with CoV = 0.03, confirming the FE model's predictive accuracy for shear capacity and failure modes across material types.

The shear failure patterns from FE simulations closely matched experimental observations, with web buckling and local yielding initiating near hole edges for unstiffened openings, and delayed buckling in edge-stiffened configurations. Load–displacement curves also exhibited good correlation in both slope and peak load.

6.2 Effect of Hole Geometry and Stiffening on Shear Capacity

6.2.1 Circular Web Holes

For both C250 and C400 sections, the introduction of unstiffened circular holes (CUH) reduced shear capacity compared to plain webs by 8–60%, depending on the hole depth ratio (dw/d_1). The reduction was most pronounced at $dw/d_1 = 0.6$, where C250-T2.0 H36 specimens dropped from 39.59 kN (plain) to 15.78 kN (CUH), a 60.1% reduction.

The addition of edge stiffeners (CEH) significantly improved performance. At $dw/d_1 = 0.6$, the shear capacity for the same section increased from 15.78 kN (CUH) to 21.80 kN (CEH S=15), representing a 38.2% improvement. Across all hole depth ratios, CEH specimens regained between 15% and 40% of the lost capacity compared to CUH.

6.2.2 Influence of Stiffener Length

Increasing stiffener length-to-web depth ratio (q/d_1) from 0.04 to 0.12 consistently improved shear capacity. For example, C400-T3.0 H38 at $dw/d_1 = 0.4$ increased from 67.73 kN (S=9) to 71.75 kN (S=15) — a 5.9% gain.

The improvement was more significant for larger hole ratios, where additional stiffening better countered the severe web distortion.

6.3 Effect of Thickness and Material Grade

6.3.1 Section Thickness

Shear capacity increased almost linearly with thickness. For C250 H36 plain webs:

- T = 2.0 mm → 39.59 kN
- T = 2.5 mm → 56.45 kN (+42.6%)
- T = 3.0 mm → 74.62 kN (+86.5%)
- T = 3.5 mm → 89.28 kN (+125.5%)

Even with large holes ($dw/d_1 = 0.5$), the same trend held, showing that increasing thickness is an effective means of restoring shear capacity in perforated webs.

6.3.2 Material Grade

For identical geometry, H38 alloy consistently outperformed H36 due to its higher yield strength. The improvement ranged between 5–9% for plain webs and 7–12% for CEH configurations. For instance, C250-T3.0 at $dw/d_1 = 0.3$ improved from 65.11 kN (H36 CEH S=15) to 68.79 kN (H38 CEH S=15) — a 5.6% increase.

6.4 Effect of Web Depth (C250 vs. C400)

Larger web depths (C400) generally provided higher shear capacity due to increased shear area. For example, with T=3.0 mm, plain web H38:

- C250 → 79.78 kN
- C400 → 97.94 kN (+22.8%)

However, the relative percentage reduction due to holes was greater in deeper webs, particularly for unstiffened configurations. At $dw/d_1 = 0.6$, C400-T2.0 H36 dropped from 45.33 kN (plain) to 20.11 kN (CUH) — a 55.6% loss, compared to 50.1% loss for C250.

6.5 Comparison with Design Standards

When benchmarked against AISI (2016) [1] and AS/NZS (2018) [2] provisions, both standards were overly conservative by 8–20% for plain webs and underestimated the beneficial effect of edge stiffening. For CEH specimens, the codes underestimated capacity by up to 25%, particularly at small shear span ratios where shear-dominated failure governed. This reinforces the need for modified shear reduction factors accounting for stiffener geometry and aluminium's lower modulus of elasticity.

6.6 Observed Failure Modes

The failure modes observed in the **parametric study** reflect the impact of hole geometry, stiffening, material grade, and section thickness on the shear behaviour of the aluminium channel sections. The following key failure modes were observed:

- **Plain Webs:** For sections with plain webs, **shear yielding** initiated at the **mid-depth near supports**, followed by the development of **inclined shear buckling waves**. The lack of reinforcement in the web leads to localized instability, especially under shear loading.
- **Unstiffened Circular Holes (CUH):** When unstiffened holes were introduced, **high stress concentrations** formed at the **hole corners**, leading to **early local buckling**. This was followed by **Vierendeel bending** between the hole edges, significantly reducing the shear capacity of the sections. The presence of holes caused substantial **capacity degradation**, with the material-grade advantage (H38 over H36) being nearly eliminated, as observed in the results from **Figs. 39 and 43**.
- **Edge-Stiffened Holes (CEH):** For sections with edge-stiffened holes, the increased **local stiffness** provided by the stiffeners delayed buckling. In these cases, failure transitioned into **web post-buckling**, with **flange distortion** observed in sections with larger holes. The stiffeners helped redistribute the applied stresses, restoring some of the lost strength compared to unstiffened holes, with the best performance seen at longer stiffener lengths (S = 15). This behavior was particularly evident for sections like **C250-T2.5-D0.6** and **C400-T3.5-D0.5**, where **H38** showed a recovery of around 4–6% in shear strength.
- **Thicker Sections (3.0 mm and 3.5 mm):** Thicker sections exhibited greater **post-buckling reserve strength**, particularly in **H38 alloy**, where the material's higher yield strength allowed it to better withstand the forces and maintain structural integrity after initial buckling. The **C400 sections** in particular showed significant improvements, with deeper holes (D0.5–D0.6) showing a more substantial recovery in shear strength when stiffened.

6.7 Key Findings

1. Edge stiffeners improved shear capacity by **15–40%** over unstiffened holes, depending on hole depth and stiffener length.
2. Shear strength loss from holes was strongly proportional to dw/d_1, with reductions up to **60%** at $dw/d_1 = 0.6$.
3. Increasing thickness was the single most effective geometric parameter for strength recovery, followed by stiffener length.
4. H38 alloy provided up to **12%** greater capacity than H36 for identical geometries.
5. Design standards do not currently capture the strength enhancement from edge stiffening in aluminium members, leading to conservative designs

Chapter 7. Design Rules

For aluminium sections, there were no design guidelines available to determine the shear strength of such sections with unstiffened and edge-stiffened web holes. However, the AS/NZS 1664.1 [2] design standards provided design equations to predict the shear strength of extruded aluminium sections with plain webs. It should be noted that the AISI [1] and AS/NZS [2] design standards offered shear reduction factor (q_s) for computing the shear strength of CFS channel sections with unstiffened web holes. The available design equations, outlined in the subsequent sub-sections, provided a valuable contribution to the understanding and calculation of the shear strength of such structural configurations.

The design standards of AISI [1] and AS/NZS [2] provide the shear reduction factor equations to determine the shear strength of aluminium sections with non-circular web holes, which were adopted from the design equations of Eiler et al. [10]. shear reduction factor equations (Equation 10, Equation 11, Equation 12, Equation 13) are given below:

$$V_{nl} = q_s V_n$$

Equation 10

$$q_s = 1 \qquad for\ \frac{c}{t} \geq 54$$

Equation 11

$$q_s = \frac{c}{54t} \qquad for\ 5 \leq \frac{c}{t} < 54$$

Equation 12

$$\boldsymbol{c = \frac{d_1}{2} - \frac{d_w}{2.83}\ for\ circular\ web\ holes\ ;\ c = \frac{d_1}{2} - \frac{d_w}{2}\ for\ non-circular\ openings}$$

Equation 13

Where, V_n = nominal shear strength of section with plain webs, q_s = shear reduction factor, c = factor for non-circular web holes.

7.1 Comparison of design strengths calculated from the available design guidelines with the FEA results

For aluminium channels having un-stiffened circular web holes, the parametric results were compared with the shear reduction factor equations of AISI [1] and AS/NZS [2]. The comparison results revealed that the design equations of AISI [1] and AS/NZS [2] were conservative or unconservative by 26 % on average, for un-stiffened circular web holes. Fig 20 present the comparison results of shear reduction factor equations [1] [2] with FEA.

From the design comparison analysis, it was found that the available shear reduction factor (q_s) [1] [2] are unsafe to predict the shear strength of aluminium sections considering with un-stiffened circular web holes (see Fig: 46).

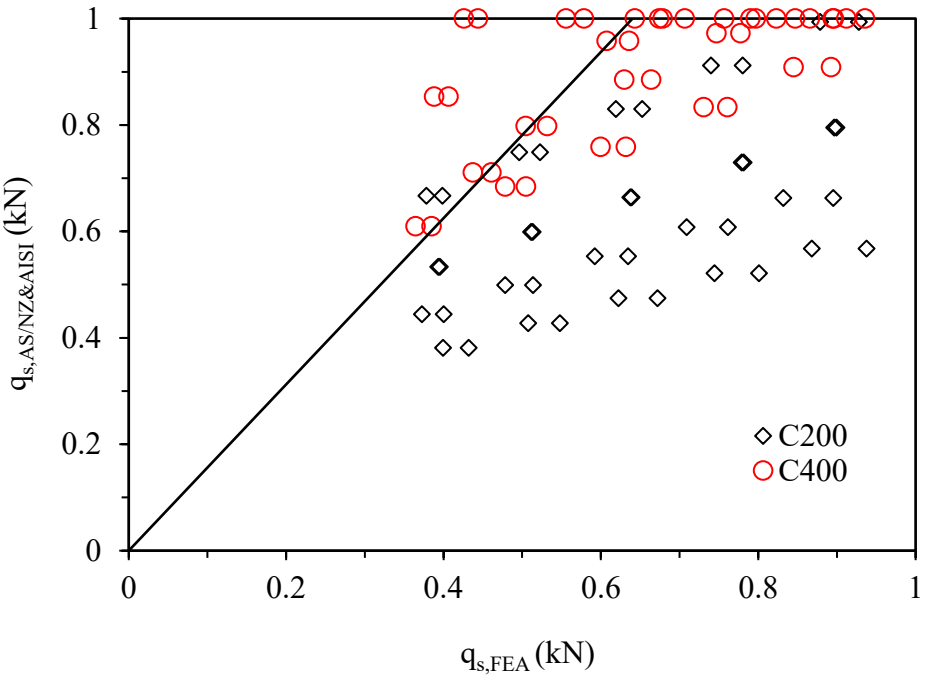

Fig: 46 Comparison of shear reduction factor equations [1] **with FEA**

7.2 Proposed shear reduction-based equations

The parametric analysis identified that the geometric ratios d_w/d_1, b_w/d_w and q/d_1 significantly influence the shear strength of aluminium channel sections containing both stiffened and unstiffened circular web holes. Based on these findings, a new shear reduction factor (q_s) for unstiffened and a shear enhancement factor (q_e) for stiffened web holes were proposed through bivariate regression analysis. The proposed design equations (Equation 14, Equation 15, Equation 16, &Equation 17) accurately estimating the shear strength of

aluminium channel sections with such web openings (see Fig: 47 and Fig: 48), which are outlined below.

For unstiffened circular web holes,

$$q_{s,Prop} = 1.00 - 0.76\left(\frac{d_w}{d_1}\right) \qquad for\ 0 < \frac{d_w}{d_1} \leq 0.30$$

Equation 14

$$q_{s,prop} = 1.10 - 1.20\left(\frac{d_w}{d_1}\right) \qquad for\ 0.30 < \frac{d_w}{d_1} \leq 0.60$$

Equation 15

For stiffened circular web holes,

$$q_{e,Prop} = 1.06 - 0.89\left(\frac{d_w}{d_1}\right) + 1.35\left(\frac{q}{d_1}\right) \qquad for\ 0 < \frac{d_w}{d_1} \leq 0.30$$

Equation 16

$$q_{e,prop} = 1.09 - 1.19\left(\frac{d_w}{d_1}\right) + 2.87\left(\frac{q}{d_1}\right) \qquad for\ 0.30 < \frac{d_w}{d_1} \leq 0.60$$

Equation 17

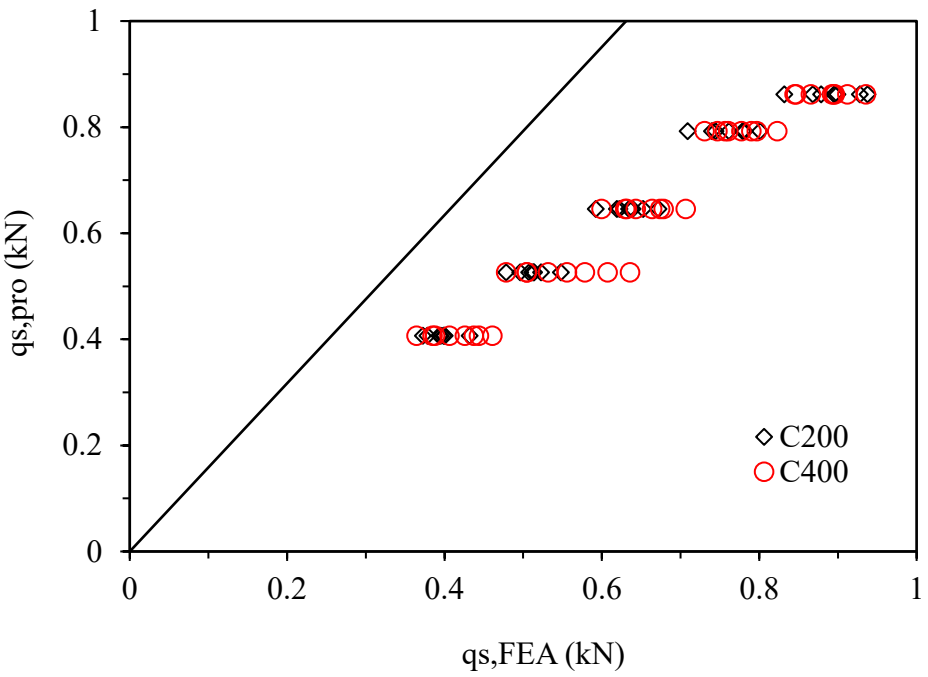

Fig: 47 Comparison of proposed shear strength reduction with FEA for aluminium channel sections with unstiffened circular web holes

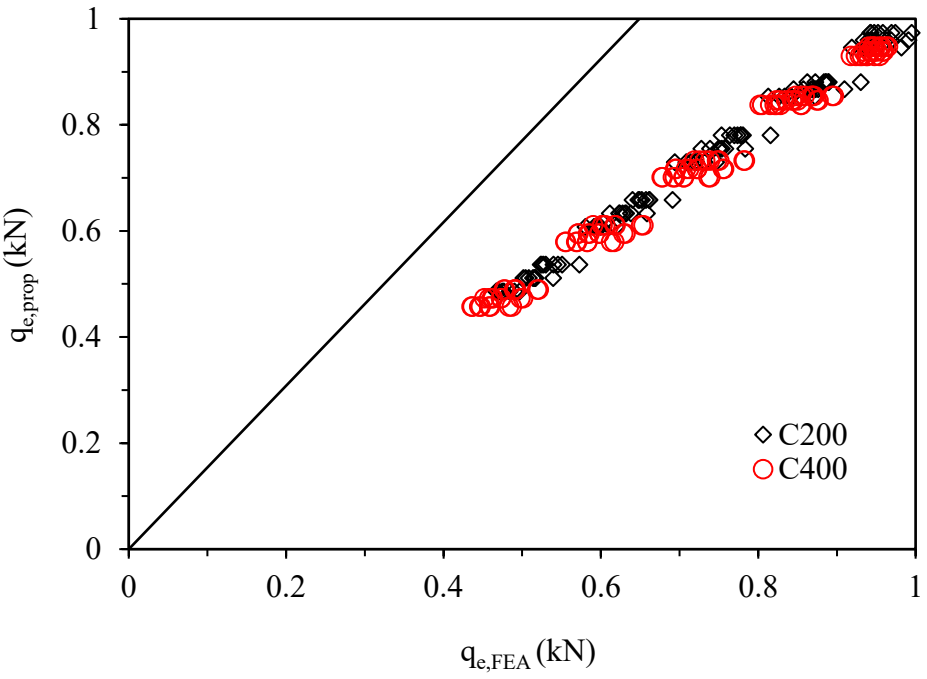

Fig: 48 Comparison of proposed shear strength reduction with FEA for aluminium channel sections with edge-stiffened circular web holes

7.3 Reliability analysis

A reliability analysis was also conducted to evaluate the accuracy of the proposed design equations of aluminium channel sections with unstiffened and edge-stiffened elongated web holes. For Thin-walled structural members, the AISI Specification [1] provides an equation Equation 18 and recommends that the lower limit of the target reliability index should be 2.5. The design equations are generally considered reliable if the reliability index (β) value is greater than or equal to 2.5. In this study, the proposed modified DSM approach was found to be reliable, while calculating the shear strength of aluminium channel sections having unstiffened and edge-stiffened elongated web holes (see Table 15).

$$\varphi = 1.52 M_m F_m P_m e^{-\beta \sqrt{\{V_m^2 + V_f^2 + C_p V_p^2 + V_q^2\}}}$$

Equation 18

Where, β = reliability index, φ = resistance factor (0.85), M_m and V_m = mean (1.1) and COV (0.1) of the material factor, F_m and V_f = mean (1.0) and COV (0.05) of the fabrication factor, P_m and V_P = mean and COV of the proposed equation, V_q = COV (0.21) of load effect, C_p = correction factor $\left[1 + \frac{1}{n}\right]\left[\frac{m}{m-2}\right]$, n = number of tests and m = degree of freedom ($m = n$-1).

Table 15 Reliability analysis results of proposed equations

	Unstiffened holes	**Edge-stiffened holes**
	$q_{s,Prop}$	$q_{e,Prop}$
	Eqs. 5&6	**Eqs. 7&8**
Number of data	80	240
Mean, P_m	1.00	1.00
Coefficient of variation, Vp	0.05	0.03
Reliability index, β	2.89	2.92
Resistance factor, φ	0.85	0.85

Chapter 8. Conclusions

The study has explored in detail the shear behaviour and design of cold-formed aluminium (CFA) channel section with circular edge-stiffened web openings, especially shear span ratios of low values and performance with respect to materials of construction. A combination of convention and available validated finite element (FE) modelling and a wide range of parametric studies, the study has numerically quantified the influence of hole geometry, stiffener type, section depth, material grade and thickness on the shear capacity of aluminium members.

Calculation of the FE models against experimental values of Rouholamin et al. [21] and Chen et al. showed great predictive excellence as the mean ratio was 1.02: aluminium specimens and 1.07: cold-formed steel specimens and coefficients of variation were insatiably low (0.06). These results showed the similarity in load-displacement behaviour and failure patterns that indicated that the developed modelling method reflected elastic buckling, post-buckling and ultimate failure behaviours.

The parametric study showed that web openings cause great degradation in shear capacity, especially at large unstiffened holes where losses could be as much as 60 percent (dw/d 1 = 0.6). Additional edge stiffeners represented a successful strengthening technique that regains 15 and 40 percent of the lost strength due to the stiffener length and hole size. Extending the ratio of stiffener length to web depth (q/d 1) improved shear strength with maximum improvement being recorded at higher openings. Section thickness and alloy grade also played a critical role: shear capacity more than doubled in most cases when the thickness was increased 2.0 to 3.5 mm and H38 alloy consistently had greater shear capacity than H36 because it has a higher yield strength.

Comparison against AISI (2016) [1] and AS/NZS (2018)[2] design standards found that the current practices are somewhat conservative in terms of aluminium members with plain webs but conservative in overestimating the positive impacts on edge stiffening, especially at low shear span ratios. The lesson in this is that new shear reduction factors and design provisions should be considered to include stiffener geometry and the specific mechanical properties of aluminium.

On the whole, the outcomes of the present study present valuable contributions to the theoretical background and practical framework of the design of aluminium alloy members with web openings. The verified FE approach and the built dataset are a good starting point to the development of future codes and the insights proposed here can serve engineers to develop

more efficient, lighter and safer aluminium structural systems. This statement places much importance on the context of narrowing the gap that existed between previous research in cold-formed steel structures and applications respectively on aluminium structures, the present work is also an important breakthrough to optimal designing guides on contemporary aluminium structures in service openings**.**

References

[1] AISI, "North American Specification for the Design of Cold-Formed Steel Structural Members, 2016 Edition," 2016. Accessed: Sep. 29, 2025. [Online]. Available: https://www.buildusingsteel.org/wp-content/uploads/2023/06/AISI-S100-16-2020.pdf

[2] AS/NZS 4600, "Cold-formed steel structures," 2018. Accessed: Sep. 29, 2025. [Online]. Available: https://www.standards.govt.nz/shop/asnzs-30002018

[3] BS NA EN 1999-1-1, "UK National Annex to Eurocode 9. Design of aluminium structures. General structural rules : British Standards Institution (BSI)," *British Standards Institution*, 2009, Accessed: Sep. 29, 2025. [Online]. Available: https://www.phd.eng.br/wp-content/uploads/2014/11/en.1999.1.1.2007.pdf

[4] B. Chen, K. Roy, A. Uzzaman, and J. B. P. Lim, "Moment capacity of cold-formed channel beams with edge-stiffened web holes, un-stiffened web holes and plain webs," *Thin-Walled Structures*, vol. 157, p. 107070, Dec. 2020, doi: 10.1016/J.TWS.2020.107070.

[5] P. Keerthan and M. Mahendran, "Shear buckling characteristics of cold-formed steel channel beams," *International Journal of Steel Structures*, vol. 13, no. 3, pp. 385–399, Sep. 2013, doi: 10.1007/S13296-013-3001-6/METRICS.

[6] B. Chen *et al.*, "Effects of edge-stiffened web openings on the behaviour of cold-formed steel channel sections under compression," *Thin-Walled Structures*, vol. 144, p. 106307, Nov. 2019, doi: 10.1016/J.TWS.2019.106307.

[7] C. Yu, "Cold-formed steel flexural member with edge stiffened holes: Behavior, optimization, and design," *J Constr Steel Res*, vol. 71, pp. 210–218, Apr. 2012, doi: 10.1016/J.JCSR.2011.09.008.

[8] “PV power plant in Thessaloniki - Energetica: Hochleistungs-Photovoltaik. Made in Austria.” Accessed: Oct. 24, 2025. [Online]. Available: https://www.energetica.at/en/portfolio-item/pv-power-plant-in-thessaloniki/

[9] B. Chen *et al.*, “Shear Capacity of Cold-Formed Steel Channels with Edge-Stiffened Web Holes, Unstiffened Web Holes, and Plain Webs,” *Journal of Structural Engineering*, vol. 148, no. 2, p. 04021268, Nov. 2021, doi: 10.1061/(ASCE)ST.1943-541X.0003250.

[10] Yu, Wei-Wen, Eiler Roger A, LaBoube, and Matthew R, “Behavior of web elements with openings subjected to linearly varying shear,” *CCFSS Library (1939 - present)*, Jun. 1997, Accessed: Sep. 29, 2025. [Online]. Available: https://scholarsmine.mst.edu/ccfss-library/149

[11] P. Keerthan and M. Mahendran, “Experimental studies of the shear behaviour and strength of lipped channel beams with web openings,” *Thin-Walled Structures*, vol. 73, pp. 131–144, Dec. 2013, doi: 10.1016/J.TWS.2013.06.018.

[12] P. Keerthan and M. Mahendran, “Improved shear design rules for lipped channel beams with web openings,” *J Constr Steel Res*, vol. 97, pp. 127–142, Jun. 2014, doi: 10.1016/J.JCSR.2014.01.011.

[13] C. H. Pham and G. J. Hancock, “Experimental Investigation of High Strength Cold-Formed C -Sections in Combined Bending and Shear,” *Journal of Structural Engineering*, vol. 136, no. 7, pp. 866–878, Dec. 2009, doi: 10.1061/(ASCE)ST.1943-541X.0000172.

[14] C. H. Pham and G. J. Hancock, “Shear buckling of thin-walled channel sections,” *J Constr Steel Res*, vol. 65, no. 3, pp. 578–585, Mar. 2009, doi: 10.1016/J.JCSR.2008.05.015.

[15] B. Chen *et al.*, “Effects of edge-stiffened web openings on the behaviour of cold-formed steel channel sections under compression,” *Thin-Walled Structures*, vol. 144, p. 106307, Nov. 2019, doi: 10.1016/J.TWS.2019.106307.

[16] B. Chen, K. Roy, Z. Fang, A. Uzzaman, Y. Chi, and J. B. P. Lim, “Web crippling capacity of fastened cold-formed steel channels with edge-stiffened web holes, un-stiffened web holes and plain webs under two-flange loading,” *Thin-Walled Structures*, vol. 163, p. 107666, Jun. 2021, doi: 10.1016/J.TWS.2021.107666.

[17] Z. Fang, K. Roy, B. Chen, C. W. Sham, I. Hajirasouliha, and J. B. P. Lim, “Deep learning-based procedure for structural design of cold-formed steel channel sections with edge-stiffened and un-stiffened holes under axial compression,” *Thin-Walled Structures*, vol. 166, p. 108076, Sep. 2021, doi: 10.1016/J.TWS.2021.108076.

[18] Z. Fang, K. Roy, J. Mares, C. W. Sham, B. Chen, and J. B. P. Lim, “Deep learning-based axial capacity prediction for cold-formed steel channel sections using Deep Belief Network,” *Structures*, vol. 33, pp. 2792–2802, Oct. 2021, doi: 10.1016/J.ISTRUC.2021.05.096.

[19] P. Keerthan and M. Mahendran, “Experimental investigation and design of lipped channel beams in shear,” *Thin-Walled Structures*, vol. 86, pp. 174–184, Jan. 2015, doi: 10.1016/J.TWS.2014.08.024.

[20] H.-T. Li and B. Young, “Cold-Formed High-Strength Steel Tubular Structural Members under Combined Bending and Bearing,” *Journal of Structural Engineering*, vol. 145, no. 8, p. 04019081, Jun. 2019, doi: 10.1061/(ASCE)ST.1943-541X.0002371.

[21] Laboube and A. Roger, *Strength of cold-formed steel beam webs in bending, shear, and a combination of bending and shear.* University of Missouri, 1977. Accessed: Sep. 29, 2025. [Online]. Available:

https://search.proquest.com/openview/062dce8fd76e24492c9021d120f08ac3/1?pq-origsite=gscholar&cbl=18750&diss=y

[22] ISO 6892-1, "Metallic materials — Tensile testing — Part 1: Method of test at room temperature," *The International Organization for Standardization*, 2009, Accessed: Sep. 29, 2025. [Online]. Available: https://www.iso.org/obp/ui/#iso:std:iso:6892:-1:ed-1:en

[23] P. Keerthan and M. Mahendran, "New Design Rules for the Shear Strength of LiteSteel Beams with Web Openings," *Journal of Structural Engineering*, vol. 139, no. 5, pp. 640–656, May 2013, doi: 10.1061/(ASCE)ST.1943-541X.0000563.

[24] D. L. Chandramohan *et al.*, "Shear behaviour and design of doubly symmetric hollow flange beam with web openings," *J Constr Steel Res*, vol. 185, p. 106836, Oct. 2021, doi: 10.1016/J.JCSR.2021.106836.

[25] Z. Fang, K. Roy, B. Chen, C. W. Sham, I. Hajirasouliha, and J. B. P. Lim, "Deep learning-based procedure for structural design of cold-formed steel channel sections with edge-stiffened and un-stiffened holes under axial compression," *Thin-Walled Structures*, vol. 166, p. 108076, Sep. 2021, doi: 10.1016/J.TWS.2021.108076.

[26] B. Young, M. Asce, and W.-M. Lui, "Behavior of Cold-Formed High Strength Stainless Steel Sections," *Journal of Structural Engineering*, vol. 131, no. 11, pp. 1738–1745, Nov. 2005, doi: 10.1061/(ASCE)0733-9445(2005)131:11(1738).

[27] E. Kanthasamy *et al.*, "Shear behaviour of doubly symmetric rectangular hollow flange beam with circular edge-stiffened openings," *Eng Struct*, vol. 250, p. 113366, Jan. 2022, doi: 10.1016/J.ENGSTRUCT.2021.113366.

[28] B. Chen, K. Roy, A. Uzzaman, and J. B. P. Lim, "Moment capacity of cold-formed channel beams with edge-stiffened web holes, un-stiffened web holes and plain

webs," *Thin-Walled Structures*, vol. 157, p. 107070, Dec. 2020, doi: 10.1016/J.TWS.2020.107070.

[29] B. Chen, K. Roy, A. Uzzaman, G. M. Raftery, and J. B. P. Lim, "Parametric study and simplified design equations for cold-formed steel channels with edge-stiffened holes under axial compression," *J Constr Steel Res*, vol. 172, p. 106161, Sep. 2020, doi: 10.1016/J.JCSR.2020.106161.

[30] B. Chen, K. Roy, Z. Fang, A. Uzzaman, Y. Chi, and J. B. P. Lim, "Web crippling capacity of fastened cold-formed steel channels with edge-stiffened web holes, un-stiffened web holes and plain webs under two-flange loading," *Thin-Walled Structures*, vol. 163, p. 107666, Jun. 2021, doi: 10.1016/J.TWS.2021.107666.

[31] United Nation Development Programme, "THE 17 GOALS | Sustainable Development." Accessed: Jan. 04, 2024. [Online]. Available: https://sdgs.un.org/goals

[32] Howick, "Floor joist system," Auckland, New Zealand, 2013. Accessed: Oct. 10, 2025. [Online]. Available: https://www.howickltd.com/applications/frames-trusses-joists/lattice-floor-joists

[33] ABAQUS/CAE, "User's Manual, Dassault Systèmes Simulia Corporation," 2014. Accessed: Sep. 29, 2025. [Online]. Available: http://130.149.89.49:2080/v2016/pdf_books/CAE.pdf

[34] M. Rouholamin, "Shear Behaviour and Design of Roll-Formed Aluminium Lipped Channel Sections With and Without Web Openings," Oct. 2020, doi: 10.25904/1912/3979.